Investigation of Mesoscale Surface Pressure and Temperature Features Associated with Bow Echoes

Submitted by

Rebecca Denise Adams Selin

Department of Atmospheric Science

In partial fulfillment of requirements

For the Degree of Master of Science

Colorado State University

Fort Collins, Colorado

Spring 2008

ABSTRACT OF THESIS

Investigation of Mesoscale Surface Pressure and Temperature Features Associated with Bow Echoes

This study examines surface features, specifically the pressure and temperature fields, associated with bow echoes occurring over Oklahoma from 2002 to 2005. Two-km WSI NOWrad data are utilized to identify bow echo cases during this period; 36 such cases are found. Cases are then classified by their appearance when mature and by their type of initiation.

The majority of bow echoes over Oklahoma in this study move in conjunction with the typical upper-level "steering" winds; generally southwest-to-northeast or southeast-to-northwest motion is observed. Additionally, there is a seasonal variability related to instability and dynamics apparent among these cases. Bow echoes such as bowing segments of a squall line tend to form in the fall, in environments of stronger shear and synoptic forcing with less instability. Less-organized bow echoes prefer formation in the summer, with higher instability and less dynamic support.

Oklahoma Mesonet data from the 2002-2005 period are used to examine surface patterns associated with the bow echo cases. The data are temporally filtered to remove synoptic signals, and a time-space transformation is performed to enhance the horizontal structure. Distinct surface pressure and temperature features associated with squall lines, the mesohigh and cold pool, are found to accompany bow echoes.

A commonly occurring surface pressure pattern preceding bowing is identified. Prior to new bowing development, the mesohigh surges ahead of the convective line,

while the cold pool remains centered behind it. Approximately 30 minutes later, a new bowing segment forms with its apex slightly to the left of the mesohigh surge. The cold pool follows the convective line as it bows. This process is termed the "pressure surge - new bowing" relationship, and a conceptual model is presented.

In one representative case, the surface signatures of the gravity waves generated by deep heating within the convective line, and shallow low-level cooling from the convective line and stratiform region, are tracked. From the calculated speed of the second wave, it is evident that the depth of cooling needed is larger than observed in previous studies of squall line MCSs. It is possible that a sudden influx of low-level cold air prior to new bowing causes a rapid increase in the overall depth of cooling in the system. This increase in depth results in a much faster gravity wave, which surges ahead of the convective line and is reflected in the mesohigh surge. The convective line and cold pool follow, forming the new bowing segment.

Rebecca Denise Adams Selin
Department of Atmospheric Science
Colorado State University
Fort Collins, Colorado 80523
Spring 2008

Acknowledgements

This research was supported by National Science Foundation Grant ATM-0500061, and a one-year American Meteorological Society Graduate Fellowship. The WSI NOWrad data was provided courtesy of the Mesoscale and Microscale Meteorology Division of the University Corporation for Atmospheric Research (UCAR). Many thanks go to David Ahijevych, for assistance in obtaining and decoding the radar data.

The members of my graduate committee, Drs. Steven Rutledge and Bogusz Bienkiewicz, have both contributed constructive feedback and helpful comments on this work. I would particularly like to thank my advisor, Dr. Richard Johnson, who has not only provided invaluable insight during the entire research process, but has also been very accommodating and flexible throughout various unforeseen circumstances.

I am very appreciative of assistance received from Paul Ciesielski and Rick Taft in coding the objective analysis of the Oklahoma Mesonet data, and Dan Lindsey in downloading and viewing radar data using the Advanced Weather Interactive Processing System (AWIPS). Dr. Pat Haertel also provided aid with the timeseries filtering process. The other members of the Johnson research group, especially Elinor Martin and Gail Cordova, have contributed very worthwhile feedback and support along the way. Thanks also go to my colleagues at the Air Force Weather Agency, particularly David Keller, for investing time and energy in proofreading this work. Finally, I would like to thank my family and my fiancé, without whose answered prayers and unending support I would have neither sanity nor finished thesis.

Contents

List of Figures

List of Tables

Chapter 1

Introduction

The type of severe storm labeled a "bow echo" has been recognized as a source of severe winds and strong downbursts ever since 1978, when T.T. Fujita first assigned the name to all curved, quasi-linear convective systems. The bow echo's association with severe winds has been both well-studied and well-documented, from Fujita's original work (Fujita 1978) to the present (Johnson & Hamilton 1988; Houze et al. 1989; Evans & Doswell 2001; Klimowski et al. 2003). However, very little work has focused on surface features, such as pressure and temperature, associated with these storms. While the arrangement of these parameters as associated with squall lines has become highly recognizable (including the mesohigh, cold pool, and wake low; Johnson & Hamilton 1988, Loehrer & Johnson 1995), it is still uncertain how strictly these patterns can be applied to the smaller-sized members of the broad class of Mesoscale Convective Systems (MCSs). This could partly be because until recently, surface observing networks have not been dense enough to capture patterns associated with such small-scale features. However, the Oklahoma Mesonet, established in 1994, now provides observations on incredibly detailed spatial and temporal scales (every 5 min and approximately 50 km). A study which utilizes this data to survey mesoscale pressure features associated with bow echoes would fill a gap in the current research, as well as extend the knowledge base for forecasters regarding these storms.

Additionally, while the term bow echo is frequently seen in the literature, its definition is not as readily apparent. As per the glossary of the American Meteorological Society, a bow echo is defined as "a bow-shaped line of convective cells that [are] often associated with swaths of damaging straight-line winds and small tornadoes...[and] have been observed with scales between 20 and 200 km, and often have lifetimes between 3 and 6 h." Other structural features mentioned as frequently (but not always) appearing in concert within the system include a rear-inflow jet and book-end vortices (American Meteorological Society 2000). It should be noted that neither the length nor time scale is given as an absolute; even Fujita's seminal conceptual model (Fujita 1978) included neither probable distances nor times. Furthermore, many of these structural features mentioned are also seen with larger MCSs, such as squall lines. This essentially results in the only delimiter between squall lines and bow echoes being an arbitrarily selected size limit. If a study of surface patterns associated with bow echoes were to reveal key differences between these patterns and those linked with squall lines, then a possible dynamic distinction between the two could be made.

Finally, it would be extremely helpful to those attempting to issue warnings for severe wind events if there was a common surface pattern which preceded development of a new bow (and therefore generally also development of stronger straight-line winds) from a previously non-curved convective line. While there have been a few features already noted in the literature which often precede bowing, such as a rear-inflow notch (Przybylinski and Gery 1983), appearance of these features does not guarantee new bowing. In addition, with this dense a mesoanalysis, perhaps clues can be gathered regarding the dynamic structure of the system as new bowing is initiated.

A review of the current literature, focusing on both bow echoes and squall lines, is considered in Chapter 2. Squall lines are included as most research has focused on the evolution and dynamics of these larger MCSs, as opposed to bow echoes. Moreover

it is likely that many of these features will also be applicable to bow echoes. Chapter 3 describes the procedures employed to complete the radar review, create the bow echo dataset, and produce the mesoanalysis. Utilizing the Oklahoma Mesonet and the Weather Services International (WSI) NOWrad 2 km composite radar archive, a dataset of surface features associated with 36 different bow echoes in Oklahoma over the four year period of 2002 through 2005 was generated. Climatological statistics of the cases in this dataset are reviewed in Chapter 4. These mesoanalyses were then examined for common patterns of behavior in the surface pressure and temperature fields at times of new bowing, and to further determine if there are patterns that are unique to these phenomena as opposed to squall lines. These results, as well as the distinctive behavior which was indeed observed, will be presented in Chapter 5. Finally, a possible dynamical explanation for this behavior will be discussed in Chapter 6.

Chapter 2

Literature Review

2.1 Bow echo definition and classification scheme development

2.1.1 Original definition and radar structure

The bow echo was first identified by Fujita, who utilitzed radar data from project NIMROD to create a conceptual model of what he would later theorize to be a downburst-driven phenomenon (Fujita 1978). His original figure is reproduced below (Fig. 2.1): important points include the downburst and associated severe winds which occur with it primarily at the apex of the bow, and cyclonic and anticyclonic rotation at opposite ends. The system would begin in a linear shape before a bulge, coupled with a strong downburst, would move quickly ahead of the rest of the line, creating the aforementioned bow shape. In this paper, Fujita suggested the bowing of the linear system was the causative factor for the downburst winds. He reversed his position a year later, finding the bow in the convective line was instead produced by the downburst (Fujita 1979). Fujita then suggested that after the downburst-induced outflow moved ahead of the system, its left (that is, left of the direction of echo motion) end would begin to develop cyclonic rotation, which would continue to intensify as the system itself weakened. Other authors (Weisman 1993; Weisman 1992) would later note that this cyclonic rotation usually appeared as part of a couplet, with anticyclonic rotation forming on the right end. This arrangement of the vortex couplet

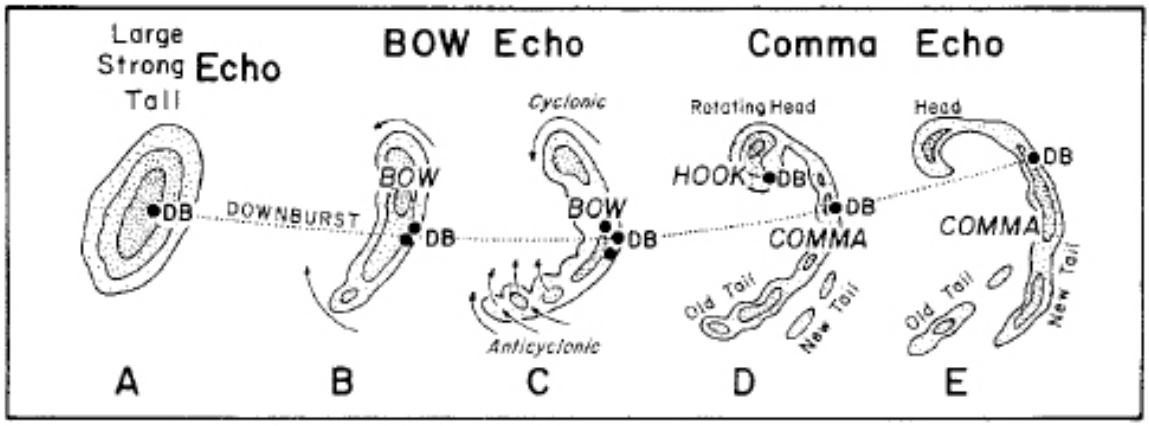

Figure 2.1: Bow echo conceptual model from Fujita (1978). 'DB' corresponds to downburst.

would earn the name "bookend vortices" (Weisman 1993). The cyclonic member often would develop a much stronger circulation (discussed further in Section 2.3.2) than the anticyclonic, even to the point of the anticyclonic vortex not being visible on radar. This is most likely why Fujita (1978) only included a cyclonic vortex in the "comma-head" stage of his bow echo conceptual model.

The question of the origins of the downburst at the apex of the system appeared to be one of the keys to predicting the severe winds so often associated with these systems. Przybylinski and Gery (1983) were among the first to note that this downburst was also accompanied by a "weak echo channel", or small region of lower reflectivity, on the back side of the system. While this channel was not found to necessarily be a precursor to the downburst reaching the surface, it was at least indicative of the presence of such a downburst.

2.1.2 Bow echo taxonomy

While Fujita was the first to recognize that these bow-shaped echoes required a separate classification from other convective types, he left the exact definition of such a feature, including its length scale, fairly open-ended, focusing solely on its curved appearance on radar. Several studies (Przybylinski 1995; Klimowski et al. 2000;

Burke and Schultz 2004; Klimowski et al. 2004) have attempted either to give a more delineated definition, to create further subcategories based on type of initiation and mature appearance, or both. However, these studies have also served to prove that not only were such tasks extremely difficult, but that bow echoes themselves are widely varying structures. Przybylinski (1995) did not attempt to define a bow echo, but instead focused solely on derechoes, a well-defined related set of long-lived, severe-wind producing systems (which, though not by definition a bow echo, often includes a large number of them). They found four separate groups of echo types, labeled Type 1 to Type 4, defined exclusively using radar data. These varied from a longer (up to 100 km) squall-line feature with smaller bowing regions (Type 1), to a isolated supercell which evolved into a bow (Type 4, no scale specified).

Klimowski et al. (2000) and Klimowski et al. (2004) (hereafter, K00 and K04) did craft a specific definition. They utilized Fujita's original identification to require "a bow or crescent-shaped radar echo with a tight reflectivity gradient on the convex (leading) edge" which must be nontransient (Klimowski et al. 2000). However, Fujita's conceptual model also included an associated downburst, which can be difficult to identify solely by radar. Thus, K00 incorporated that the echo must appear to be "outflow dominated"; in other words the radius of curvature of the bow must get smaller with time. Finally, the motion of the bow must not exactly correspond to the mean tropospheric steering flow. This definition has been utilized by both Burke and Schultz (2004) and Klimowski et al. (2003) to create their bow echo data sets for their respective climatologies, and by K04 for their classification scheme, all with success.

K04's classification scheme found four groups of echo types, some of which overlapped with Przybylinski's (1995). These four types were the Classic Bow Echo, Bow Echo Complex, Cell Bow Echo, and Squall Line Bow Echo, and are exhibited in Fig. 2.2. The Classic Bow Echoes were those which appeared most like Fujita's 1978

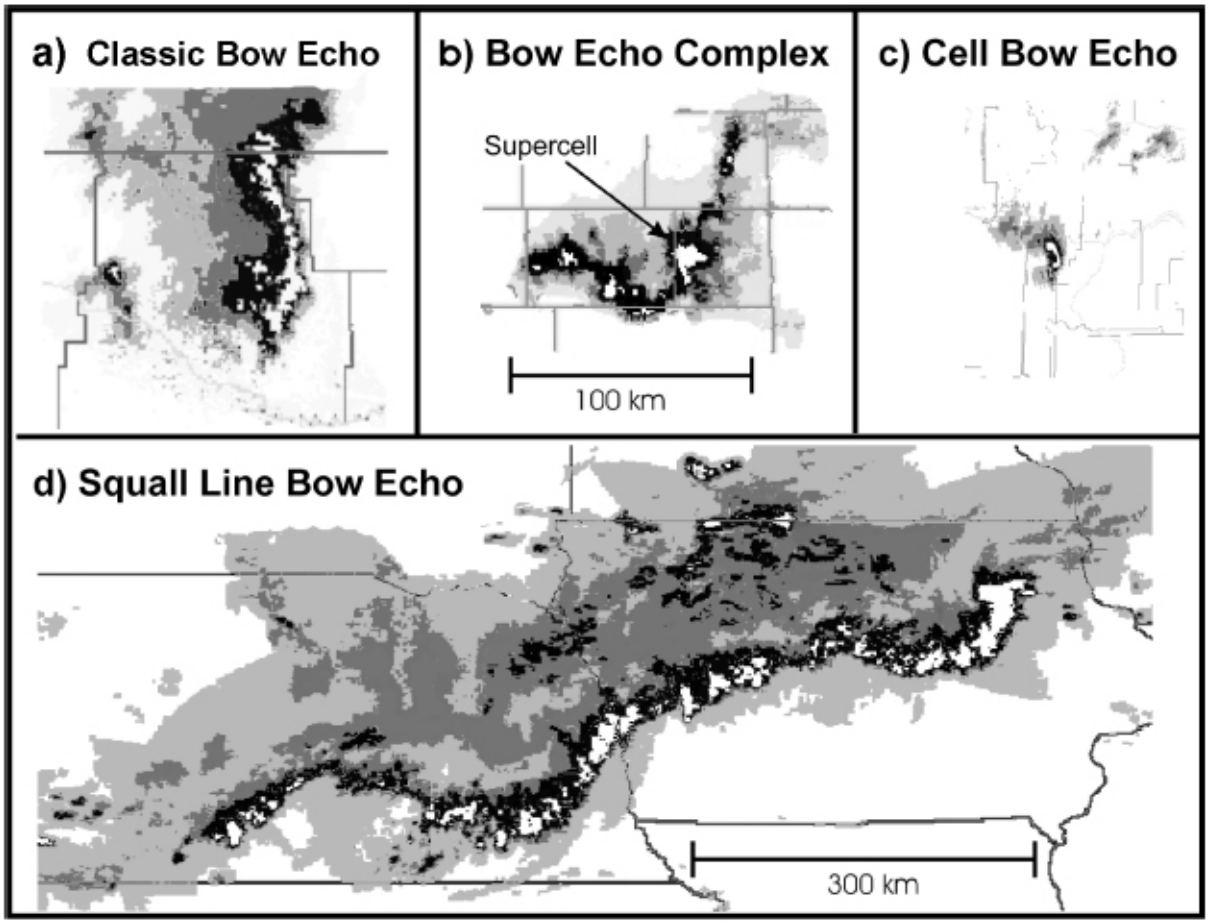

Figure 2.2: Schematic presentation of the four types of bow echoes, as identified by Klimowski et al. (2004): (a) classic bow echo, (b) bow echo complex, (c) cell bow echo, (d) squall line bow echo. Descriptions are given in the text.

conceptual model; they were of a length scale larger than an original thunderstorm and smaller than a squall line, and were generally isolated from other convection. The Bow Echo Complex had a convective line which incorporated other convective types. A Cell Bow Echo was just as its name described, a strong thunderstorm cell (usually a supercell) which had bowed out (similar to Przybylinski (1995)'s Type 4). This was described on scale with or slightly larger than a single thunderstorm (10-25 km). And last, the Squall Line Bow Echo, much like Przybylinski (1995)'s Type 1, has smaller

bowing segments within a longer squall line. K04 were the first to further categorize by type of initiation, breaking the echoes down into those which began as weakly organized cells, a squall line, and a supercell (these will be discussed further in Chapter 3). This classification system, by both lifecycle behavior and initiation type, appears to be the most intuitive thus far, and has the strongest dynamic underpinning in the reasoning for its category division.

2.2 MCS radar-observed lifecycle evolution

Most of the research on system lifecycle evolution has focused not just on the specific organization of bow echoes, but instead on the organization of Mesoscale Convective Systems (or MCSs). While these do include bow echoes, studies have mainly concetrated on the larger scales in the spectrum of MCSs, such as squall lines. However, a review of these features will still be instructive, as it is probable that they apply at least in part to the smaller-scaled bow echoes as well. A typical squall line consists of a convective line and an associated region of stratiform precipitation which may be in front (leading), behind (trailing), or parallel (Parker and Johnson 2000; Houze et al. 1989). The remainder of this review will focus on the trailing stratiform cases, as not only are those the most commonly studied and understood, but that is also where the stratiform region is almost always found with the bow echoes examined in this study. A conceptual model depicting the trailing stratiform MCS composition and lifecycle evolution is displayed in Fig. 2.3.

The squall line consists of two primary regimes of flow, as can be seen in Fig. 2.4. Front-to-rear flow originates as inflow ahead of the storm, which flows into the intense updraft on the leading edge of the convective line, and eventually extends over the stratiform region to the rear (Smull and Houze 1985). It carries with it ice particles from the convective region to the stratiform, which are able to be spread farther behind the convective line due to the slower rate at which they fall out of the flow

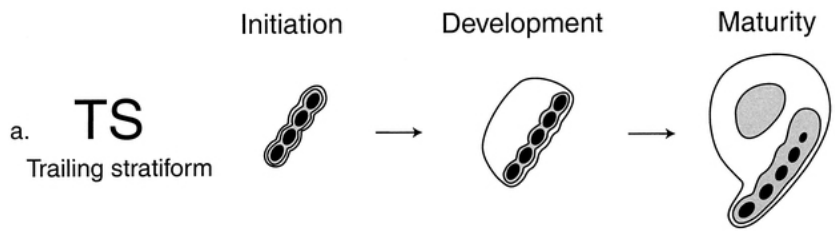

Figure 2.3: Archetypical evolution of a leading convective line, trailing stratiform MCS. Revised from Parker and Johnson (2000).

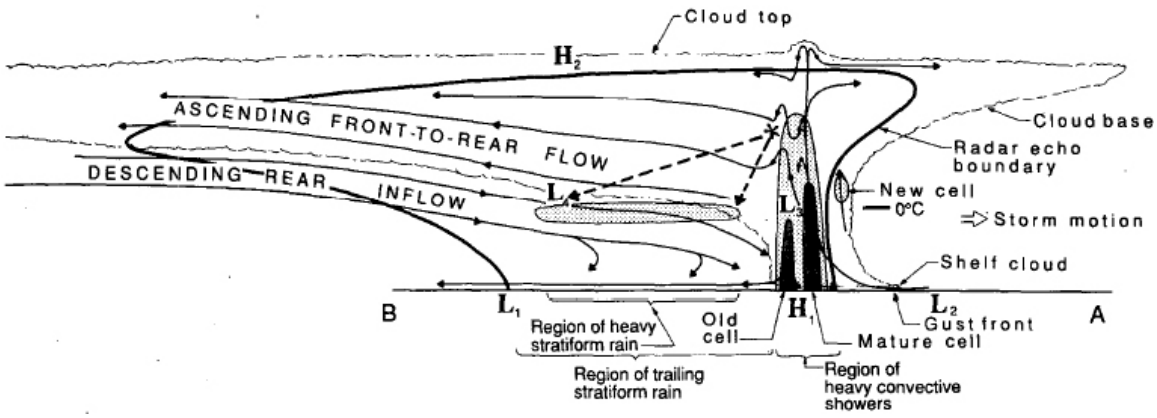

Figure 2.4: Conceptual model of flows in a squall line MCS with trailing stratiform region. The convective line is positioned perpendicularly to the viewed plane. From Houze et al. (1989).

(Fovell and Ogura 1988; Gallus 1996). These hydrometeors, along with other liquid moisture carried backward by the same current, create the stratiform precipitation region. Rear-to-front flow begins in the mid-levels, behind the stratiform area. Drier, higher-momentum air is funneled into the back of the system, creating a rear-inflow notch in the radar returns at the back of the stratiform area (Smull and Houze 1985; Przybylinski and Gery 1983). Later discussion in Section 2.3 will look at explanations for what has now become known as the rear inflow jet. This jet contributes to the rear-to-front outflow at the surface of the leading edge of the system.

Over the lifetime of the system, the trailing stratiform region drifts from being symmetrically placed behind the convective line, to being asymmetrically arranged behind its left end as shown in Fig. 2.3 (Houze et al 1989; Loehrer and Johnson 1995;

Hilgendorf and Johnson 1998). Meanwhile, cells on the right end of the convective line become stronger than those on the left. A study by Skamarock et al. (1994) provided three-dimensional model simulations of these systems with and without inclusion of the Coriolis force; those MCSs with Coriolis evolved from the symmetric to asymmetric mode over a period of about 6 hours, while those without remained symmetric. Skamarock et al. (1994) theorized that, if the front-to-rear and rear-to-front flows are maintained over a suitable period of time for the Coriolis force to act, each will be turned to the right. Thus, the front-to-rear flow, which provides the nuclei and moisture for the stratiform region, would be redirected to its right (or the left end of the convective line). Meanwhile the rear-to-front flow, which serves as the impetus for the initial lifting for the convection, would focus on the right edge of the line, strengthening the convection there. However, Hilgendorf and Johnson (1998) noted that the mean flow in which these systems developed typically had a large southerly component. As these systems were also characteristically aligned north-south, the repositioning of the stratiform region could partly be a result of advection by the mean flow.

These flow structures also have tendencies to create warm and cold pools of air at or near the surface. The cold pool is generated by evaporation and melting/sublimation of liquid and frozen precipitation in the downdrafts of the convective line (Fujita 1959), and stretches from the leading edge of that line well back into the stratiform region. This region of colder air was found to play a large role in the longevity of the system, and will be discussed in the next section. Given the correct conditions, a region of warmer air can be found behind the cold pool just above the surface, at the back edge of the stratiform region. The method of production of this warm region was for a time under some debate, as will be seen in Section 2.4.

2.3 Bow echo dynamics

2.3.1 Interplay between vorticity production by cold pool and shear

As has already been noted, many of the theories which have been created for the larger-scaled MCSs, such as squall lines, could also be applicable to their smaller-scaled brethren, such as bow echoes. Thus, a description of the theory developed by Rotunno et al. (1988) (hereafter, RKW) for long-lived squall lines would not be out of place, especially as that same theory was also used by Weisman (1993) to discuss long-lived bow echoes. The essential premise behind this RKW theory is the balance of the vorticity associated with the surface cold pool with that from the environmental low-level shear. Since RKW considered the squall line as a two-dimensional feature, then the horizontal vorticity (η) equation for a north-to-south oriented line could be reduced to:

$$\eta = \frac{\partial u}{\partial z} - \frac{\partial w}{\partial x}. \tag{2.1}$$

As defined in RKW, u and x were velocity and distance perpendicular to the convective line, respectively; and w and z were vertical velocity and distance (or height). Essentially, then, in Eq. 2.1 the only factors contributing to horizontal vorticity would be the horizontal changes in buoyancy in the x direction (which would affect vertical motion, $\frac{\partial w}{\partial x}$), or change in line-perpendicular wind speed with height ($\frac{\partial u}{\partial z}$). At the right edge of the cold pool produced by the system, as displayed in Fig. 2.5b, the $\frac{\partial w}{\partial x}$ term would be positive, resulting in negative horizontal vorticity. On the other hand, these systems almost always develop in sheared environments where the low-level shear vector has a component pointing perpendicularly away from the system, meaning $\frac{\partial u}{\partial z}$ would be positive, and thus would create positive vorticity. Overall, the updraft would tilt upshear or downshear accordingly depending on which vorticity source, shear or cold pool, was stronger, like in Figs. 2.5a,c. The ideal situation

would be one where the two were balanced over the lower levels, allowing for an upright updraft with its stronger lifting, as displayed in Fig. 2.5b. Over time, cold air production by the system would create a cold pool that would be simply too strong for the ambient low-level shear, and thus the system would tip backward over the cold pool and ultimately die.

This theory was later applied to bow echoes in Weisman (1992, 1993). As explained by Weisman, the convective line would begin by being tilted downshear, as it had not yet time to produce a cold pool (Fig. 2.5a). The vorticity supplied by the horizontal buoyancy gradients in the cold pool would then begin to balance the ambient low-level shear, until eventually the updraft would be upright (Fig. 2.5b). As the system would continue to strengthen, so would the cold pool, until it would overwhelm the vorticity provided by the low-level shear; the system then would lean upshear over the cold pool (Fig. 2.5c). This would create a strong gradient in buoyancy where the updraft air, heated by latent heat release, would overtop the dense cold pool. This arrangement could then generate its own vorticity, which would act in concert with the circulation from the rear edge of the cold pool to strengthen any rear inflow into the storm, also depicted in (c). This inflow could be further concentrated, up to 30-50% (Weisman 1993), by the cyclonic/anticyclonic vortex couplet found at the ends of bow echo systems. The elevated rear inflow jet combined with the shear would be able to balance the vorticity created by the cold pool, letting the updraft remain erect and permitting deep lifting (d). Occasionally, since the rear inflow jet would be feeding cooler, mid-level air directly into the surface cold pool, the cold pool would strengthen to such an extent that the system would be briefly tipped upshear. The inflow jet would be able to more directly transport higher momentum air to the surface, leading to damaging downbursts, before providing enough vorticity to tip the updraft upright again.

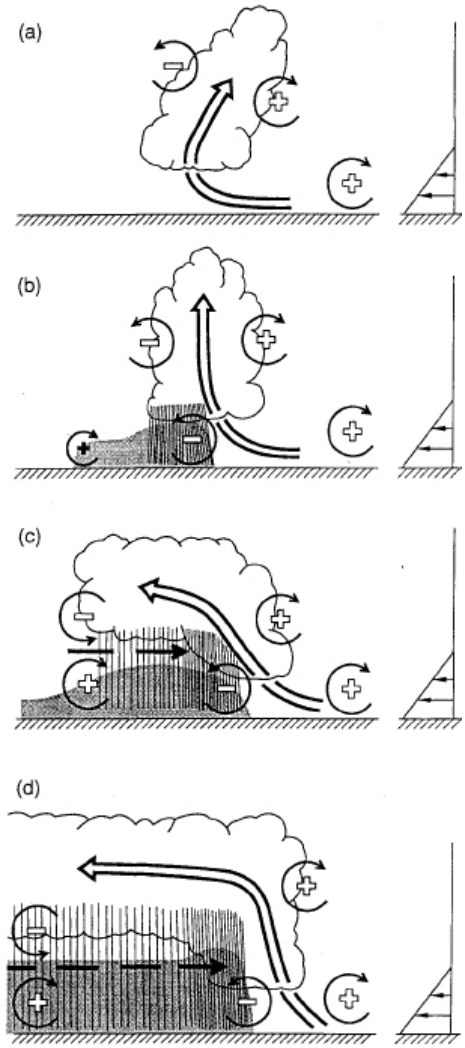

Figure 2.5: Representation of the interplay between vorticity produced by the cold pool, environmental shear, and the rear inflow jet. Thin circular arrows depict positive and negative vorticity, while the wide arrow displays the major flow fields in the bow echo. Note that the low-level shear vector points perpendicularly away from the system. (a) shows an initial updraft with no downdraft or cold pool; the updraft has been tipped downshear. (b) displays a mature thunderstorm with both cold pool and low-level shear; the two are able to balance so the updraft remains upright. In (c), the cold pool has grown stronger than the ambient shear, slanting the updraft backward overtop it. The resultant buoyancy gradient then would channel the rear inflow jet. (d) shows how the vorticity produced by the cold pool was balanced by that from the elevated rear inflow jet and the ambient shear. From Weisman (1993).

Environmental characteristics, as modeled by Weisman (1992, 1993), played a large role in determining whether the rear inflow jet would remain elevated until almost the convective line before descending sharply to the surface (as depicted in part (d) of Fig. 2.5), or instead gradually slope downward and spread along the surface. With less strong ambient low-level shear and thus an upshear-tilted updraft, parcels would rise more slowly, leaving more time for entrainment to cool the updraft. As a result the buoyancy gradient overlying the cold pool would be weaker, resulting in correspondingly weaker rear inflow. Lower environmental instability values would also denote slower lifting, a warmer cold pool and cooler updraft, and as a consequence a more ineffective horizontal buoyancy gradient. Thus, both higher instability and shear is ideal.

However, a number of observational studies have since been completed which do not confirm the optimal cold pool – low-level shear balance theory expressed by RKW88 and Weisman (1993). Evans and Doswell (2001) and Coniglio et al. (2004) both examined environmental soundings obtained within the proximity of derechos, which as mentioned earlier very often contain one or more bow echoes. In those soundings, almost no correlation between the low-level shear and environmental instability (as measured by CAPE, convective available potential energy) was found. Additionally, many of these systems formed with low-level shear distinctively less than 15 m s^{-1}, the minimum threshold given by RKW as needed to offset the vorticity produced by the cold pool. Neither was there any significant change in the low-level shear over the lifecycle of the system, nor did systems decay when they entered an environment with lesser low-level shear. Evans and Doswell (2001) noted that derecho systems which formed in regions near a strong synoptic system could often initiate and be quite long lived in environments which had both little CAPE and low-level shear. Strong shear was instead found over a deeper layer, from 0-5 km according to Evans and Doswell (2001), or even as high as 5-10 km, noted in Coniglio et al. (2004). Both

studies suggested this deeper shear value might be more useful for forecasting the formation and longevity of derecho systems, particularly in strongly forced synoptic environments. However, Evans and Doswell (2001) did observe a decrease in mid-level storm relative winds (along with a corresponding increase at the low levels, thereby indicating stronger low-level shear) that was distinctively more pronounced in weakly forced derechos. Thus it is possible that the theories developed by RKW and Weisman (1993) are indeed valid, but only for a subset of the bow echo population. In any case, while these theories should be viewed as instructional, it should be noted that they have not been fully borne out by observational evidence.

2.3.2 Vortex development

Mid-level vortex couplet

In the previous section, the role of the bow echo mid-level vortex couplet in forming the rear inflow jet was mentioned. The origination of this vortex couplet itself has been suggested to be dependent on the cold pool-shear dynamical balance discussed above (Weisman and Davis 1998). At first, it was thought by Weisman (1993) that the positive vorticity created by the westerly low-level shear was tilted vertically by the updraft of the convective line, and then retilted back downward by the downdraft (Fig. 2.6b), creating the north-south cyclonic-anticyclonic couplet so often seen. This theory was then restructured in Weisman and Davis (1998). There, they suggested that the downward tilting of environmental low-level shear was primarily responsible for the lower-level meso-γ vortices (considered in the next section). The larger, mid-level bookend vortices instead appeared to be a product of upward tilting of negative vorticity from the cold pool edge, by the updraft alone (Fig. 2.6a). However, it is also possible that these bookend vorticies form simply by shearing effects at the end of the convective line (Weisman 1993). The cyclonic vortex was found, however, to often be much stronger than the associated anticyclonic member. Weisman and Davis (1998)

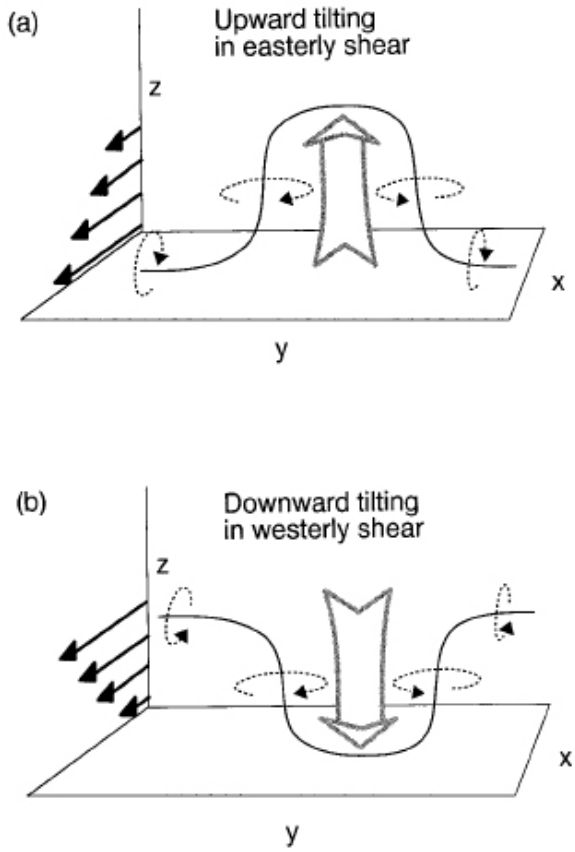

Figure 2.6: Archetypes of vertically tilted horizontal vorticity, shown in the dotted arrows. Schematic (a) shows negative vorticity, such as from a cold pool tilted upward; (b) shows postive vorticity, such as from the ambient shear, tilted downward. Note that each produces the same vortex couplet. From Weisman and Davis (1998).

determined that stretching of planetary vorticity in the updraft could supplement this vortex; this same mechanism would act to reduce the circulation of the anticyclonic vortex, explaining its infrequent appearance on radar.

Low-level meso-γ vortices

Previous theories for the causes of the severe winds typically associated with bow echoes have attributed them to surface manifestations of the rear-inflow jet (Fujita (1978), Weisman (1992), Weisman (1993)). However, Weisman and Trapp (2003) and Trapp and Weisman (2003) utilized a three-dimensional modeling study to suggest a new paradigm for severe wind generation. They noted that within damage

surveys of bow echoes, often a pattern would be found of smaller, more intense damage among a larger swath of somewhat lesser damage; additionally, these more severe pockets would almost always be located to the north of where the radar placed the apex of the bow echo at that time. It had already been theorized that there were smaller, meso-γ scale (2-40 km) vortices embedded in the convective line at low-levels that were responisble for these stronger winds, while the previously conjectured rear inflow jet caused the wider, less severe damage. The existence of such meso-γ scale vortices were noted in numerous observational studies of bow echoes, such as Funk et al. (2003) DeWald and Funk (2000), and Miller and Johns (2000). These smaller vortices were separate and unique from the larger, mid-level bookend vortices in both structure and formation, although Weisman and Trapp (2003) did suggest that through stretching one of the small vortices could build upward and become a mid-level vortex. It should be noted that these meso-γ vortices are on a much smaller length scale (2-40 km) than both the bow echoes they are associated with, and the pressure and temperature perturbations discussed in Chapter 5. While bow echo pressure and temperature perturbations are not directly related to the small vortices, a discussion of them would still be relevant in order to fully examine all processes within bow echoes which can contribute to extreme winds.

Through their idealized simulations, Trapp and Weisman (2003) (hereafter TW03) thought these low-level vortices were formed by the the tilting in a downdraft of horizontal, baroclinically-generated vorticity. This process is shown schematically in Fig. 2.7. Essentially, the horizontal variations in buoyancy across the leading edge of the cold pool, as previously mentioned in Section 2.3.1, would form a band of crosswise vorticity (that is, parallel to the convective line and perpendicular to the storm-relative inflow). This vorticity would then be tilted by a localized downdraft of cold outflow at the front periphery of the system, creating a small-scale vortex couplet. The enhancement of the cyclonic vortex from stretching of planetary vorticity would cause

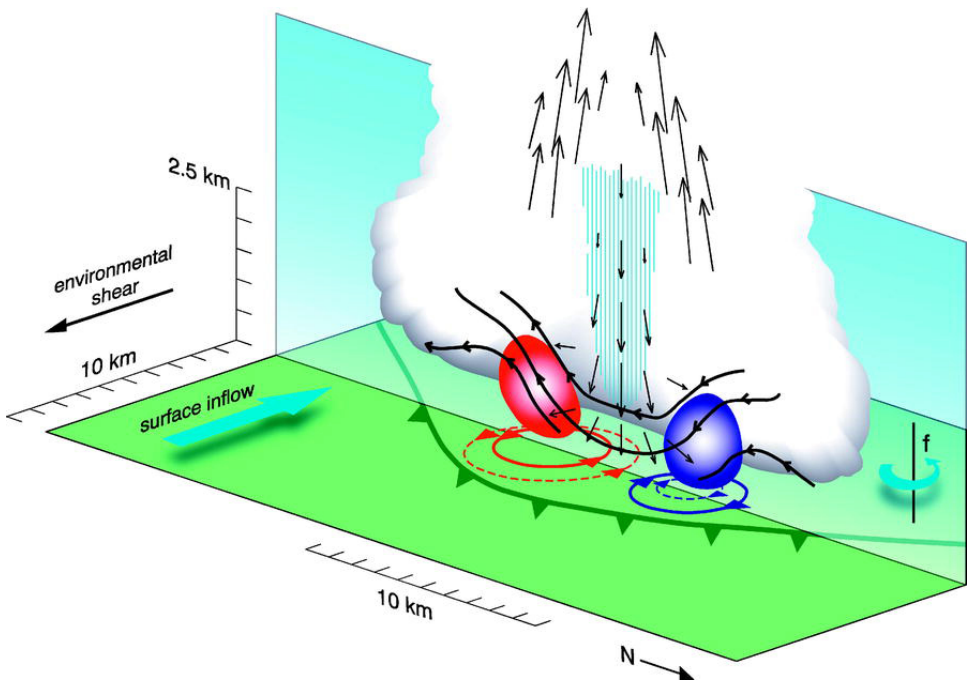

Figure 2.7: Conceptual model of the downward tilting of crosswise, horizontal, baroclincally generated low-level vorticity. The resultant vortex couplet is depicted in the red and blue bubbles, for the cyclonic and anticyclonic members, respectively. Eventually the cyclonic vortex is enhanced through stretching of planetary vorticity; this is shown beneath in the red and blue circulations. From Trapp and Weisman (2003).

it to expand, and the anticyclonic portion of the couplet to fade away. The cyclonic vortex, by virtue of the fluid shear terms in the pressure perturbation equation, would induce lower pressure in its center. This lowered pressure would generate a downward-directed pressure gradient force, which would enhance the surface outflow at that point. Hence, according to TW03, sections of stronger winds would be found centered within the smaller-scale low-level cyclonic circulation.

However, Wakimoto's (2006a,b) detailed case study of an Omaha, NE bow echo which occurred during BAMEX (Bow Echo and Mesoscale Convective Vortex Experiment) found that the area of strongest winds actually corresponded to a region within the right side of the low-level cyclonic vortex (Wakimoto et al. 2006a). In their examination of the lower-levels of the system, while there was a perturbation pressure gradient associated with each mesovortex, air parcels did not accelerate di-

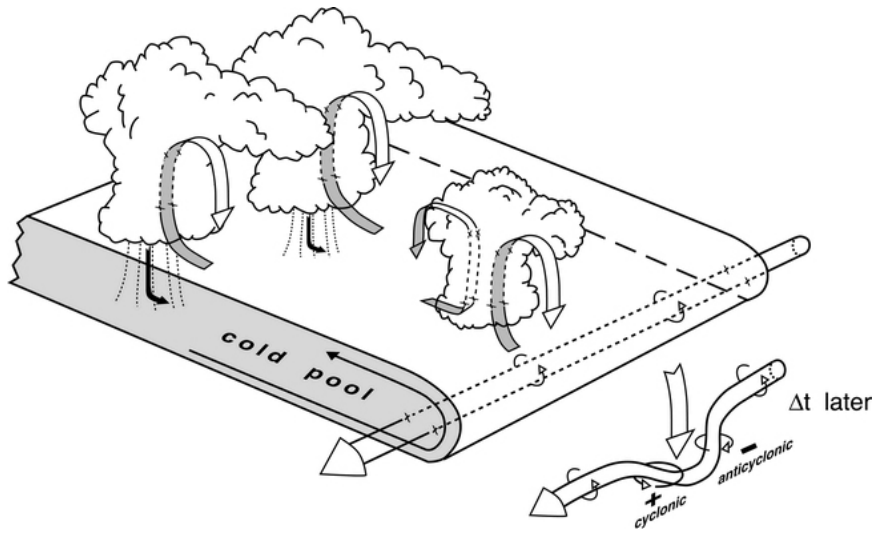

Figure 2.8: Figure from Wakimoto et al. (2006b) detailing the source of the downdraft which would affect the baroclinically-generated vorticity at the leading edge of the cold pool; note that the cell just formed is not yet mature enough to have a rain-filled downdraft. The stretched vortex tube in the bottom right shows how the couplet is produced over time δt.

rectly along this gradient from high to low pressure. If they had, as expected from Trapp and Weisman (2003), the strongest winds would have been found at the end of this acceleration, in the center of the cyclonic vortex. Instead, the pressure gradient mainly acted to increase the rotation speed about the vortex. The strongest surface winds fit with the part of the vortex where its rotation, plus the storm motion, would combine most effectively. In other words, if one considers the storm motion vector to be straight ahead, then the right side of a cyclonic rotation would produce the strongest winds.

Wakimoto et al. (2006b) suggested another change in TW03's mesovortex production model. TW03 would require a downdraft to tilt the vorticity produced by the cold pool at the leading edge of the storm. They suggested this downdraft had been created by air cooled from evaporation of rainfall. Yet, thunderstorm cells at the leading edge of the cold pool are in their initial state and have not yet had time to develop a rain-induced downdraft that would reach the surface. Thus, Wakimoto et al. proposed that this downdraft was instead dynamically generated in order to

balance the convective updraft, as displayed in Fig. 2.8. However, both TW03 and Wakimoto et al. agreed that these mesovortices were only present in bow echoes in environments of strong low-level shear. Those which developed in weaker low-level shear had wider, more uniform damage swaths, fitting with winds produced by a rear inflow jet.

2.4 Description of mesohighs and wake lows

2.4.1 Overview

The association of surface mesoscale high pressure regions with convection was first noted back in 1949, during the summary report of the Thunderstorm Project by Byers and Braham (1949). Fujita was then the first to provide a conceptual model of the positioning of the mesohigh (which he termed a "thunderstorm high") within a squall line complex; he added a mesoscale low pressure region in the wake behind the mesohigh, which he called the "wake depression" (Fujita 1955). The mesohigh was located directly beneath the convective line downdraft, as exhibited in Fig. 2.9. Even though many of the following studies have been confined to surface pressure and temperature features associated with squall lines, the current study hopes to explore the similarities between these features and those coupled with bow echoes; therefore it is entirely appropriate to examine these squall line characteristics.

Within the downdraft, precipitation would be evaporating, melting, or sublimating during its descent, cooling the parcel; the mesohigh would then be a hydrostatic manifestation of this denser air (Fujita 1959). Additional nonhyrdrostatic effects, such as the downdraft physically impacting the surface, could also increase the pressure, and will be discussed in 2.4.3. The wake depression (now termed wake low) was placed directly behind the mesohigh. Originally, Fujita thought that this low pressure area was the result of flow blocking by the mesohigh (hence the "wake" terminology), but this would later be shown to not be the case (see Section 2.4.4).

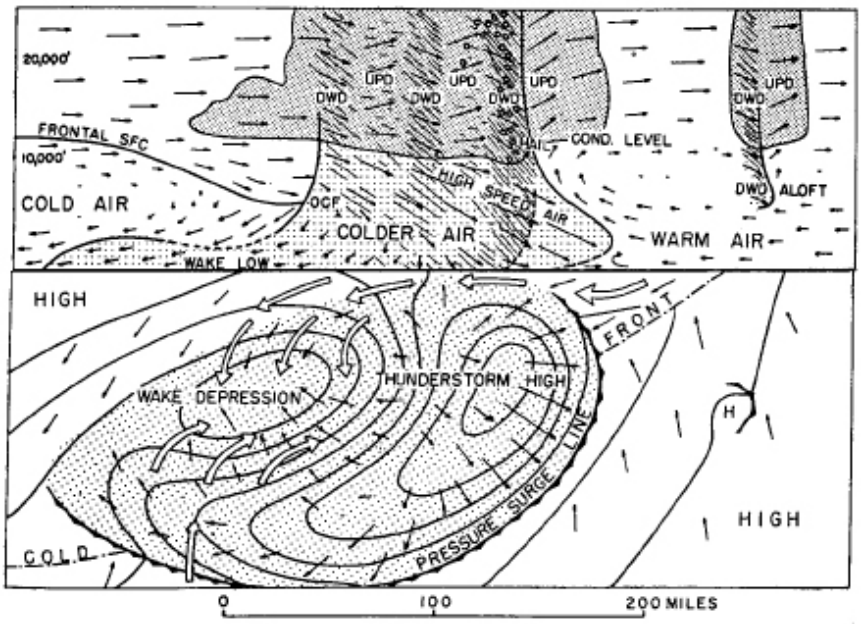

Figure 2.9: Vertical cross-section (top) and horizontal plan view (bottom) of Fujita's original conceptual model of pressure features associated with squall lines. DWD and UPD stand for downdraft and updraft, respectively. From Fujita (1955).

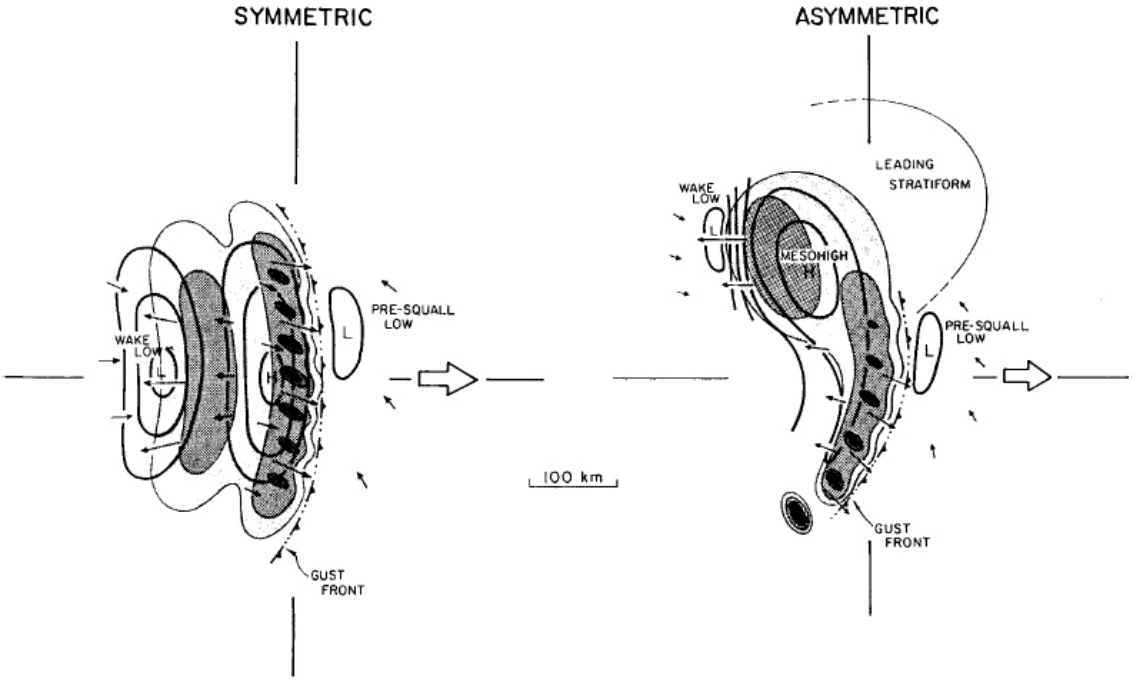

Figure 2.10: Conceptual model of the surface pressure features of a MCS as it evolves from symmetric to asymmetric throughout its lifecycle. Large arrows indicate direction of storm motion; small arrows indicate system-relative winds. The shading corresponds to increasing levels of radar reflectivity, with the heaviest being in the convective line. From Loehrer and Johnson (1995).

Johnson and Hamilton (1988) (hereafter, JH88) also produced an idealized diagram of mesoscale surface pressure features associated with squall line MCSs, slightly modified from Fujita's original model; their figure appeared very similar to Fig. 2.10a. Much like Fujita's model, the mesohigh was located beneath the strongest downdraft and cooling within the system. The wake low was positioned at the back edge of the stratiform precipitation region; the reasoning behind that decision will be elaborated in Section 2.4.4. As was already stated in the section regarding MCS lifecycle evolution, MCSs were shown to evolve from a symmetric to asymmetric structure with time. Loehrer and Johnson (1995) designed a surface pressure conceptual model for asymmetric MCSs. Note the mesohigh and wake low have followed the stratiform precipitation region, hinting at a connection between the three. A new feature introduced by Hoxit et al. (1976) and JH88 was the pre-squall low, a small low pressure region located ahead of the convective line.

Another alteration to Fujita's original model was the relocation of the axes of divergence and convergence. Instead of being centered within the mesohigh and wake low, respectively, they were placed behind them (Johnson and Hamilton 1988; Loehrer and Johnson 1995). JH88 noted that as these pressure features moved with the system (which usually has strong forward motion), surface air parcels were not able to remain within the pressure gradients long enough for the main axes of divergence and convergence to be located directly within the pressure features themselves. Nor were these parcels able to accelerate to the full hurricane force wind speed to which a strong gradient would typically correspond (Vescio and Johnson 1992). As the fastest winds were usually found in the surface outflow at the leading edge of the system, Vescio and Johnson (1992) suggested this was because not only were parcels being accelerated forward by the pressure gradient at that location, but the pressure gradient itself was moving forward with the storm system. Thus, parcels were able to maintain their presence in that gradient longer, and could accelerate more. On

the other hand, parcels traveling through the (often stronger) gradient between the mesohigh and wake low would be accelerated backward, while the gradient was moving forward. Therefore these parcels would have a shorter residence time and could not achieve such high speeds.

2.4.2 Lifecycle as expressed through timeseries

In addition to the evolution of the system as it migrates from symmetric to asymmetric, the surface pressure features also undergo change as the MCS completes its entire lifecycle, from initiation to dissipation. Fujita described this process for squall lines in his 1959 paper using station timeseries traces of surface pressure; his figure is reproduced here as Fig. 2.11. Essentially, a surface pressure trace from a station passed over by the center of the squall line would indicate the time the leading edge of the thunderstorm outflow and mesohigh reached the station with a large jump in pressure, which would then drop down to the following wake low before returning to its original state. He listed five stages: initiation, development, mature, dissipation, and remnant, and illustrated them using these surface pressure traces (corresponding to timeseries one through five in Fig. 2.11). In the initiation and development stages of the squall line, only a mesohigh was present; the wake low would not appear until the storm was fully mature. Then, as the system dissipated, so would the mesohigh, until eventually only a wake low would remain.

Other observational studies - one of a gust front (Wakimoto 1982), and another of a squall line (Johnson and Hamilton 1988) - confirmed that actual timeseries from a station as a mature system passed overhead were in fact very similar to that proposed by Fujita in step 3. Additional information about the spatial arrangement of these surface pressure features could also be gathered from these traces. Evident in the JH88 trace was a dip in pressure corresponding to the wake low occurring at the end of the stratiform rain; this agreed with the conceptual model produced in the same

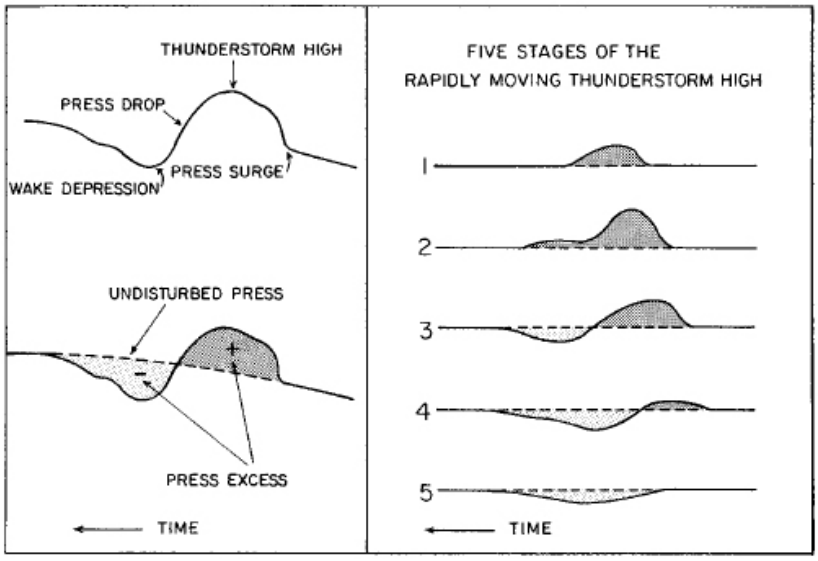

Figure 2.11: Surface pressure traces of Fujita's five identified stages of a squall line, from initiation, development, maturity, dissipation, and remnant (labeled 1 through 5). Time increases to the right. From Fujita (1955).

paper placing the wake low at the back edge of the stratiform rain region. The wind speed peaked at that point as well, which would correspond with JH88's positioning of the rear inflow jet (described later in Section 2.4.4).

2.4.3 The mesohigh

As previously stated the majority of the mesohigh is thought to be hydrostatically induced from cold air, produced by evaporating rainfall (and melting/sublimating frozen precipitation). Additional nonhydrostatic sources could be precipitation loading (that is, the added mass of rain and ice within the downdraft) (Wakimoto 1982), and the dynamic pressure rise as the downdraft impinged upon the ground (Fujita 1955). Wakimoto's idealized trace of surface pressure, windspeed, wind direction, and temperature is displayed in Fig. 2.12. Note that here, the pressure trace actually began to increase before the cold pool passage (evidenced by the temperature starting to drop). This pressure increase was attributed to the nonhydrostatic effect of the cold pool colliding with the air mass ahead of it.

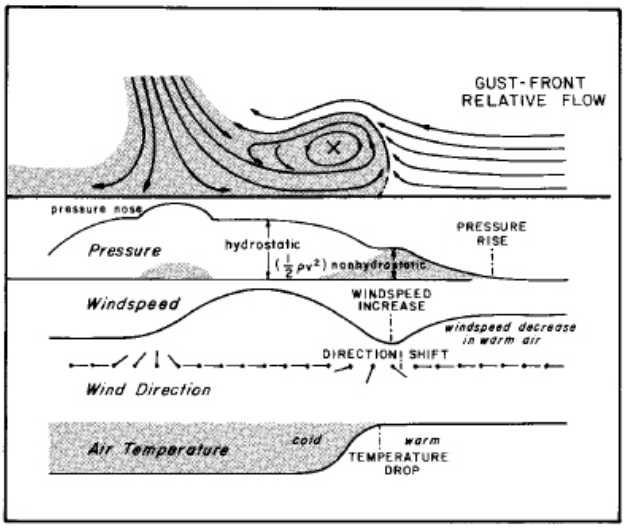

Figure 2.12: Wakimoto's (1982) idealized conceptual model of pressure, wind speed and direction, and air temperature during a mature gust frontal passage. Time increases to the left.

2.4.4 The wake low and rear inflow jet

The reason for the existence of the wake low has been the subject of much debate in the literature. Williams (1963) found that the wake low was hyrdostatically induced by subsidence warming from descending air above it. However, the source of this descent was unknown for quite some time. Ultimately, it was JH88 that proposed the wake low was the "surface manifestation" of the rear inflow jet. This rear inflow would descend as it flowed into the stratiform precipitation region, descending as it went (explanations for its descent are provided later in the section). Within the region itself, evaporation and melting/sublimation of precipitation could help offset the subsidence warming. This would not be the case in back of the stratiform region, and the wake low would be hydrostatically generated by the adiabatically warmed descending air reducing the depth of the cold pool over that point. Figure 2.13 illustrates this process. This would also explain the rear inflow "notch" often seen at the back edge of the stratiform region (Przybylinski and Gery 1983); that would be the mid-level, drier inflow evaporating the precipitation as it descended into that

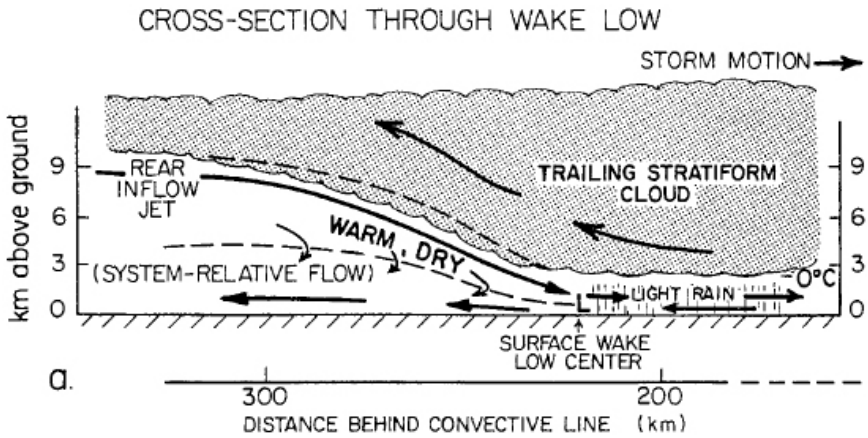

Figure 2.13: Idealized vertical cross-section through the center of a trailing stratiform precipitation region of a squall line. The arrows show streamlines of system-relative flow, and the dashed line indicates where this flow is zero. From Johnson and Hamilton (1988).

region. The subsidence-warmed, descending flow might or might not appear in surface observations, depending on its ability to penetrate through the stable cold pool to reach the surface. To descend that far, it would "overshoot" its level of neutral buoyancy with its high momentum, and would be so strongly adiabatically warmed a heat burst could occur (Johnson 1983). Haertel and Johnson (2000) further updated this idea to indicate that a mesohigh-wake low couplet could form as a result of low-level cooling associated with the stratiform region. The rear inflow jet could then amplify the wake low.

JH88 also suggested that the intensity of the rear inflow jet was proportional to the intensity of the stratiform precipitation directly ahead of it; so the subsidence warming (and therefore intensity of wake low) would be most amplified behind the stongest reflectivity returns in the stratiform region. This was confirmed in an observational study of an MCS with an intense wake low by Stumpf et al. (1991). Incidentally, if the strongest part of the rear inflow jet was located behind the strongest reflectivity and collocated with a reflectivity notch, it would follow that it would also be located behind the strongest gradient in reflectivity; this arrangement was also ob-

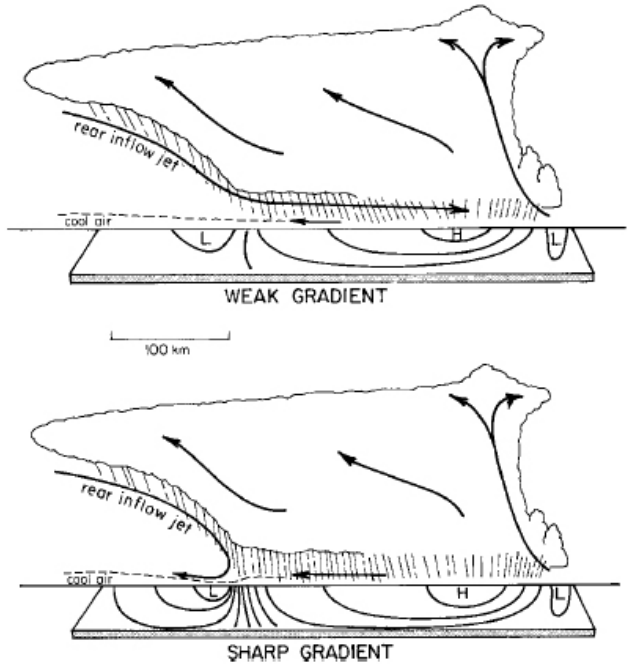

Figure 2.14: Conceptual model showing vertical cross-section through the center of a MCS. The top illustrates a rear inflow jet which descends gradually to the surface through the stratiform region, and results in a weak pressure gradient between the mesohigh and wake low. The bottom shows a rear inflow jet which descends sharply to the surface behind the stratiform region, corresponding to a strong pressure gradient. From Johnson (2001).

served in Stumpf et al. (1991). They found that the rear inflow fully evaporated the lighter precipitation at the back edge of the stratiform region as it descended (also seen in Smull et al. 1991). Additionally, the rear inflow jet was placed not above the wake low, but instead the area of the most rapidly dropping surface pressure. The more quickly the rear inflow would descend, the stronger the gradient between the wake low and mesohigh, and the more intense the wake low. Those MCSs associated with weaker mesohigh-wake low pressure gradients would have a more gradually descending rear inflow jet; both situations are exhibited in Fig. 2.14.

Stumpf et al. (1991) also observed in the asymmetric stage of their MCS that the wake low had remained behind the stratiform region; no low was found behind the portion consisting of just the convective line. Thus, since the descent of the rear inflow jet is reflected on the surface as a wake low, both features are probably coupled

in some way to the region of stratiform precipitation. According to Stensrud et al. (1991) and Gallus and Johnson (1995), the rear inflow was first evaportively cooled by the moisture in the stratiform region, rendering the inflow negatively buoyant. Once all the precipitation in that region was evaporated (or melted/sublimated), the already descending flow would continue to descend through inertia, and would be adiabatically warmed, as already described above. However, microphysical effects alone were not necessarily enough to drive a descent that would create an intense wake low of magnitude corresponding with observations. Gallus (1996) completed a modeling study to examine this question, and found that while the stratiform region was still mature, cooling from the evaporation, melting, and sublimation would indeed begin to induce descent, but would also fully offset all adiabatic warming. Not until the stratiform region began to collapse, eliminating this offset, would the adiabatic warming become strong enough to induce an intense wake low. Thus, as such powerful wake lows often appear in concert with mature stratiform regions, it appears as though there are other mechanisms at least partially responsible for the initial descent of the rear inflow. These will be more fully examined in the discussion about gravity waves in Section 2.5.

2.4.5 The pre-squall mesolow

The method of formation for the pre-squall mesolow was found to be somewhat similar to that of the wake low, in that it is produced by convectively-induced subsidence ahead of the convective line (Hoxit et al. 1976). This subsidence, also like that of the wake low, occurs above the surface feauture, in the mid- and upper-levels. Because there is no strong inflow into this region, the pre-squall mesolow is much weaker than the wake low. Gravity wave dynamics may also play a large role in producing this feature, as will be stated in the next section.

2.5 Gravity currents and waves

2.5.1 Surface cold pool as a gravity current

The movement of the surface cold pool could also be considered as a gravity current. By definition, a gravity current is "a mass of high density fluid, flowing along the horizontal bottom and displacing an ambient fluid of lesser density" (Charba 1974). Charba (1974) was also the first to make this comparison quantitatively: he looked at the similarities in speed between a squall line gust front and laboratory experiments of a gravity current. Utilizing the equation

$$V = k\sqrt{gd\frac{\rho_1 - \rho_2}{\rho_1}} \tag{2.2}$$

for the theorized gravity current speed, they found that the laboratory current and gust front observed speeds were very similar. (Here, d was the mean depth of the cold air, ρ_2 was the density of the cold air, ρ_1 was the density of the environmental air, g was the gravitational constant, and k was chosen to be the square root of the cold air Froude number.) Additionally, the general shape of the gust front cold pool as it flowed was congruous with the laboratory observed shape of a gravity current in motion.

2.5.2 Gravity wave generation and effects

While the cold pool and mesohigh might be looked at as a gravity current, that explanation would not provide for the existence of the pre-squall mesolow or the wake low. Schmidt and Cotton (1990) examined the linear effect of gravity waves generated by convective heating within a simulated squall line, in both the lower and upper troposphere. Their results as depicted in a conceptual model are shown in Fig. 2.15; the three plots illustrate simulations with increasing shear. The updraft was protected from the environmental flow by not only the mass divergence at its top, but

also by the circulation around the upshear upper-level gravity wave (labeled upper left wave, or ULW, on their diagram) blocking the mean flow. With no shear, this feature would propagate away quickly, but as the ambient shear increased the wave stayed closer to its source, the updraft, and provided more efficient blocking allowing the updraft to further strengthen. This circulation also shifted the rear inflow downward and warmed it, helping serve as the impetus for the initial descent of the rear inflow jet. Thus, the height of the stable layer along the surface was reduced and the surface pressure was lowered. The interaction between the upshear upper and lower tropospheric waves (ULW and LLW), both prevented from propagating away by the shear vector, also helped focus the rear inflow by channeling it and thereby increasing its speed. This would further lower the surface pressure beneath this feature, further intensifying the wake low.

Meanwhile, the downshear lower tropospheric wave (lower right wave, or LRW) served as the leading edge of the cold outflow of the squall line, and triggered upward motion along its forward edge. This propagation speed of this feature would decide the overall propagation speed of the entire system; the bottom outgoing portion of its circulation would also provide additional strength to the surface outflow. Note that this entity would be the same as the gravity current described in the previous section, except elevated above the surface. The pervasive environmental stable layer at the surface kept the feature aloft, ensuring a gravity wave.

Nicholls et al. (1991) did a similar simulation with no shear, and looked not just at gravity waves generated by convective heating, but instead those produced by combined heating and cooling profiles. The convective profile of heating throughout the troposphere was incorporated with the stratiform profile of cooling in the lower levels and heating aloft. The gravity wave mode produced by the deeper convective heating moved quickly away from its source, producing a pervasive region of lower pressure surrounding the system. Were this simulation to be repeated with shear,

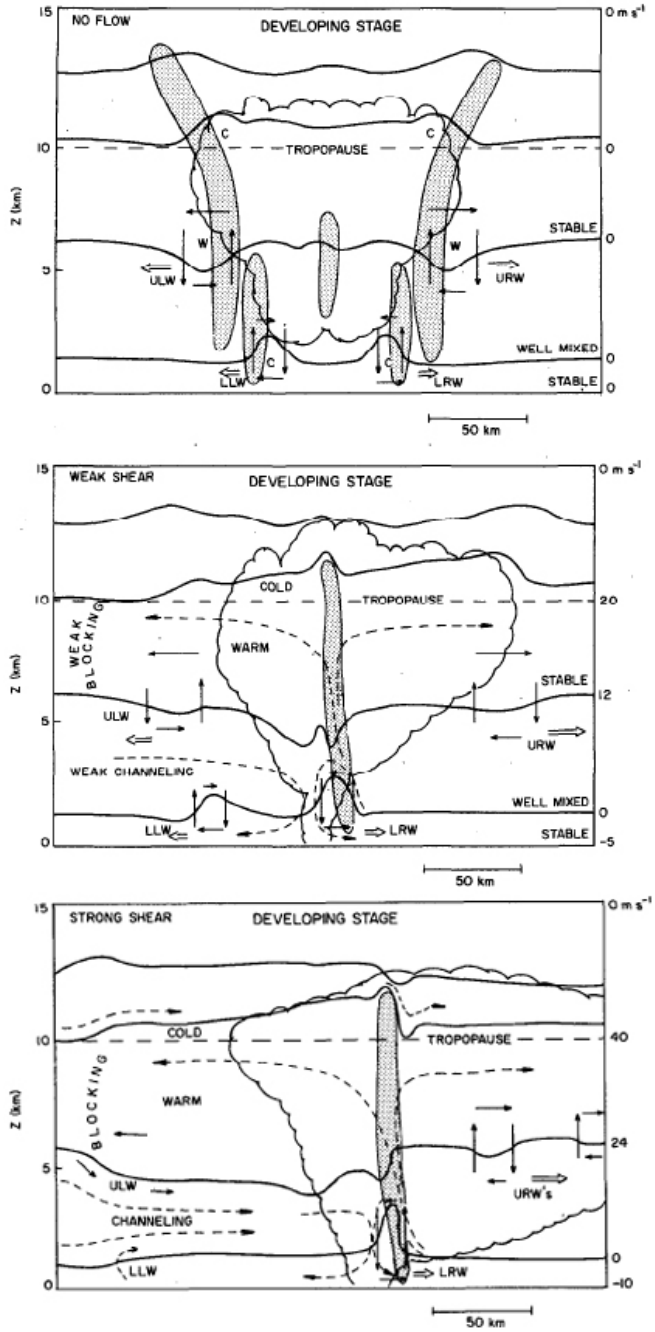

Figure 2.15: Gravity waves generated by convective heating in a linear model. The top figure corresponds to no shear, the middle to weak shear, and the bottom to strong shear. ULW, LLW, URW, and LRW are abbreviations for Upper Left Wave, Lower Left Wave, Upper Right Wave, and Lower Right Wave, respectively. The solid arrows are perturbation flow in u and w, dashed arrows are streamlines of resultant flow from the waves, and double arrows are the gravity wave direction of motion. The solid lines are θ contours. The numbers on the right-hand vertical axis are the mean ambient horizontal flow. Shaded areas correspond to the main updrafts. From Schmidt and Cotton (1990).

the upshear portion of this low pressure would remain closer to the convective source (Haertel 2007). This could perhaps correspond to or help intensify the pre-squall mesolow or wake low. The wave mode yielded by the stratiform profile of shallow cooling propagated more slowly away from the source, and produced a mid-level inflow (similar to that described as the channeled rear inflow by Schmidt and Cotton 1990) and upper- and lower- level outflow. The speeds of these two waves were given by

$$c = \frac{NH}{n\pi} \tag{2.3}$$

where N is the Brunt-Väisälä frequency, H is the vertical depth of the atmosphere, and n is the vertical mode of the temperature perturbation.

Finally, Haertel and Johnson (2000) and Haertel et al. (2001) developed another linear model of gravity wave production, but this time using only a source of cooling to simulate the diabatic profile in the lower levels of the stratiform region. This cooling prompted decreased heights at upper levels in the atmosphere (not shown). The dip in heights quickly divided in two and propagated away from the source at the speed of sound as acoustic waves; as these decreased heights moved away from the cooled air they were duly reflected at the surface as a short period of lowered pressure (Fig. 2.16d). In addition, the relocation of the decreased heights resulted in extra mass over the source of cooling, so high pressure and subsidence appeared in the lower levels at that point, allowing the cooled air to spread. (Fig. 2.16a-c).

Assuming a low-level inversion (such as is often present at nighttime) above the surface, this lower-level subsidence would also produce two elevated gravity waves at the density discontinuity at the inversion. These waves were termed "forced" waves as they were forced by a precise mass source; they propagated away from this source due to horizontal convergence at their edges, and were reflected at the surface by an increase in pressure. Since the forcing (i.e., the cooling from the stratiform region) was

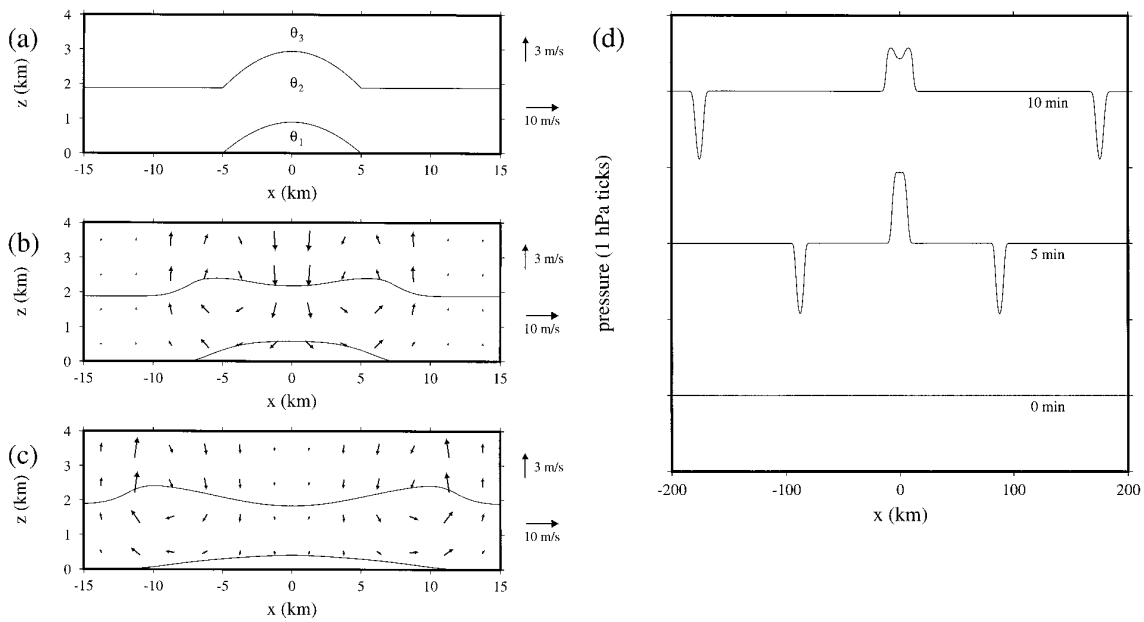

Figure 2.16: Depiction of gravity wave and gravity current outflow, produced from low-level cooling, within an idealized linear model, at (a) 0 min, (b) 5 min, and (c) 10 min. The solid lines are theta surfaces. (d) is perturbation surface pressure at 0, 5, and 10 min. From Haertel et al. (2001).

moving as well, the magnitude of this high pressure was increased for the downshear wave, particularly so if the forcing was moving at about the same speed as the forced gravity wave (Haertel and Johnson 2000).

Meanwhile, the stratiform region had also cooled air near the surface. Once the acoustic waves at upper levels had propagated away, the resultant high pressure and subsidence left behind created a gravity current at the surface as the cooled air spread away from its source. This was exactly like the gravity wave above it, except that the leading edges of the gravity current were moving by actual advection of cold air, as opposed to propagation (Fig. 2.16a-c).

A station at x = 10 km in Fig. 2.16a-c would experience a number of effects from both the gravity wave above it and gravity current, as per Haertel et al. (2001). A sample timeseries is reproduced from Haertel et al. (2001) in Fig. 2.17. When the initial acoustic wave passed overhead, the station would show a short lowering in

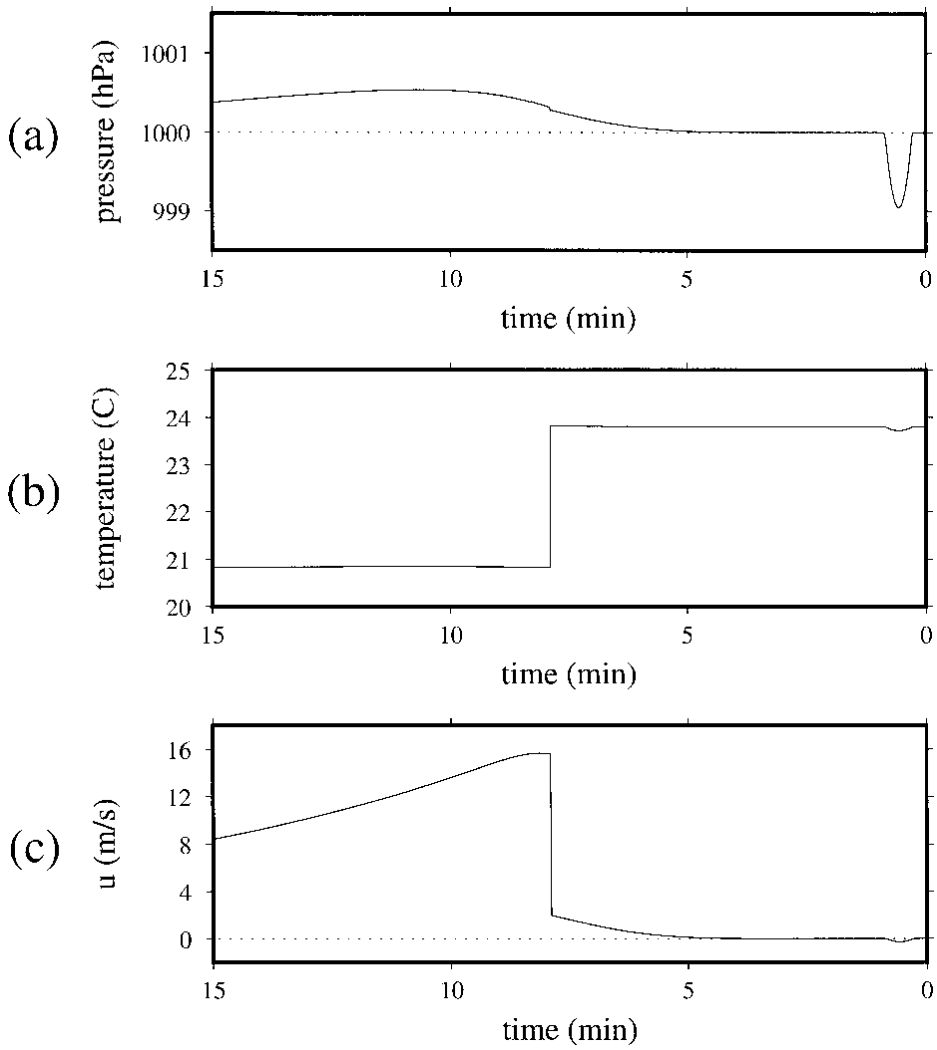

Figure 2.17: Pressure (a) hPa, temperature (b) C, and u (c) m/s observations from a station experiencing both gravity wave and gravity current passage forced by low-level cooling. Time increases to the left. From Haertel et al. (2001).

pressure before returning to its original level. A small shift in temperature and wind might appear as well. The forced gravity wave would pass overhead next, yielding an increase in pressure and wind at the surface but no temperature change as the cold air was still elevated. Finally, the gravity current would arrive, producing a further pressure rise and increase in wind, as well as a drop in temperature.

Haertel and Johnson (2000) found that when the source of the cooling was sustained, allowed to move with a speed similar to that of the forced gravity wave, and

simulated in a three-dimensional model, a mesohigh/wake low couplet was generated. Primarily this was found to be because of vertical motions both preceding and after the downshear forced gravity wave. On its downshear side, there was rising air, which decreased the buoyancy of the air and amplified the high pressure signature at the surface. On the other hand, there was subsidence to be found near the actual cooling (as was mentioned above). Once the cooling was stopped, the subsidence continued, producing warmed air and eventually lower pressure - the wake low. Haertel and Johnson (2000) also found that often the speed of the forced gravity wave was very similar to the speed of a typical squall line, allowing for amplification of the pressure response into a strong mesohigh. Thus, the mesohigh-wake low couplet could very well be a result of gravity wave dynamics produced by low-level cooling from the stratiform region.

2.6 Summary

This review of the literature shows that while bow echoes and their larger relatives, squall lines, have both been well-studied, there are a few gaps which could be duly filled by that which this study proposes.

It is obvious that the pressure and temperature features associated with the larger end of the spectrum of MCSs, such as squall lines, are understood in at least general terms. The mesohigh, mostly hydrostatically induced from the cold air produced by evaporating rainfall and melting precipitation, can be found centered directly behind the convective line of the squall system. Other non-hydrostatic sources for the mesohigh include precipitation loading and the physical impact of descending air on the ground. The wake low, also typically hydrostatically produced – from subsidence warming connected with descending air in the rear inflow jet – should be located behind the strongest portion of the stratiform precipitation region. Circulations fostered by gravity waves produced by both the deep heating and low-level

cooling associated with the convective line and stratiform region can also assist in the formation of these pressure features, as noted by Schmidt and Cotton (1990), Nicholls et al. (1991), Haertel and Johnson (2000), and Haertel et al. (2001).

Much work has been accomplished with regard to bow echoes as well. K04's new classification system has allowed a more systematic approach to collecting and analyzing large bow echo datasets, as well as inter-comparison between types. Various research has been done to understand sudden instances of severe wind production by bow echoes, including new theories regarding meso-γ vortices put forward by Trapp and Weisman (2003) and Wakimoto et al. (2006b). The "optimal" environmental state for long-lived bow echoes has also been a well-researched field, even if the current theory, RKW theory, is not yet fully satisfactory. Yet, there is still need to appraise potential links between the characteristics of larger (squall lines) and smaller (bow echoes) MCSs. It is possible that examination of bow echo surface pressure and temperature fields may reveal new insights into both the "optimal" environment and the production of severe winds. Furthermore, if patterns of behavior in surface observations are observed which are distinctively different from those associated with squall lines, then there are possibilities for a more dynamical separation (other than an arbitrary size limit) of bow echoes from these typically larger and more commonly occurring squall lines.

Chapter 3

Methodology

3.1 Oklahoma Mesonet data accrual and manipulation

The Oklahoma Mesonet, an observational network of unprecedented spatial and temporal resolution first fully operational in 1994, provides environmental observations every five minutes from over 110 stations across Oklahoma. A map of these stations is provided in Fig. 3.1. Observed variables utilized in this study include 1.5 m air temperature (°C), station pressure (hPa), and average five-minute 10 m wind speed (m s^{-1}) and direction (degrees).

3.1.1 Diurnal cycle and constant height pressure corrections

Before utilizing Mesonet surface pressure data for mesometeorological studies, the raw observations need to be treated to remove effects of the diurnal and semi-diurnal tides, and the station elevation. For the atmospheric tidal correction, the following procedure was utilized. Initially, a mean pressure, $\overline{P}(station)$, was calculated for each station on a monthly basis. A mean pressure value for each observation time throughout the day (e.g., 1100 AM, 1105 AM, 1110 AM, etc.) for each month was then also computed, $\overline{P}(station, observation\ time)$. A "diurnal variation" value for

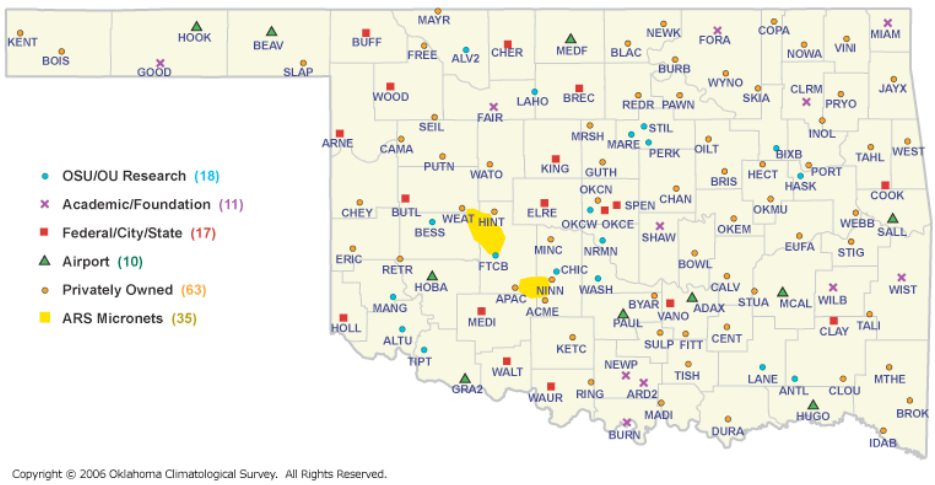

Figure 3.1: Oklahoma Mesonet stations as of 2006. Found online at www.mesonet.org/sites/.

each station was then obtained for each observation time:

$$P_{diurnal}(station, observationtime) = \overline{P}(station, observationtime) - \overline{P}(station) \tag{3.1}$$

In this way a "diurnal variation" value was obtained for each observation time and month at each station. This value would then be subtracted from each pressure observation to give a corrected pressure.

After that process, the pressure observations were then adjusted to 356.5 m (the mean height of all Mesonet stations). Virtual temperature was used for this correction, as given below:

$$P_{OK} = P_{station} * exp\left(\frac{z_{station} - \overline{z}_{OK}}{29.3 * T_v}\right) \tag{3.2}$$

where $T_v = T(1 + 0.61r)$ is the virtual temperature (found using the mixing ratio, r) in degrees Kelvin. The subscript *station* is used to indicate the station pressure and height, while P_{OK} is the pressure adjusted to the mean height of all the stations in the Mesonet ($\overline{z}_{OK}$).

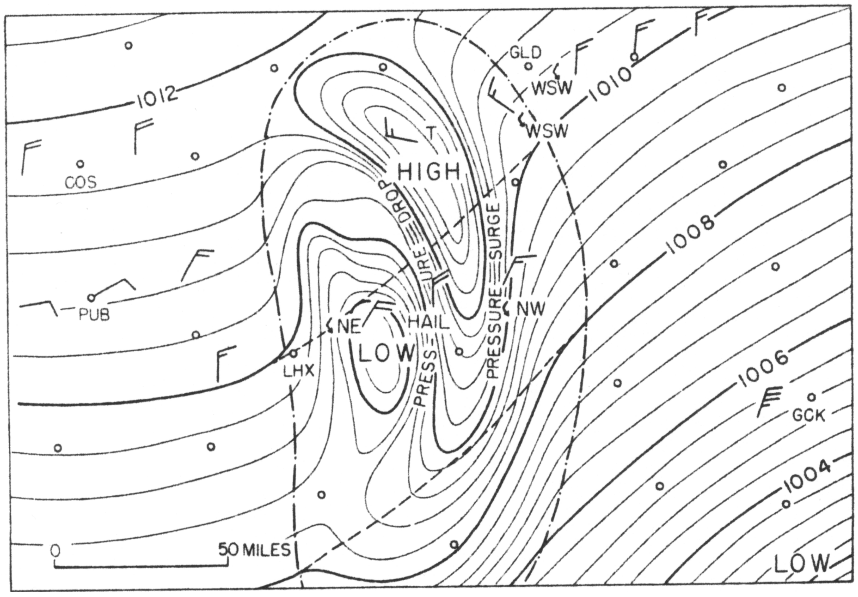

Figure 3.2: Pressure contours associated with a thunderstorm high. The dot-dash line shows the spatial realm of influence of the storm, while the dashed lines are the synoptic scale pressure pattern undisturbed by storm-scale features (i.e., the low-frequency data). From Fujita (1955).

3.1.2 High-pass Lanczos filter

As this study focused on mesoscale features, it was desirable for the synoptic scale features, such as longer-lasting pressure troughs and ridges, to be removed. This was not without precedent; such a procedure was done subjectively by Fujita in his 1955 paper. In that analysis, the entire pressure field was plotted, and then the contours at points considered to be outside the influence of the thunderstorm system were connected across the system itself (see Fig. 3.2). From this one could easily pick out the larger-scale (what Fujita termed the "undisturbed") pressure pattern, as well as the mesoscale, thunderstorm-produced ("excess") pressure pattern. While this method was straightforward and intuitive, it would not be ideal for examining a large number of cases as done in this study; nor would it provide reproducible results as it was left up to the researcher's discretion what was outside the influence of the convective line. Thus the process of time series filtering, a popular method of removing specific frequencies in a time series, would be useful.

For this task, a Lanczos high-pass Fourier filter was chosen. To examine the effects such a filter would have on a time series, one can look at its response function. This function is the ratio of the amplitude of the filtered time series to the unfiltered time series, and is a function of the different frequencies available (which range from one cycle over the whole time series to one cycle over two time steps.) The filtered series is obtained by multiplying the original series by the filter's weighting function. The ideal response function for a high-pass filter would be a step function, of value one for all frequencies higher than the chosen cutoff frequency and equal to zero for all lower frequencies, with a sharp delineation in between.

A running-mean filter, with its boxcar-style weighting function, is generally considered to be the worst-case filter. Its response function contains oscillations on either side of the frequency cutoff where the response function actually is negative; these would indicate the weighting function is introducing large phase shifts which contain spurious data. Also, the frequency cutoff itself is more gradual than preferred; including more surrounding points in the weighting function (i.e., increasing its width) would help this, but then more points would be excluded from each end of the filtered time series. Thus, this filter alone would not provide high-quality results.

The Lanczos filter is found by performing running-mean smoothing on the response function of a running-mean filter (Duchon 1979). As a running mean will precisely remove frequencies that are multiples of the number of weights used, this method can be employed to effectively eliminate the negative oscillations surrounding the frequency cutoff in the pure running-mean response function, as they occur in set periods. According to Duchon (1979), the weighting function which results from smoothing the response function with a running mean can be calculated by multiplying the original weighting function by a sigma factor, or

$$\sigma = \frac{sin\frac{\pi k}{N}}{\frac{\pi k}{N}} \tag{3.3}$$

where k ranges over all wave numbers from 1 to N, and $2N + 1$ is the width of the weighting function used. The response function produced by a high pass filter using this method is shown in Fig. 3.3, for a weighting function of width 61 and a cutoff wave number of 100. Obviously, there are no negative oscillations, and though the wave number cutoff is still somewhat gradual, this method reaches much closer to the ideal step function than the running mean. As already mentioned, the sharpness of the cutoff can be increased by adding to the width of the weighting function. The data set used in this study contains four years of data at five minute intervals, or 420,768 time steps; losing a few extra points at each end will not be a difficulty. Therefore, a high-pass Lanczos filter will be used for the following analysis. After trial and error, a weighting function width of 81 points was selected; higher widths did not offer significant improvement.

It would be ideal to filter out all features with periods longer than the lifetime of each bow echo case. In order to generalize the filter cutoff period so it could be applied to all cases, a common period was selected using the definition for the upper (longer) end of meso-timescales, the pendulum day ($\frac{2\pi}{\Omega sin(\phi)}$, where ϕ is the latitude and Ω the angular speed of the earth.) For the average latitude in Oklahoma (35.5°N), this corresponds to perturbations of 41.2 h in length, or a cutoff period of 82.4 h. (Note that meteorological perturbations are actually half wavelengths, so a 41.2 h pressure perturbation would actually correspond to a feature with an 82.4 h period.)

3.1.3 Time-space transform and objective analysis

In order to add additional detail to these mesoanalyses, a time-space transformation (Fujita 1955) was performed on the data during the periods that bow echoes were within the state. Although not strictly true, the meteorological fields associated with these bow echoes were assumed to remain in a steady state for 15-minute periods. For each 15-minute period during the system's lifetime, the velocity ($\overrightarrow{u}$) of the

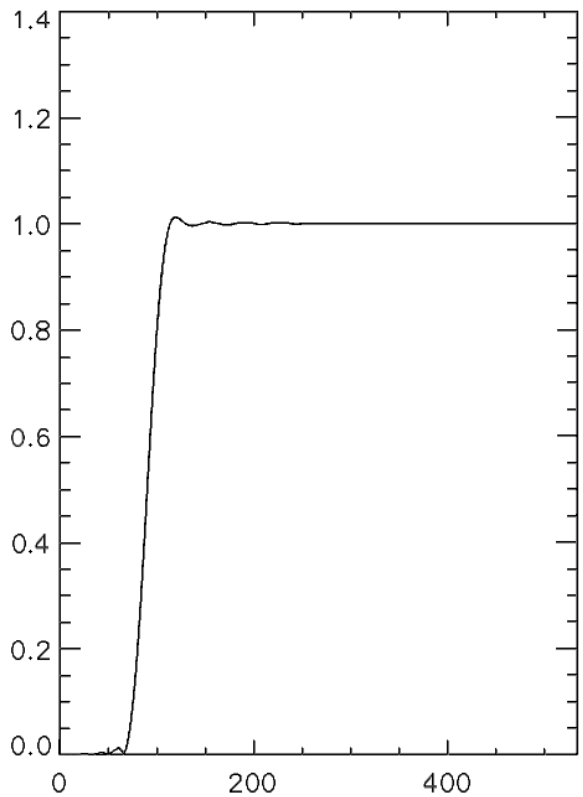

Figure 3.3: Response function for a 61-point width high-pass Lanczos filter with a cutoff wavelength of 100. Vertical axis is the response function value; horizontal axis is the wavelength for a 500-point length timeseries.

bow apex was calculated. This was done utilizing the heading-speed tool in AWIPS (Advanced Weather Interactive Processing System). WSR-88D NEXRAD radar data for each case were downloaded from the National Climatic Data Center Hierarchical Data Storage System (accessible via http://has.ncdc.noaa.gov) and then converted to AWIPS-viewable format.

Once the bow apex velocity was calculated, the observations surrounding the bow would be shifted $\overrightarrow{u}n\Delta t$ in space with the bow echo, where n is the number of timesteps and Δt the interval between timesteps. Each observation could then be attributed to that new position at time $t - n\Delta t$. Here Δt was five minutes. However, while it is reasonable to apply this procedure to observations near each convective event, it was not appropriate to extend it to all observations throughout Oklahoma.

Thus, the time-space transformation was only applied over a movable, latitude- and longitude- defined box, redefined every 15 minutes, which followed the bow echo.

After the data field was enhanced by this procedure, the observations were then objectively analyzed using the multiquadric interpolation scheme (Nuss and Titley 1994). This scheme was chosen for its better analysis of smaller, mesoscale features as compared to the Barnes, Cressman, and optimal interpolation methods (as according to Nuss and Titley (1994)). Because this scheme does not perform as well in regions with sparse observations, contour patterns in the Oklahoma panhandle (where only three Mesonet stations are located) were not examined. The newly gridded data was then read into GEMPAK, which could draw the resultant contours.

WSI NOWrad mosaic base reflectivity data at 15-minute resolution was added to these GEMPAK analyses after being downloaded from the National Center for Atmospheric Research's (NCAR) Mesoscale and Microscale Meteorology Division (MMM) at http://www.mmm.ucar.edu/imagearchive/WSI. Because this data was only available in native WSI NOWrad format (easily visualized using GEMPAK) for the full years 2002 through 2005 when this study began, it was limited to those years.

Plots of adjusted surface pressure, surface temperature, and gridded surface wind speed, overlaid on radar data, were produced at 15-minute intervals for all bow echo cases found over this four-year period. These plots will be examined in detail in Chapters 5 and 6.

3.2 Bow echo definition

Four years' worth of radar images were obtained from MMM's online image archive, found online at http://www.mmm.ucar.edu/imagearchive. These images were of 30-minute (or occasionally higher) resolution, so if a bow-shaped feature was found, the 15-minute resolution WSI NOWrad radar data for that date would be downloaded and examined using GEMPAK. If a feature met the necessary criteria (discussed

below) it would be included as one of the cases, from either the start of convection or when the bow apex entered the state, to the exit of the stratiform precipitation region to another state or the conversion or merging of the bow echo into a larger system. Climatological statistics regarding these cases will be discussed in Chapter 4. Unfortunately, 14 days of radar data were missing from this archive, during the period of 9 June 2002 to 22 June 2002. A full listing of cases from each year and their classifications is included in Appendix A.

The definition for a bow echo used in this study drew heavily on the work of'Klimowski et al. (2000), discussed in 2.1.2. As mentioned there, the feature must appear "bow or crescent-shaped" on the radar return, and must display a strong gradient in reflectivity at the leading, or convex, edge of the bow. This feature must also last long enough so that it is obvious that the bow shape was not just a fortunate arrangement of cells for a few radar sweeps. Because the temporal resolution of the WSI NOWrad data was 15 minutes, it was natural to require that a feature must persist for at least 30 minutes, preferably longer if any conclusions about the surface observations attendant with the system are to be drawn. Thus, the following time constraints were included in the bow echo selection criteria for this study:

- The bow or crescent-shape of the radar echo must endure for at least one hour.
- "Active bowing" – when the radius of curvature of the echo is decreasing with time – must persist for at least 30 minutes during this same period.

In addition, these time constraints must both be met while the apex of the bow is within the state of Oklahoma (excluding the panhandle.)

Further specifications were required to ensure the Mesonet would be able to adequately sample any surface pattern associated with the bow. For this reason, the bow needed to be large enough to cover the average distance between two Mesonet stations, or about 50 km, throughout the duration of the time periods listed above.

The resultant number of bow echoes which were found during the four years examined will be discussed in Chapter 4.

It is possible, however, for such one bow echo case to contain several bowing segments. These multiple segments could occur at the same time and be located within the same bow, or could appear sequentially. Thus, each instance of new bowing development or active bowing within a case is referred to as a "bowing episode." Bowing episode development and its attendant surface patterns will be addressed in Chapter 5.

3.3 Bow echo classification

The bow echo cases selected were then each divided into categories based on both the behavior of the system during the mature, or active bowing, portion of its lifecycle, and the manner in which the system initiated. The work of Klimowski et al. (2004) was utilized here. As already mentioned in Chapter 2, this system of bow echo classification had the strongest dynamic underpinning of all those reviewed for its category choices. In addition, because categorizing the echoes in this study needed to be done entirely with radar, it was important that the classification system used lend itself easily to that end.

K04's convective initiation types were the merger of weakly organized cells, bowing of a squall line, or bowing of a supercell. These three types were essentially reused; the first two categories were termed "Merger" and "Linear," respectively, in this study. The third category was simplified to the bowing of an isolated single cell ("Isolated"), as not enough information was available using solely radar to determine whether the cell was officially supercellular. Occasionally the feature would form outside the state of Oklahoma where the method of initiation remained unseen; in those cases the bow echo was classified by active bowing structure only.

The active bowing structure groupings were also borrowed from K04: the Classic Bow Echo (CBE), the Bow Echo Complex (BEC), and a Squall Line Bow Echo (SLBE), all discussed in Chapter 2. A radar-depicted conceptual model of each of these, as per K04, was provided in Fig. 2.2. The Cell Bow Echo, describing the bowing of an isolated cell, was not included due to the imposed spatial restrictions of the echo stretching at least 50 km. The number of echoes which fell into each category will be considered in Chapter 4.

Chapter 4

Climatology of Bow Echo Cases

Thirty-six total bow echo cases were identified during the 2002-2005 period using the criteria outlined in Chapter 3. Once the cases were selected, an analysis of the distribution of these cases among classification categories was performed to find if one of the categories was preferred during the period. The number of cases which occurred were also examined by season for annual preferences. Frequency of severe wind reports associated with each classification was also studied to see if one structure or initiation type was a more effective producer of severe winds. Unfortunately, because so many cases initiated or dissipated outside the state, a diurnal frequency distribution of storm formation was not possible.

4.1 Distribution of cases by classification

4.1.1 Classification by initiation type

The breakdown of cases by initiation type (and active bowing structure as well) is shown in Table 4.1. There were instances of all three initiation modes throughout the period studied. Merger was by far the most frequent type of initiation: it comprised 55.6% of the 36 total cases (Table 4.2). Within this category, the Bow Echo Complex was the most common structure, seen 70.0% of the time. The relationship between Merger initiation and BEC structure appears straightforward. Specifically,

Table 4.1: Number of Oklahoma bow echoes in each classification for 2002-2005. Columns are mature or active bowing structure, and rows are initiation type. As in Chapter 3, CBE corresponds to Classic Bow Echo; BEC to Bow Echo Complex, and SLBE to Squall Line Bow Echo.

	CBE	BEC	SLBE	Total
Isolated	2	1	0	3
Merger	6	14	0	20
Linear	3	0	3	6
Unknown	4	3	0	7
Total	15	18	3	36

not all of the pre-existing weaker convection needed for a Merger initiation would actually merge, and that which remained would form other types of convection in the immediate area–resulting in a Bow Echo Complex situation. The least frequent mode of initiation was the bowing out of an isolated cell. It is probable that these event types are actually more numerous, but the exclusion of Cell Bow Echoes (which would naturally initiate through the bowing of an isolated cell) weighted the results.

The distribution of initiation types given in Table 4.2 compare well with the climatological study done by Klimowski et al. (2004) for the Southern Plains (defined there as Texas, Oklahoma, Kansas, and eastern portions of New Mexico and Colorado). In that study, just over half (51%) of the 40 Southern Plains cases initiated from a Merger, with squall line (Linear) and supercell (Isolated) cases accounting for 33% and 16%, respectively.

4.1.2 Classification by active bowing structure

Bow Echo Complexes were the most frequent active bowing form in this study, composing 50.0% of all cases (Table 4.3). This is markedly different than Klimowski et al. (2004), where no Bow Echo Complexes were found within the Southern Plains throughout the entire study. This suggests a distinct difference in application of the BEC definition between the two studies. In Klimowski et al. (2004), Bow Echo Complexes are defined as "those mesoscale convective systems in which the bow echo is

Table 4.2: Number of bow echoes and frequency statistics for each initiation type, subdivided by active bowing structure. Cases where the initiation type is unknown are not included.

Isolated Initiation	Events	Percentage of Isolated	Percentage of Total
CBE	2	66.7%	5.6%
BEC	1	33.3%	2.8%
SLBE	0	0.0%	0.0%
Total	3	100.0%	8.3%
Merger Initiation	**Events**	**Percentage of Merger**	**Percentage of Total**
CBE	6	30.0%	16.7%
BEC	14	70.0%	38.9%
SLBE	0	0.0%	0.0%
Total	20	100.0%	55.6%
Linear Initiation	**Events**	**Percentage of Linear**	**Percentage of Total**
CBE	3	50.0%	8.3%
BEC	0	0.0%	0.0%
SLBE	3	50.0%	8.3%
Total	6	100.0%	16.7%

the primary, but not the only, organized convective structure." According to Dr. Klimowski (Klimwoski 2007), the requirement for organization of the secondary convective structure was strictly applied. However, in this study, such a requirement was much more relaxed, to the point that even unorganized secondary convection associated with a bow echo would place the system in the Bow Echo Complex category. This categorization was deemed more useful in this study, as any secondary convection, organized or not, would affect surface pressure and temperature patterns.

Within this study, mergers were most favored for BECs, also shown in Table 4.3. They were also the most common initiation type for Classic Bow Echoes, although CBEs were distributed across all initiation types more than Bow Echo Complexes were. All Squall Line Bow Echoes were initiated from the bowing of a linear structure, as was predetermined by the definition of the SLBE classification. The Squall Line Bow Echo active bowing structure was also the least frequent, although ironically the first bow echo simulations (Weisman 1993) were of the SLBE type. This is not to say

Table 4.3: Number of bow echoes and frequency statistics for each active bowing structure, subdivided by initiation type.

Classic Bow Echo	Events	Percentage of CBE	Percentage of Total
Isolated	2	13.3%	5.6%
Merger	6	40.0%	16.7%
Linear	3	20.0%	8.3%
Unknown	4	26.7%	11.1%
Total	15	100.0%	41.7%
Bow Echo Complex	**Events**	**Percentage of BEC**	**Percentage of Total**
Isolated	1	5.6%	2.8%
Merger	14	77.8%	38.9%
Linear	0	0.0%	0.0%
Unknown	3	16.7%	8.3%
Total	18	100.0%	50.0%
Squall Line Bow Echo	**Events**	**Percentage of SLBE**	**Percentage of Total**
Isolated	0	0.0%	0.0%
Merger	0	0.0%	0.0%
Linear	3	100.0%	8.3%
Unknown	0	0.0%	0.0%
Total	3	100.0%	8.3%

few squall lines were observed moving through the state during this period; rather, often none of their bowing segments would be located within Oklahoma.

4.2 Distribution of cases by geographic location

Figures 4.1 and 4.2 display the paths taken as bow echoes moved across Oklahoma, categorized by active bowing structure (Fig. 4.1) and initiation type (Fig. 4.2). The tracks were determined from the path of the bow apex. The beginning point was selected as either when the bow apex entered the state, or when the system first initiated bowing. The end point was chosen as either when the system exited the state or bowing activity stopped. Bowing activity was considered finished when the convective line contained no returns greater than 50 dBZ, or the system no longer retained its bowed shape. (Note that systems which tracked only across the state's panhandle were not included in this study.)

According to these figures, there did not appear to be any favored locations for bow echoes to form or track across the state, other than a basic west-to-east profile. Bow echoes could be found in any part of Oklahoma. There can, however, be seen two primary directions of motion: southwest to northeast, and northwest to southeast. Only four cases were close to propagating directly eastward. As predominant upper-level patterns over Oklahoma almost always feature upper-level steering winds in one of these two directions, this result was also expected. Finally, even the shortest tracks covered at least 150 km, owing to the time and spatial restrictions on cases. It is the smaller bow echoes, such as Cell Bow Echoes not included here, that have shorter life spans and track lengths.

In Fig. 4.1, the tracks are color-coded by active bowing structure. None of the structures appears to favor either of the two primary track directions. Nor do they favor one portion of the state over another, instead being evenly dispersed throughout. The colors in Figure 4.2 correspond to the initiation type. Again, the categories were uniformly spread throughout the state with no preferred geographic region. However, while the Linear and Isolated type cases have tracks which traveled in a multitude of directions, the majority of the Merger type cases (12 of 19, or 63.1%) moved from southwest to northeast. Environments with upper-level southwesterly flow over Oklahoma often contain more moisture than those with northwesterly flow, and more moisture results in more convection. If this type of situation were to evolve into a bow echo, it would be likely to initiate through a merging of this extra convection.

4.3 Distribution of cases by season

The largest number of bow echoes took place during either the spring or summer seasons, as can be seen in Tables 4.4 and 4.5. (Note that here winter is defined conventionally as Dec.-Feb., spring Mar.-May, summer Jun.-Aug., and fall as Sep.-Nov.) Since the summer months are typically the ones that provide environments

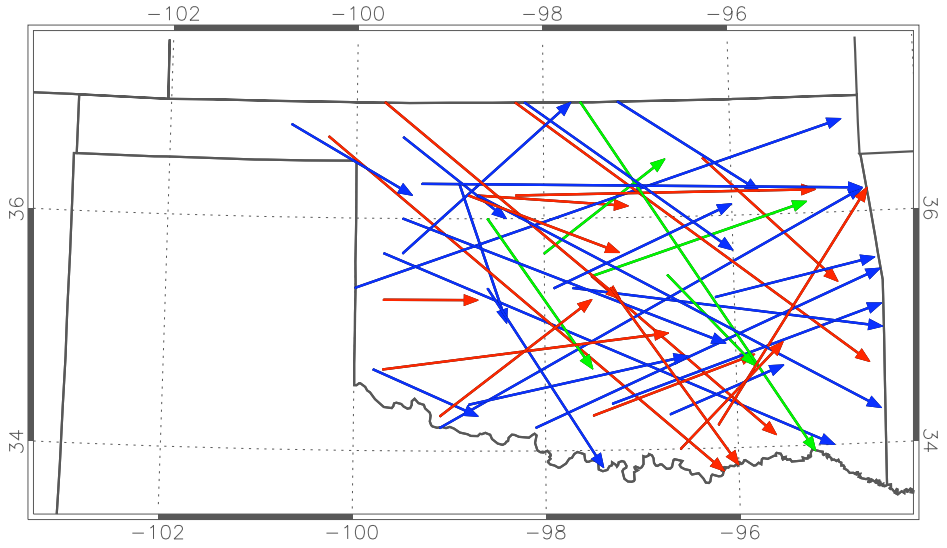

Figure 4.1: Tracks of the 36 bow echoes in Oklahoma during 2002-2005, color-coded by active bowing structure. Red: Classic Bow Echo; Blue: Bow Echo Complex; Green: Squall Line Bow Echo.

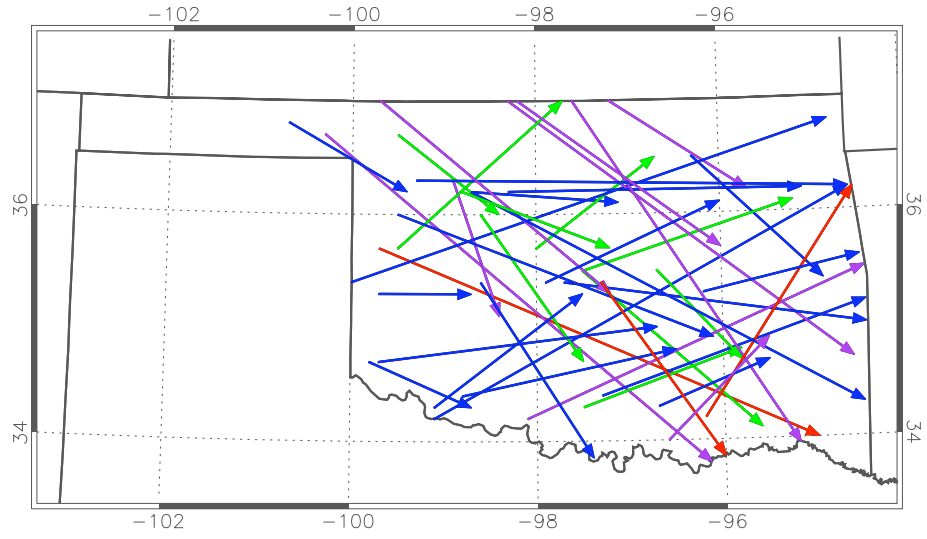

Figure 4.2: Tracks of the 36 bow echoes in Oklahoma during 2002-2005, color-coded by initiation type. Red: Isolated; Blue: Merger; Green: Linear; Purple: Unknown.

with greater instability and less synoptic forcing, it could be expected that Merger initiations were most plentiful during that time, as was the case (Table 4.4). The weaker, scattered convection needed prior to Merger initiation would be more expected in that type of environment. Meanwhile, the linear initiation category, which would require the most synoptic forcing to form, was the only classification with cases that occurred during the fall months. Again, however, it should be noted that the unavailable radar data during 09-22 June 2003 could have slightly biased these results.

The distribution of the different active bowing structures across the seasons somewhat underscored this instability-dynamics relationship (Table 4.5). The largest number of Bow Echo Complexes were found during the summer months. This could hint that these BECs do not need as dynamically strong a situation in which to form when compared to the other active bowing structures. Classic Bow Echoes were most frequent in the spring, suggesting a combination of instability and dynamic forcing were preferred by these systems. On the other hand, Squall Line Bow Echoes, which would naturally require the most synoptic forcing of all the classifications, were most numerous in the fall when the availability of stronger synoptic forcing would likely outweigh availability of instability.

There were no cases found during this four-year period which took place during the winter. This signified that there was at least a minimum amount of moisture and warmth required to initiate a bowing system over Oklahoma. It would be reasonable to assume that the state is located too far north for such an environment to exist with any frequency in the winter months. However, it should be noted that at least one instance of all active bowing structures were found in all of the other seasons (with two exceptions: no SLBEs in spring and no BECs in fall). Thus, while a predisposition of certain environments to particular structures and initiation types might be suggested, these are certainly not proposed as absolute rules.

Table 4.4: Number of bow echoes occurring during the four three-month periods, Dec-Feb (winter), Mar-May (spring), Jun-Aug (summer), and Sep-Nov (fall); subdivided by initiation type. Unknown initiation type cases were not included.

Initiation Type	Dec–Feb	Mar–May	Jun–Aug	Sep–Nov
Isolated	0	2	1	0
Merger	0	9	11	0
Linear	0	2	1	3
Total	0	13	13	3

Table 4.5: Number of bow echoes occurring during the four three-month periods, Dec-Feb (winter), Mar-May (spring), Jun-Aug (summer), and Sep-Nov (fall); subdivided by active bowing structure. Abbreviations for active bowing structure as described in Fig. 4.1.

Active Bowing Structure	Dec–Feb	Mar–May	Jun–Aug	Sep–Nov
CBE	0	8	5	2
BEC	0	7	11	0
SLBE	0	0	1	2
Total	0	15	17	4

A plot of bow echo tracks by season (not shown) demonstrates that there does not appear to be a storm track favored by bow echoes during specific seasons. Both southwest-to-northeast and northwest-to-southeast tracks can be found in each season.

4.4 Percentage of severe wind reports across classifications

The criteria set for finding bow echo cases did not include severe wind reports. (Here, a severe wind report was defined as a Storm Prediction Center storm report which occurred in time and space conjunction with the bowing system - either on the convective line or within the stratiform region.) The reasoning for not including a severe wind requirement is twofold. First, bow echoes can and often do form at night above a stable boundary layer. Severe winds associated with the system may occur, but in some instances may not penetrate this stable layer to reach the surface. Secondly, severe winds associated with a system may simply not be recorded. The subjectiv-

ity of the Storm Prediction Center severe wind report database has already been noted elsewhere in the literature (Trapp et al. 2006). However, the positioning of the Mesonet stations assured that an objective report of severe winds was available every five minutes, if only at approximately 50 km resolution. An examination of which classifications produced more cases associated with severe wind reports would therefore be instructive.

A full 75.0% of cases (27 of 36) were associated with severe wind reports. Unfortunately, due to the small number of cases within each classification, it was difficult to draw conclusions about which type may typically produce more severe wind reports. Tables 4.6, 4.7, and 4.8 showcase the number of cases that produced severe wind reports, divided by active bowing structure and initiation type. The results shown in Table 4.6 demonstrate that the Linear initiation mode had a slightly higher percentage of severe cases (83.3%, or 5 of 6) than Merger initiation cases (65.0%, or 13 of 20). This would agree with prior findings in the literature (Evans and Doswell 2001) that strongly forced environments (conventional forebears of Linear cases) were favorable to more severe bow echoes; whereas situations with weaker forcing and more instability (more typical of Merger cases) were not. It is unlikely that this result is entirely an artifact of the size of Linear cases, as the Merger cases examined were on average just as large and yet had a much lower severe wind report rate. With only three Isolated cases no deductions regarding that initiation type can be made.

Such conclusions should not be carried too far as Bow Echo Complexes (frequently initiated by Merger) actually had the most cases with severe wind reports (83.3%, or 15 of 18). It is possible, however, that this is a consequence of the larger size of Bow Echo Complexes. On average, the bowing segments of the Complexes were larger (a longer and "thicker" convective line) than both the Classic and Squall Line bowing segments. Nevertheless, such results would indicate that just because a bow echo

does not appear in a "classic" shape on the radar does not mean it is less likely to cause severe damage.

Table 4.6: Number and percentage of initiation types associated with severe wind reports.

Initiation Type	Number with wind reports	Total number	Percentage
Isolated	3	3	100.0%
Merger	13	20	65.0%
Linear	5	6	83.3%
Total	21	29	72.4%

Table 4.7: Number and percentage of active bowing structures associated with severe wind reports.

Active Bowing Structure	Number with wind reports	Total number	Percentage
CBE	10	15	66.7%
BEC	15	18	83.3%
SLBE	2	3	66.7%
Total	27	36	75.0%

Table 4.8: Percentage of combined initiation type and active bowing structure associated with severe wind reports.

Percent Severe	CBE	BEC	SLBE	Total
Isolated	100.0%	100.0%		100.0%
Merger	33.3%	78.6%		65.0%
Linear	100.0%		66.7%	83.3%
Unknown	75.0%	100.0%		85.7%
Total	66.7%	83.3%	66.7%	75.0%

Chapter 5

Surface Patterns Associated with Bow Echo Initiation and Dissipation

The cases will now be examined by mature structure for patterns in high-pass filtered surface pressure, temperature, and wind. The similarities of the squall line conceptual model of pressure and temperature fields as compared to those found to be attendant with bow echoes will also be noted. Following the discussion of one case study from each category, a synthesis of all cases will be presented.

5.1 Classic Bow Echoes

5.1.1 All initiation types

As almost all of the CBE cases' surface patterns exhibited the same behavior regardless of initiation type, just one case will be examined that best exemplified the patterns associated with the systems. This bow echo case existed from 0530 to 0745 UTC on 13 March 2003. If a large fraction of CBE cases contained a feature which differed from the behavior of this case, such behavior will be noted in the text.

Figures 5.1a,b display the typical arrangement of the mesohigh and cold pool in relation to the convective line prior to the start of new bowing. The exact timing of the formation of the mesohigh varied throughout the cases; for Merger cases a

mesohigh would already be associated with the merging convection, while for Linear and Isolated cases the mesohigh would appear no more than 45 minutes after the line of convection or isolated cell appeared (not shown). After this 45 minutes, however, the mesohigh in almost all cases appeared very similar to Fig. 5.1a: located just behind the right side of the convective line.

The time the cold pool developed also varied among initiation types. For Merger cases, just like the mesohigh, a cold pool would already be associated with the convection merging to form the convective line. For the Initiation and Linear cases, the cold pool would appear after the mesohigh, about 1.5 hours after the convective line or isolated cell initiated (not shown). After the 1.5 hours, just like with the mesohigh development, the location of the cold pool for almost all cases was very similar to Fig. 5.1b, centered behind the convective line and to the left of the mesohigh. Around this same time, as is also discernible in the figure, stratiform precipitation began to form, centered behind the convective line. However, the timing of its formation in relation to the formation of the cold pool was quite variable and did not allow for conclusion regarding a relationship between the two.

The wind field in this case also exhibited the one main feature evident in all CBE cases. An axis of convergence was located just ahead of and parallel to the newly initiated convective line, somewhat evident just ahead of the left side of the convective line in Fig. 5.1a. This figure also displays a divergence axis perpendicular to the right side of the convective line, which was a feature unique to this case. Also evident in Figs. 5.1a,b are the larger area of low pressure ahead of the convective line, somewhat collocated with a smaller but more intense area of warming.

At some time between 15 and 120 min after the formation of the convective line (for all the cases), the mesohigh surged wholly or partially ahead of the right side of the convective line, as it did for the case on 13 March (Fig. 5.2a). Meanwhile, the cold pool remained centered behind the convective line with the isotherms parallel along

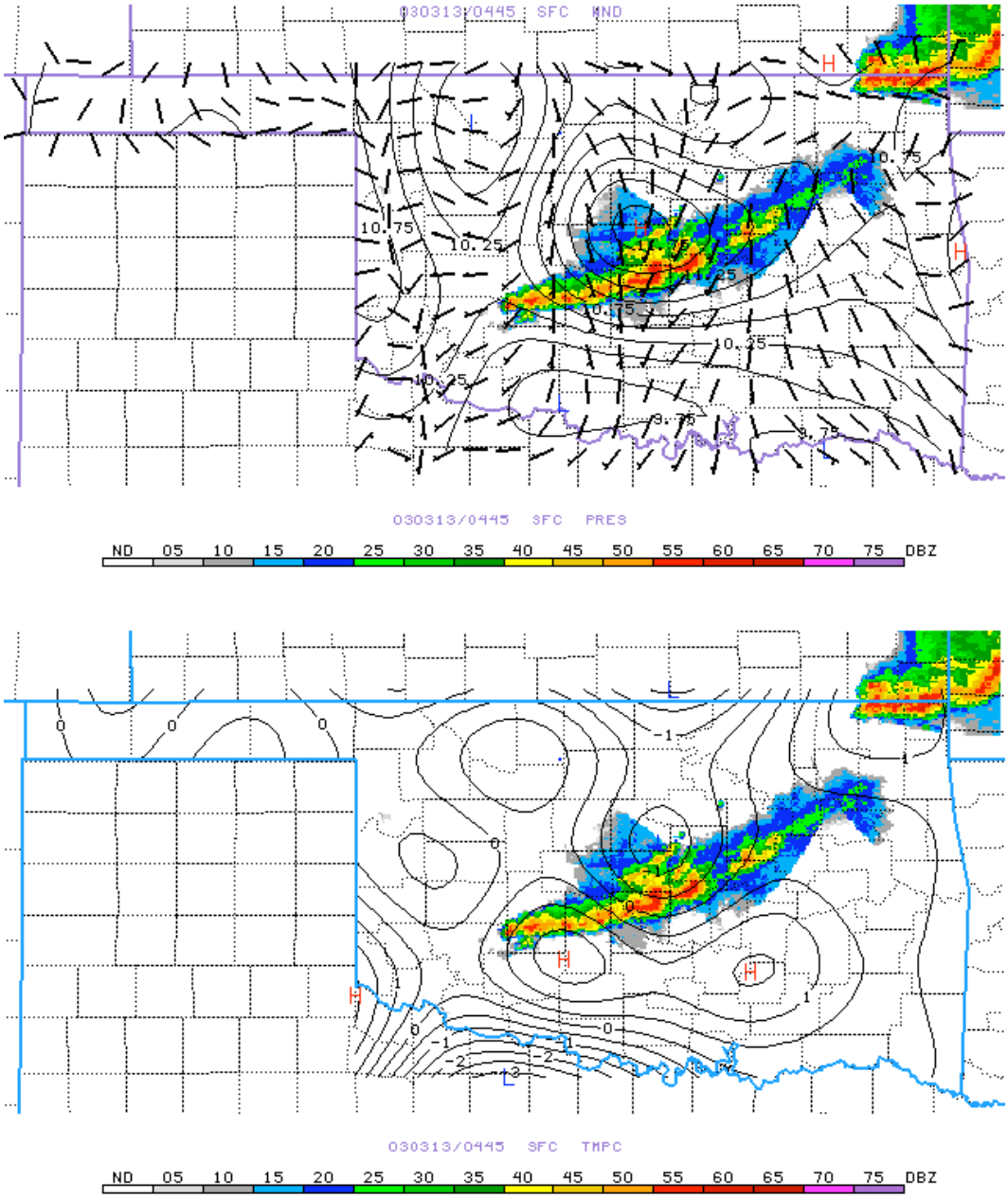

Figure 5.1: Figure (a): high-pass adjusted pressure (0.25 hPa) and high-pass gridded winds (knots) from 0445 UTC 13 March 2003. WSI NOWrad base reflectivity in color. Figure (b): high-pass temperature (0.5 °C) from the same time.

its entire length, illustrated in Fig. 5.2a. Thirty minutes later (Fig. 5.2b), new bowing development formed just to the left of the mesohigh surge. The cold pool remained centered behind the convective line, although the cold air expanded outward with the new bow. This pattern will be referred to later in the chapter as the "pressure surge – new bowing" pattern.

If the convergence axis (or wind shift) surged with the pressure in advance of the convective line, that would be indicative of either a gravity wave (Haertel et al. 2001) or strong downward momentum transport surging ahead of the convection. Unfortunately, even with the gridded winds the resolution in the mesoscale analysis is not fine enough to determine if that was the case. Thus, timeseries plots of observed high-pass pressure, temperature, and wind, as well as rain rate, at a station which experienced both the pressure surge and new bowing were examined. Such a timeseries, typical of the majority of Classic Bow Echo cases, is shown in Fig. 5.3 at station VANO (see Fig. 3.1 for a map of the mesonet stations). There, the wind shift occured just after 0530 UTC, at the same time as the increase in wind speed. The pressure had begun to rise slowly about 20 min before, although it also began a sharp increase right at the same time as the wind shift. The rain began 20 min later than the wind shift, just before 0600 UTC, at the same time the station encountered the cold pool.

Station NRMN, whose timeseries is shown in Fig. 5.4, experienced the passage of the convective line at 0430 UTC, before both bow and pressure surge developed. The wind shift occurred at 0415 UTC, followed about 15 min later by the onset of the rain and the arrival of the cold pool. In this timeseries, the wind shift occurred about 15 min after the pressure started to rise, and there was no change in the rate of pressure rise at the time of the wind shift. These two timeseries exhibited a pattern which was evident in a number of the other cases. A "bowing" station would show a sharp increase in the pressure rise rate at the same time as the wind shift passage, followed around 20 minutes later by the onset of rain and the cold pool. The "non-

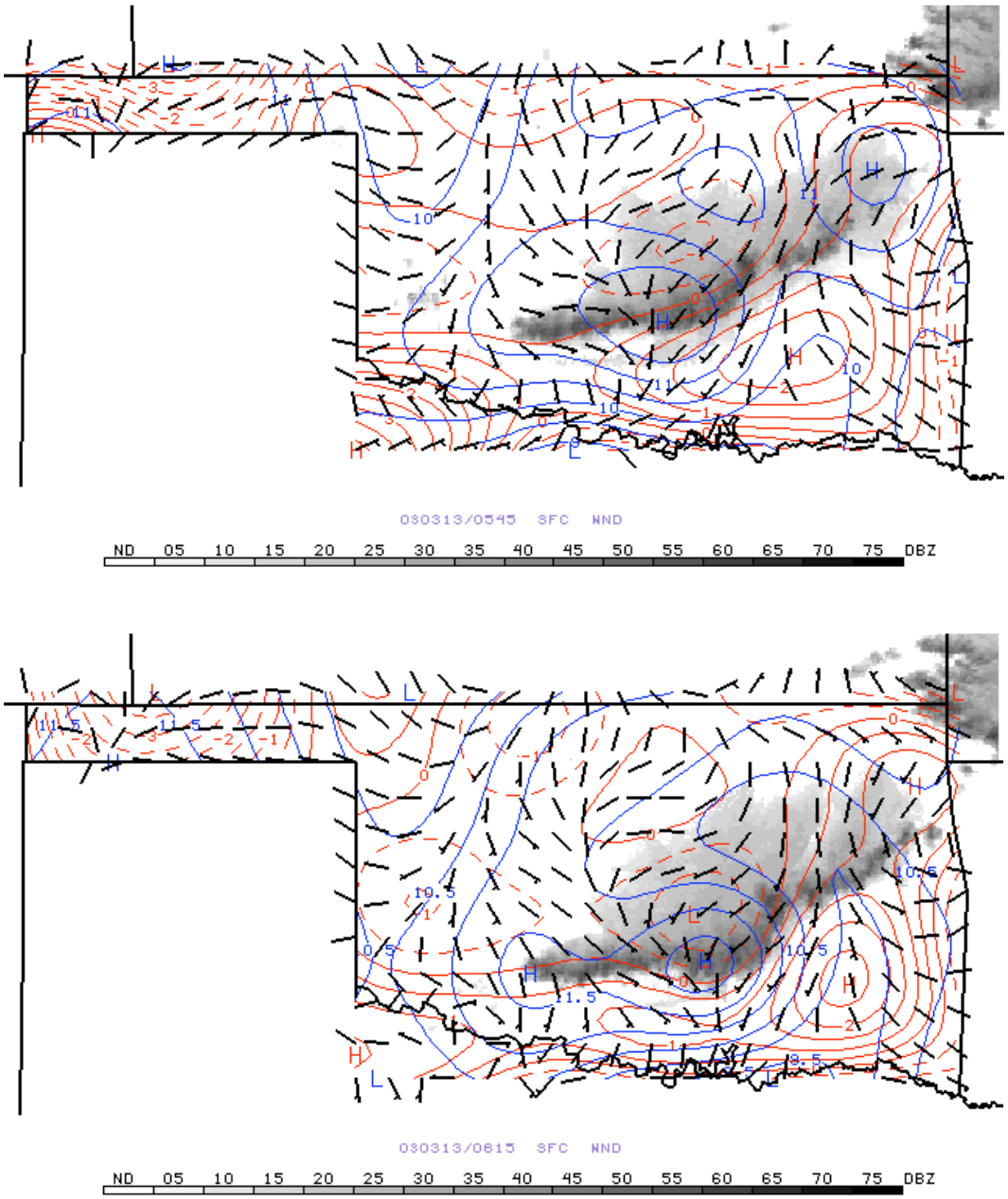

Figure 5.2: Figure (a): high-pass adjusted pressure (blue, 0.5 hPa) and temperature (red, 0.5°C, negative dashed) from 0545 UTC 13 March 2003. Barbs are gridded high-pass winds, in knots. WSI NOWrad base reflectivity in gray. Figure (b): same as (a), but for 0615 UTC.

bowing" stations would not exhibit this sharp pressure rise, and the onset of rain and arrival of cold pool would follower sooner or even simultaneously. However, it should be stressed that there were still exceptions to this pattern; the main point should simply be there were generally sharper pressure rises associated with the "bowing" stations, as well as a longer lag between the pressure rise/wind shift and the onset of rainfall/cold air.

One could theorize that the slower pressure rise rate prior to the wind shift was due to the non-hydrostatic effect of colliding air masses (Wakimoto 1982). The following sharper increase in pressure would be the leading edge of the mesohigh; this would match with the sudden experience of higher pressure observed at a typical "bowing" station. Since the mesohigh characteristically surged ahead of the convective line in bowing cases, this would also explain the longer interval between the wind shift/pressure rise and the start of the rain. Thus, at least from the examination of these timeseries, it would appear that the wind shift axis did surge with the mesohigh. A discussion of the dynamical implications of this will follow in Chapter 6.

Another feature apparent in Figs. 5.2a,b is the shift of the stratiform precipitation region to the left side of the convective line. This typically occurred between 30 to 120 minutes after the original appearance of the stratiform region in association with the convective line, depending if (as in the Merger cases) stratiform precipitation was already in existence when the convective line formed. On average, the larger the convective line/stratiform precipitation system, the longer the time period between the formation of the stratiform region and its shift to the left hand side. In addition, this shift could take place before or after the pressure surge - new bowing pattern. In the particular case of 13 March 2003, the stratiform region had shifted fully to the left within an hour after it had formed, which was 15 minutes prior to the start of new bowing.

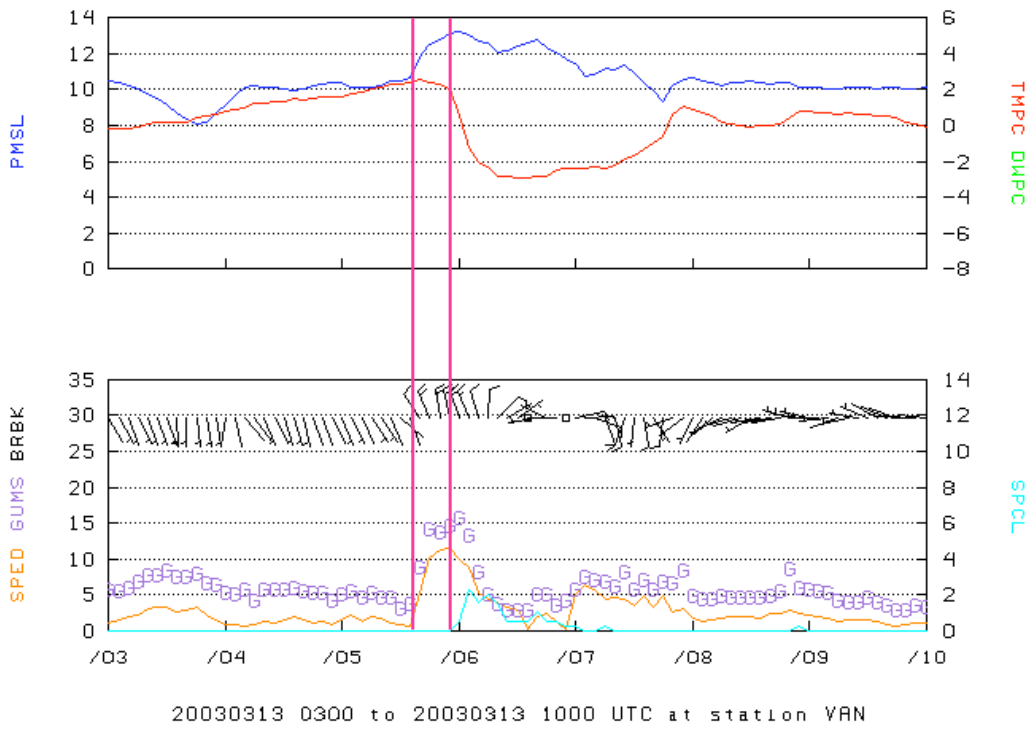

Figure 5.3: Timeseries display high-pass filtered data for station VANO, which experienced both the pressure surge and the newly bowed segment of the squall line. Adjusted pressure is in blue (hPa) with its scale on the upper left axis; temperature in red (°C) with its scale on the upper right axis; wind (knots) in the black barbs on the lower graph; unfiltered wind gusts (m sec^{-1}) in purple and sustained wind speed in orange with their scale on the lower left axis; and unfiltered precipitation rate (mm $(5\ min)^{-1}$) in aqua with its scale on the lower right axis. Time increases to the right, running from 0300 UTC on 13 March 2003 to 1000 UTC, same date. The wind shift occurred just after 0530 UTC, and the convective line along with the cold pool arrived just prior to 0600 UTC; these events are marked by vertical pink lines.

As the system continued through its lifecycle, the cold pool stayed centered behind the convective line and the bow, with its isotherms aligned with both (Fig. 5.5). Also noticeable in this figure is the wind convergence axis still running parallel to and just in front of the convective line and bow.

In this case, less than 2 h after the new bowing episode developed, the convective line began to dissipate. In other Classic cases, this time interval varied greatly, but was generally not longer than 3 h. The mesohigh, shown in Fig. 5.6a, was elongated backward and to the left, farther behind the convective line into the stratiform region.

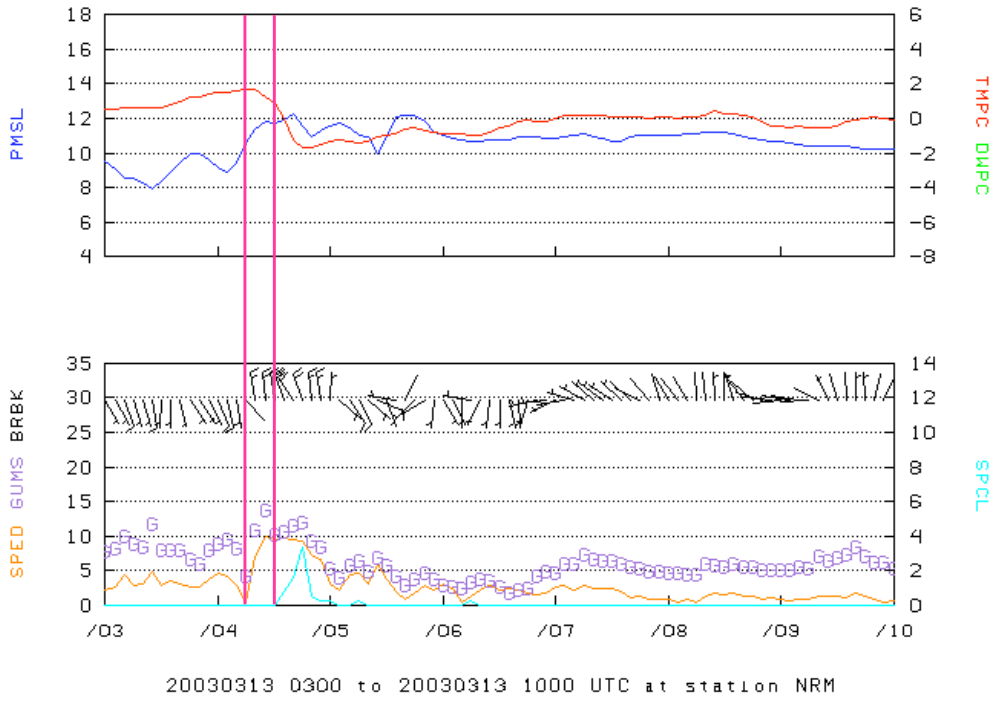

Figure 5.4: Same as Fig. 5.3, but for station NRMN, which experienced neither bowing nor pressure surge. The vertical pink lines correspond to the wind shift that occurred at 0415 UTC, and the convective line that passed at 0430 UTC.

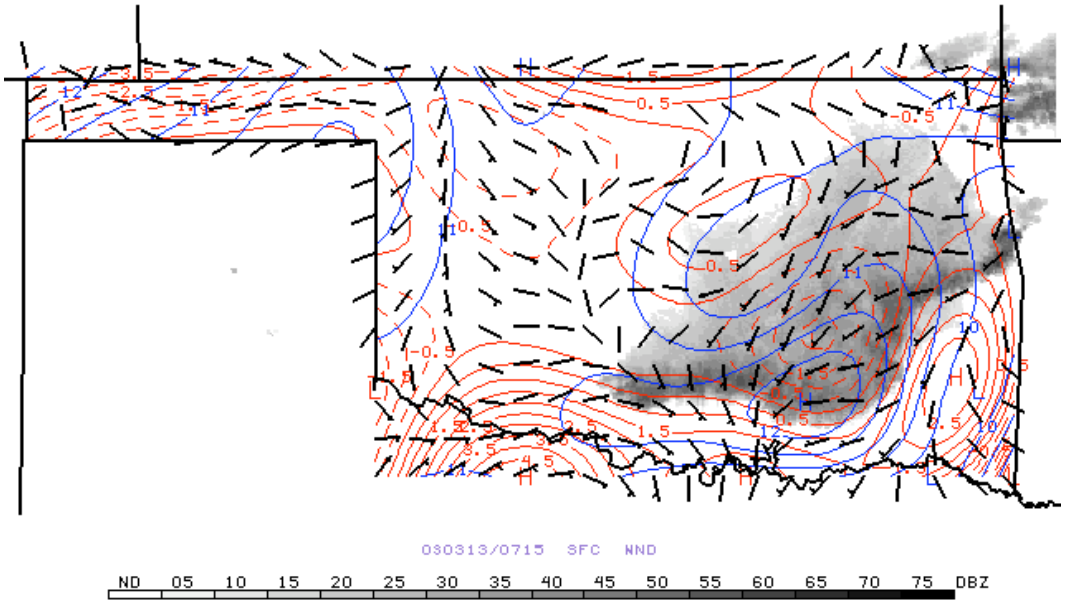

Figure 5.5: As in Fig. 5.2, but for 0715 UTC 13 March 2003.

While it is still about 25 km forward of the the cold pool (Fig. 5.6b), the two are much closer together than even 45 minutes prior (as was displayed in Fig. 5.5). The cold pool remained centered behind the bow apex as the convective line continued to dissipate. As the system had reached the edge of the observational analysis area at this time, it was difficult to fully trace an axis of convergence ahead of the convective line, but one was partially visible along the left side in Fig. 5.6a.

The above arrangement during dissipation, with only one mesohigh and cold pool both in the stratiform region and somewhat centered behind the dying convective line, was evident generally in only the smaller Classic bows. The case presented here was the largest Classic bow to still exhibit such behavior. However, when some of the larger bows entered the dissipation portion of their lifecycle, the mesohigh - cold pool arrangement instead appeared like that of Fig. 5.7, a Classic case of Merger initiation type, shown in its dissipation stage. The convective line runs north-south through the east-central portion of the state, and then curves to run about 200 km east-west along the southern Oklahoma border. There are two mesohighs in this dying system; one behind the left end of the convective line in the stratiform precipitation, and the hint of another on the right end of the convective line. Meanwhile, the cold pool remains centered about 75 km behind the convective line.

5.1.2 Classic Bow Echo discussion

After examining all of the cases in this category, there were a number of common patterns that appeared. While the ways in which the mesohigh and cold pool formed depended on the type of initiation, eventually the mesohigh shifted so it was about 25 km behind the right-center portion of the convective line, while the cold pool was centered about 50 km behind the convective line. There was also a large area of low pressure ahead of the convective line, and a region of warmer air in advance of the cold pool. A convergence axis ran parallel to the convective line.

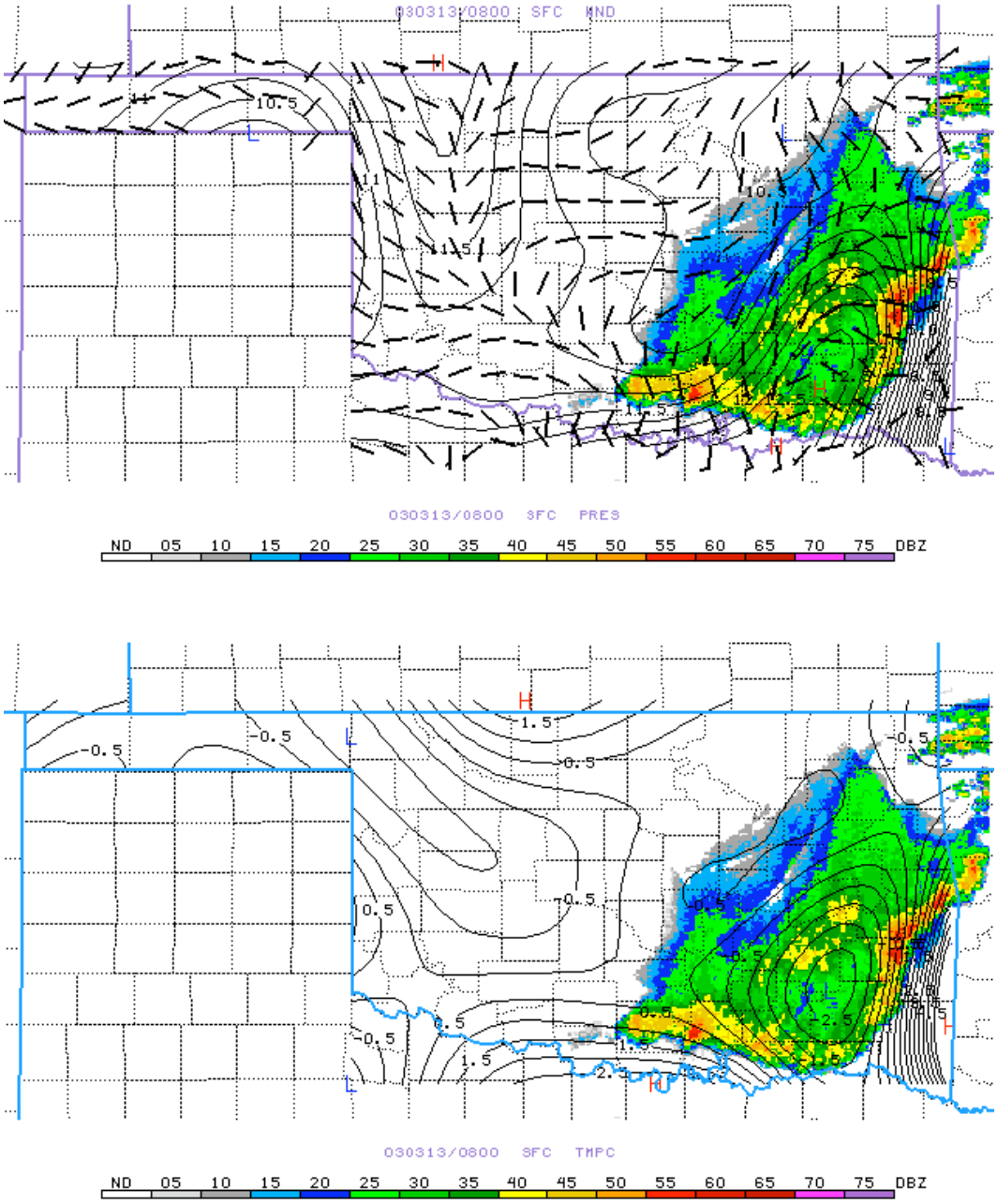

Figure 5.6: Figure (a): as in Fig. 5.1, but for 0800 UTC 13 March 2003. Figure (b): as in Fig. 5.1b, but for the same time as (a).

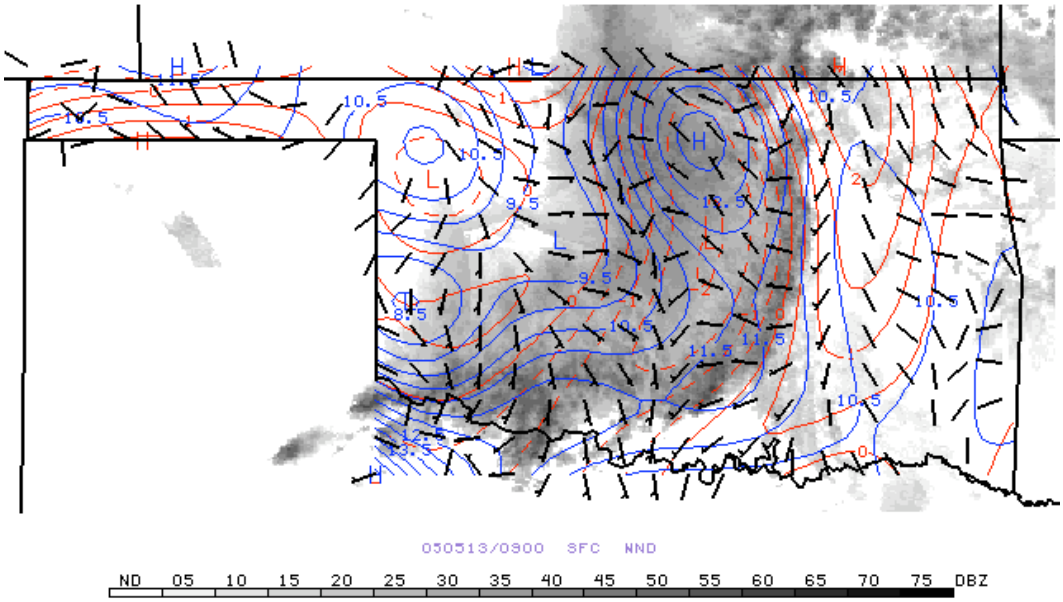

Figure 5.7: As in Fig. 5.2, but for 0900 UTC 13 May 2005.

Around the time of new bowing development, the mesohigh partially surged ahead of the convective line, while the cold pool stayed centered behind it. A new bowing segment formed to the left of the pressure surge, while the isotherms of the cold pool conformed to the new curved shape of the convective line. According to the various time series examined, the wind shift axis did surge with the pressure. Additionally, either prior to new bowing development or simultaneous to it, the stratiform precipitation region shifted to the left side of the convective line.

Table 5.1 displays the relationship between the pressure surge and the start of each new bowing episode which initiated within the state and was larger than 50 km. The largest plurality of cases followed the timeline outlined here, where the pressure surge preceded new bowing development by an average of 25.7 min. While the timing of the surge varied in relation to the start of new bowing, almost all cases exhibited a surge at some time associated with the new bowing.

As each case began to dissipate, there were two distinct behaviors of the mesohigh among the cases. Generally, the smaller cases exhibited only one mesohigh, which

Classic Bow Echoes

	Pressure Surge - New Bowing Relationship					
Initiation Type	Before	Simul.	After	None	Total	Surge/No Bow
Linear	3	0	0	0	3	0
Isolated	0	0	0	0	0	0
Merge	1	1	1	2	5	2
Total	7	4	3	3	17	4
Percent of Total	41.1%	23.5%	17.6%	17.6%	100%	
Mean Interval (min)	25.7	0	30.0			

Table 5.1: Number of Classic Bow Echo bowing episodes which were preceded by (Before), simultaneous to (Simul.), followed by (After), and not associated with (None) surges of the surface mesohigh. Surges not followed by new bowing (Surge/No Bow) are also indicated. The totals reported are larger than the figures in the column above as cases with an unknown initiation were included. Only episodes that, at start of bowing, were both larger than 50 km and inside the state were counted. Also noted is the mean time interval between the surge and onset of new bowing, in minutes.

shifted behind the center of the bow apex into the stratiform precipitation region. In the larger cases, the mesohigh split; one was located about 25 km behind the right side of the convective line, while the other was farther behind the left end of the convective line in the stratiform precipitation region. In both instances, the cold pool remained centered behind the bow apex, although it might shift further behind the convective line. The location of the mesohigh and cold pool in relation to each other as the system was dissipating, however, varied.

The reader will note that no reference to the wake low, a common feature associated with squall lines, was included in this discussion. While a wake low was often present with all cases (over all mature structures), its timing of development, positioning (other than generally behind the stratiform precipitation region), and appearance in relationship to the convective line varied so widely that a discussion of its common behaviors was impossible. This was made more difficult by the small geographical region of the Mesonet. Often portions of the stratiform precipitation region (and therefore, presumably, the wake low) were outside the state even though the convective line and associated mesohigh were within the boundaries. With a larger

observational region, perhaps typical characteristics of the wake low could be noted. This will be discussed further in Chapter 7. In the following case studies, however, while the reader can assume a wake low exists, assumptions regarding its placement and evolution should not be made.

5.2 Squall Line Bow Echoes

5.2.1 Linear initiation

All Squall Line Bow Echo cases were of Linear initiation. The case which best exemplified the surface patterns associated with these systems occurred on 06 June 2003; the squall line began to form at 0130 UTC. Both a mesohigh and a cold pool had already been associated with nearby convection; at this point they shifted so both were behind the right end of the most intense part of the squall line. This can be seen in Figs. 5.8a,b. While both are about 100 km behind the convective line, the mesohigh is 25 km farther to the right (to the southwest) than the cold pool; this alignment of the mesohigh farther right than the cold pool was not found in all cases, however.

Another feature which can be seen in Figs. 5.8a,b is the area of both lower pressure and warmer air ahead (to the southeast) of the newly forming squall line. At that time, the two were in the same location. This arrangement was also found in the other cases, although their colocation was perhaps not quite as precise. Also evident in the gridded high-pass filtered winds in Fig. 5.8a is the axis of convergence situated parallel to and just ahead of the newly forming squall line.

Thirty minutes later at 0200 UTC, the system entered a period very similar to the pressure surge - new bowing period found in the Classic structure bow echoes. Figures 5.9a,b depict this stage. In Fig. 5.9a, one can see high pressure surging ahead of the convective line. The cold pool remained centered behind the squall line with its isotherms aligned with the line itself; there was no surging of the cold pool. At

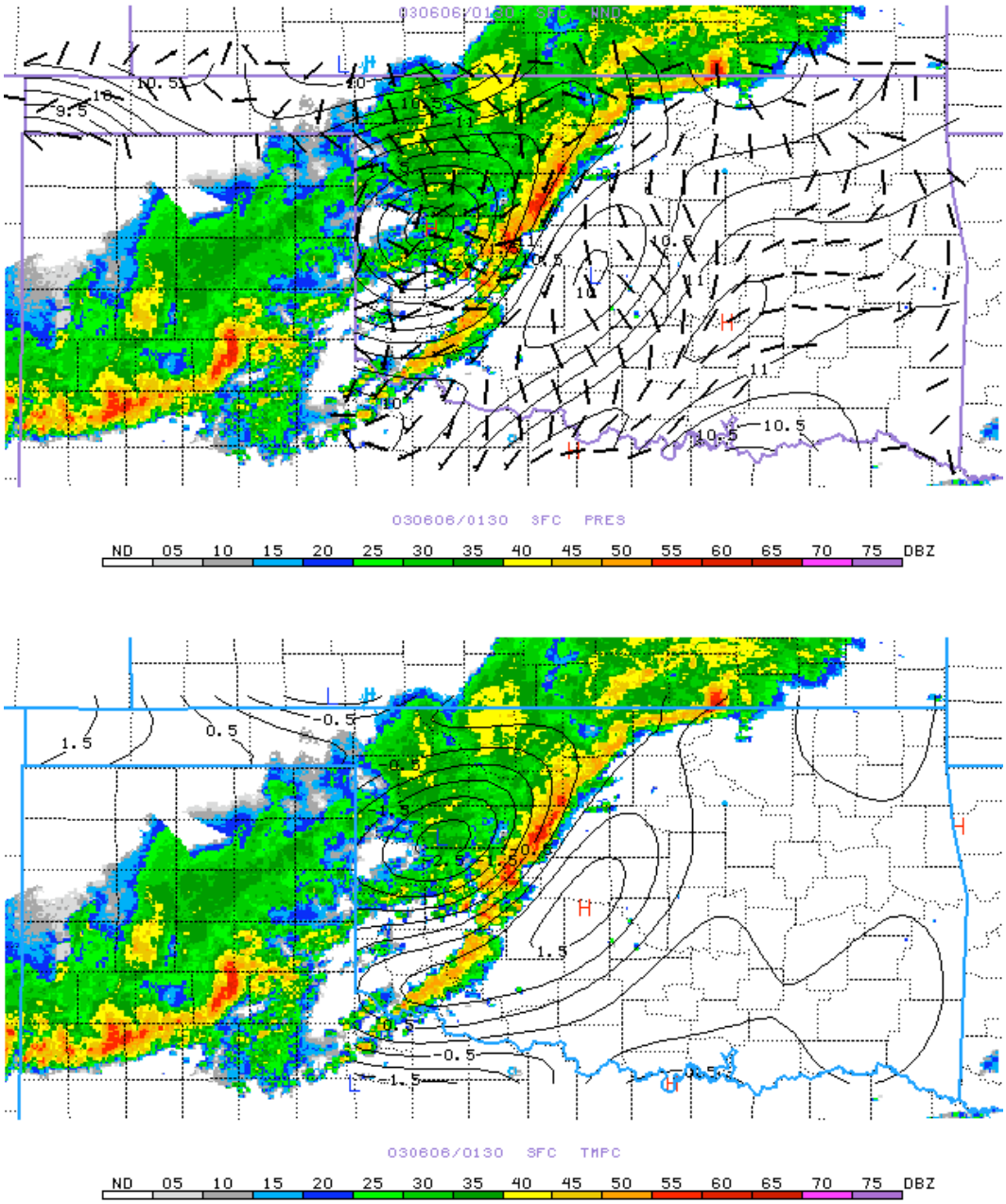

Figure 5.8: Figure (a): same as Fig. 5.1, but for 0130 UTC 6 June 2003. WSI NOWrad base reflectivity in color. Figure (b): high-pass temperature (0.5 °C) from the same time.

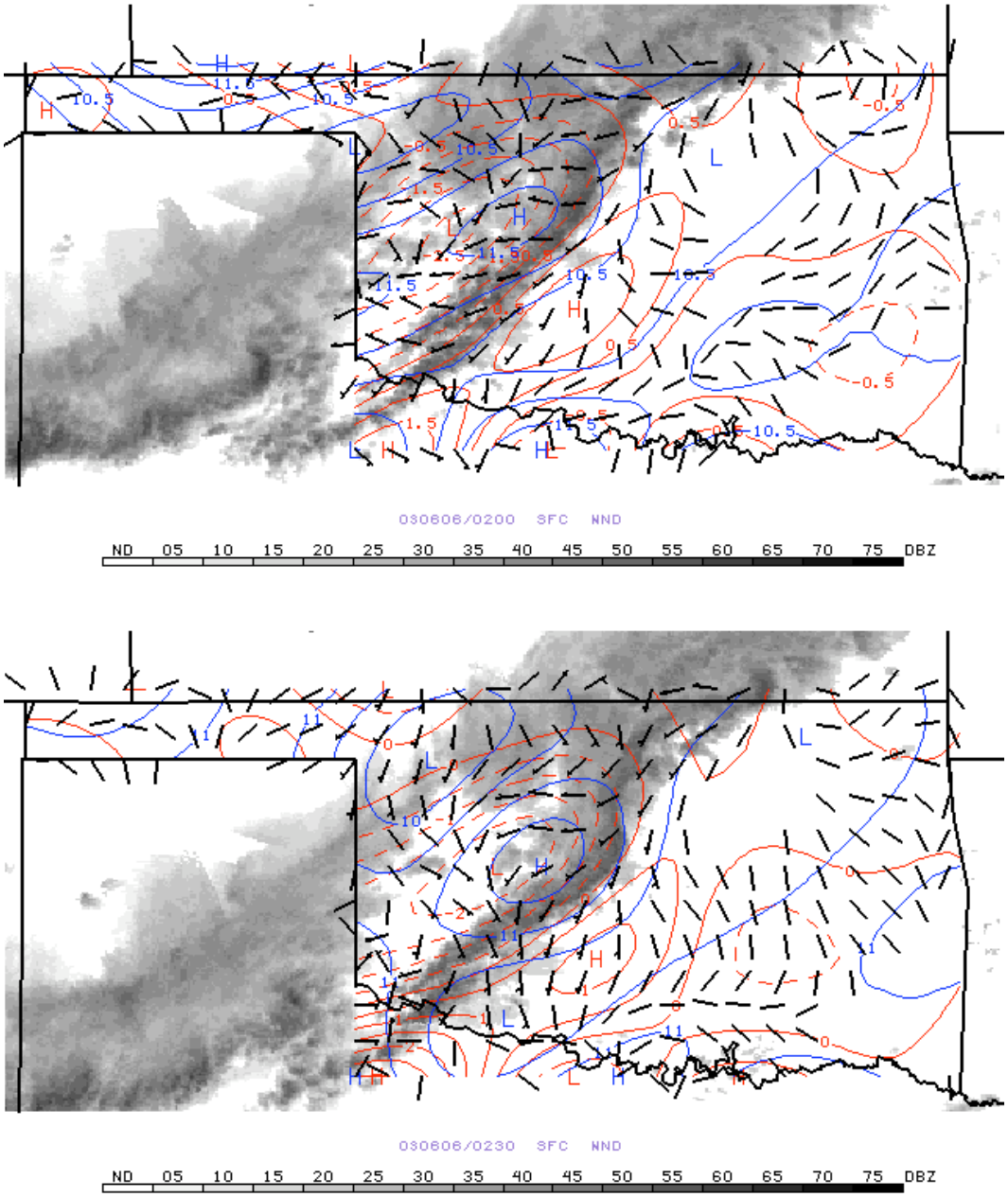

Figure 5.9: Figure (a): same as Fig. 5.2, but for 0200 UTC 6 June 2003. Figure (b): same as (a), but for 0230 UTC.

0230 UTC, shown in Fig. 5.9b, a bowing segment formed within the squall line, about 25 km to the left of the surge. The isobars still crossed the convective line, but the isotherms continued to conform to the line as it bows.

Even utilizing the gridded winds, at this resolution it is still difficult to examine whether the convergence (wind shift) axis ahead of the squall line surged with the mesohigh or remained parallel to the convective line itself. Timeseries of the surface data recorded at two different stations are presented in Figs. 5.10 and 5.11. Figure 5.10 is from a station which encountered both the pressure surge and the newly bowed squall line; the squall passed the station at 0230 UTC. Figure 5.11 is from a station the squall line passed at 0130 UTC, before both the pressure surge and bowing development. The location of these two stations (SPEN and WATO, respectively) is given in Fig. 3.1 in Chapter 3. In Fig. 5.10, (the "bowing" station) the pressure began rising at approximately 0220 UTC, prior to the wind shift which occurred at 0250 UTC. However, the pressure rise rate increased at the same time as the wind shift, just like in the "bowing" timeseries for the Classic bow echoes. The rain and cold air arrived just over 10 min later.

Meanwhile, in Fig. 5.11 (the "non-bowing" station), the pressure began to rise and the wind shifted both at 0100 UTC. The rain arrived and temperature dropped about 5 min later. While there was no distinct increase in the pressure rise rate at the time of the wind shift, the interval between the wind shift and rain/cold air onset was much smaller. Moreover, these timeseries would also seem to indicate that the wind shift axis surged with the mesohigh.

Also during the period from 0200 to 0230 UTC, there was still a region of warming ahead of the squall line that appeared in advance of the cold pool, shown in Figs. 5.9a,b. However, the region of low pressure originally associated with this warming had spread and weakened, so that there was merely a large region of slightly lower pressure located ahead of the entire squall line length. Additionally, the stratiform precipitation region shifted farther toward the left end of the convective line, giving the system an asymmetric appearance. This asymmetric behavior was found

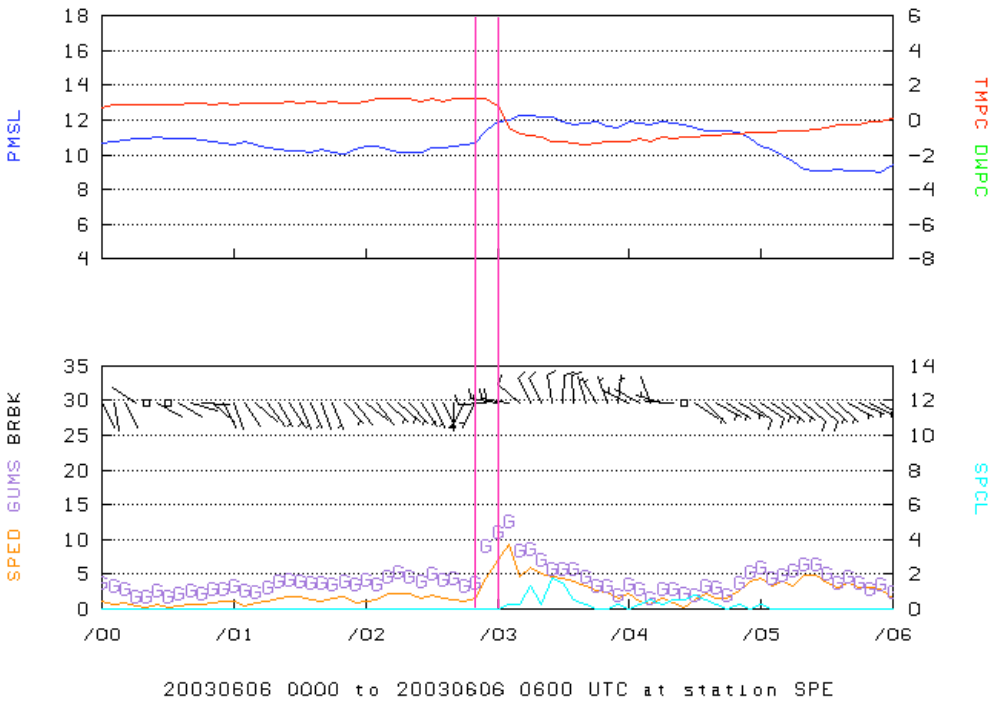

Figure 5.10: Timeseries display high-pass filtered data for station SPEN, which experienced both the pressure surge and the newly bowed segment of the squall line. Plotting convention same as Fig. 5.3. Time increases to the right, running from 0000 UTC on 06 June 2003 to 0600 UTC, same date. The vertical pink lines correspond to the wind shift that occurred at about 0250 UTC, and the convective line arrived at 0300 UTC.

in all the cases save one; in that case the stratiform region remained centered behind the squall line (not shown).

As the life of the system continued, the cold pool remained centered behind the more intense portion of the squall line; the isotherms also remained aligned with the convective line. Figure 5.12 displays this for the 6 June 2003 case. The warm region, originally in advance of both the squall line and cold pool, shifted to the right (southward) out of the state; very possibly it relocated nearer a stronger cold pool associated with the stronger convection in that part of the squall line. Also evident in Fig. 5.12 is the mesohigh's closer proximity to the squall line than the cold pool. The center of the mesohigh also persisted in its location to the right of the more intense

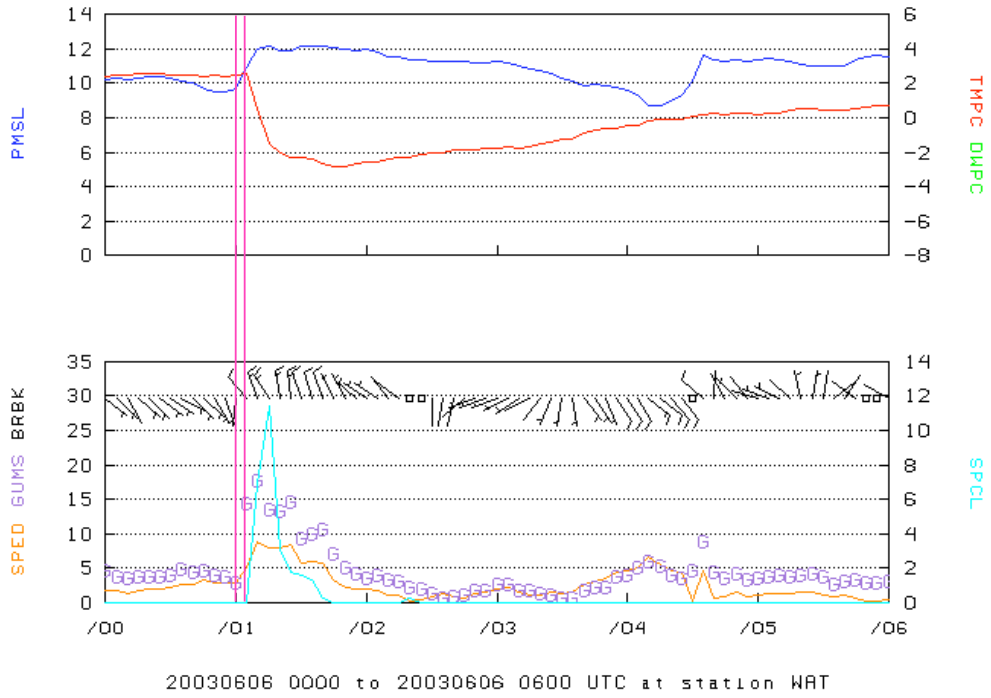

Figure 5.11: Same as (a), but for station WATO, which experienced neither bowing nor pressure surge. The wind shifted at 0100 UTC, and the squall line passed 5 min later; these are marked by vertical pink lines..

convection. The gridded winds in Fig. 5.12 show that the axis of convergence grew less defined; this trend continued as the squall line dissipated.

Dissipation commenced around 0400 UTC. At that point, as seen in Figs. 5.13a,b, what was the convective line at the leading edge of the system had almost entirely converted to stratiform precipitation, at least in the state of Oklahoma. Meanwhile, there was no longer a well-defined axis of convergence preceding the squall line evident in the gridded wind field. The mesohigh split into two: one continued to follow the convective line to the right of what was once the bowing segment (typically now the most intense part of the convective line); the other shifted so it was collocated with the strongest stratiform rain at the left edge of the system (Fig. 5.13a). As the squall continued dissipating, the mesohigh proceeded behind the most intense part of the leading edge of the squall line.

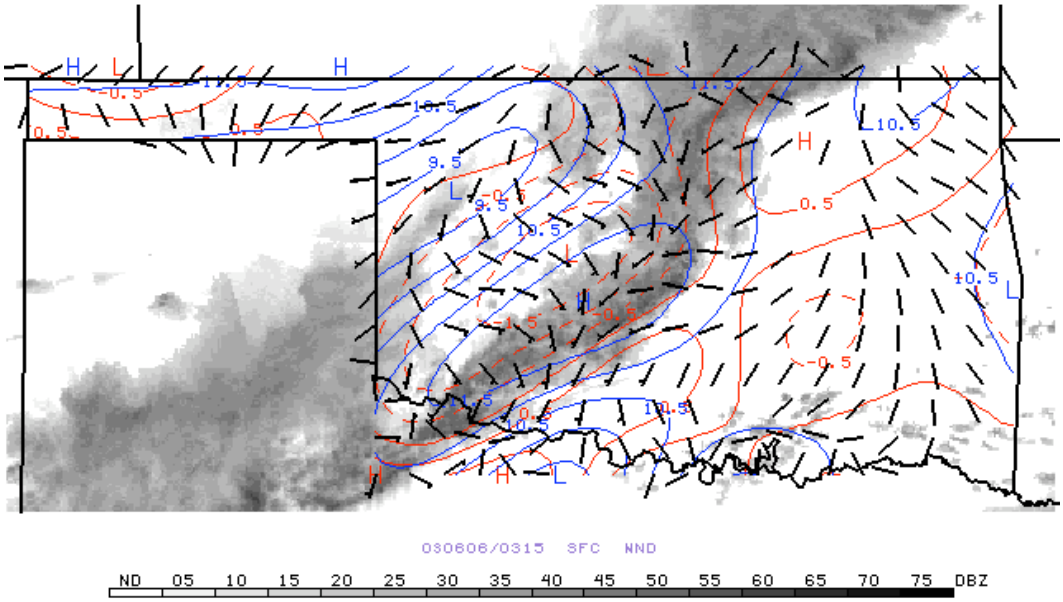

Figure 5.12: As in Fig. 5.1, but for 0315 UTC, same date.

The cold pool was still centered behind what was left of the convective line, depicted in Fig. 5.13b; a second cold pool appeared to be located to the left, in the most intense region of stratiform rain. Both of these cold pools were between 25-50 km behind their respective mesohighs, and continued in these positions until the squall line fully decayed. The splitting behavior of both the mesohigh and the cold pool was observed in all cases in this category, with the exception of the case with stratiform precipitation remaining centered behind the squall line throughout its lifetime (not shown).

5.2.2 Squall Line Bow Echo discussion

The key features the Squall Line Bow Echo cases generally exhibited were very similar to those of the Classic Bow Echoes. At the initiation of the convective line, a mesohigh was already associated with it. In this category the mesohighs were found to the right of the more intense convection along the squall line. A cold pool was collocated here, in the same general area as the mesohigh. There was also a well-

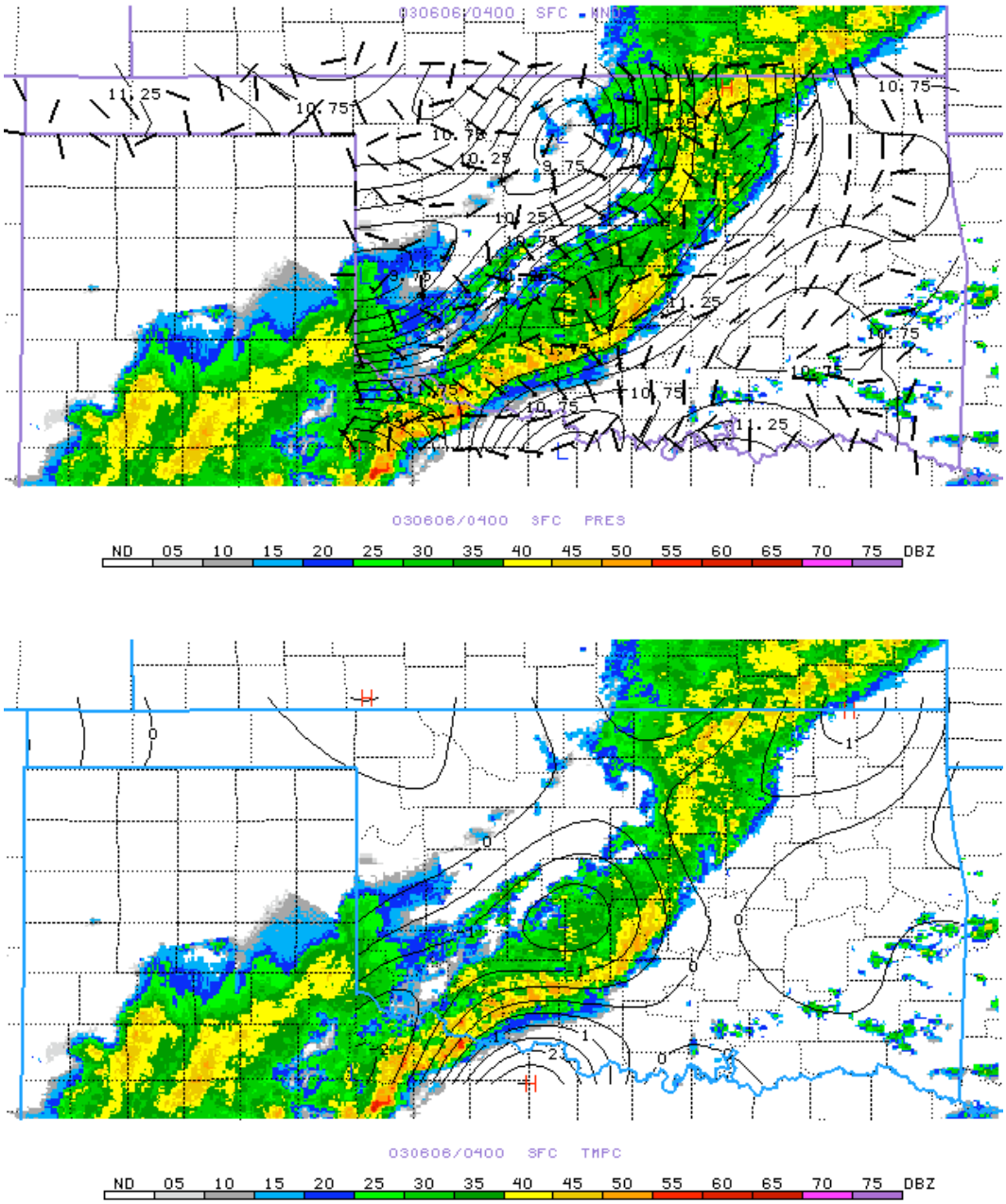

Figure 5.13: Figure (a): as in Fig. 5.8a, but for 0400 UTC. Figure (b): as in Fig. 5.8b, but for 0400 UTC.

Squall Line Bow Echoes

	Pressure Surge - New Bowing Relationship					
Initiation Type	Before	Simul.	After	None	Total	Surge/No Bow
Linear	3	1	0	0	4	0
Total	3	1	0	0	4	0
Percent of Total	75.0%	25.0%	0.0%	0.0%	100.0%	
Mean Interval (min)	20.0	0	N/A			

Table 5.2: As in Table 5.1, but for Squall Line Bow Echo bowing episodes.

defined axis of convergence located about 25 km ahead of the convective line. This was possibly either a manifestation of a gust front or fine line ahead of the actual convection; finer resolution than the current observational system allows would be needed to resolve this. A region of lower pressure and warmer temperatures preceded the convective line and appeared to be associated with the cold pool. While over time the lower pressure region dissipated, the region of warming associated with the cold pool remained throughout the system's lifetime.

A little over an hour after the squall line formed, the leading edge of the mesohigh surged ahead of it at one location. The associated cold pool generally stayed centered behind the line. A segment of the line bowed out shortly thereafter, with the apex of this new bow to the left of the pressure surge. This process could be repeated multiple times before the squall line dissipated. Information about the pressure surge - new bowing behavior is provided in Table 5.2. One of the bowing episodes that fell in this category did not meet the 50 km size requirement; otherwise all of the episodes exhibited an associated pressure surge. In addition, in three of the four episodes in this category this surge preceded the new bowing by an average of 20 min. With examination of station timeseries plots, it appeared that the wind convergence axis surged with the mesohigh; however more cases will be needed for a definitive conclusion.

As the squall line began to dissipate, the mesohigh split into two: one part still remained on or just behind the right end of the more intense portions of the convective line, while another formed in the stratiform region near the area of most intense stratiform rain. Meanwhile, there were also now two cold pools, both about 25-50 km behind each mesohigh. There was no longer a clear convergence axis ahead of the squall line, indicating the lack of a sharp delineation between the storm outflow and air ahead of the system.

5.3 Bow Echo Complex

5.3.1 All initiation types

As there was only one case in the Bow Echo Complex category that was not of the Merger initiation type, this section will focus on patterns found among all the Bow Echo Complexes at once. As in the previous two sections, one case which seemed to exemplify the main characteristics of the type will be presented; points in which cases differ from this will be noted. Although 14 of 15 BEC cases had Merger initiations, the case with Isolated initiation on 17 May 2002 was typical of almost all BEC cases. The isolated cell entered the state at 0400 UTC (not shown.) At 1130 UTC, the system had not completely dissipated but at that point exited the state.

Because the convection which formed the convective line in a Bow Echo Complex has other convection surrounding it, often a mesohigh and cold pool would already be nearby when the system initiated. Figures 5.14a,b depict the beginning stages of the 17 May 2002 bow echo. Note the mesohigh and cold pool were both located together and centered behind the new bow. (As the new bow in this case formed so soon after entering the state, it is impossible to state with certainty that both the mesohigh and cold pool were already in existence. However, this pattern was common in numerous other BEC cases.) These two features were originally associated with the convection to the north and east of this case; they shifted toward the new bow as it formed. A

wind shift or convergence axis can be seen parallel and very close to the front edge of the new bow in Fig. 5.14a.

Also evident in these figures was the positioning of the stratiform precipitation region to the left side of the newly formed bow. With so much convection already existing in the area, by the time the convective line of the complex formed there was not only stratiform precipitation associated with it, but it was also already shifted to the left side of the convective line. This behavior was apparent in a large majority of the cases.

Located about 200 km ahead (to the southeast) of the bow echo were both a warm region and a pre-squall mesolow (seen in Figs. 5.14a,b). At this point in the lifecycle, they are in the same location; this was apparent in most of the cases. A feature unique to Bow Echo Complexes was that not only did the warm pool appear to be almost as intense as the cold pool, but the pre-squall mesolow was almost as intense as the mesohigh. Perhaps since the circulations attendant with the formation of the mesohigh persisted longer, they were also able to further amplify the pre-squall mesolow and warm region. However, while the warm anomalies did remain more intense, the stronger pre-squall mesolow did not persist throughout the complex's lifecycle, as will be seen.

Figures 5.15a,b display the typical pressure surge - new bowing relationship for the Bow Echo Complex cases. In Fig. 5.15a, the mesohigh partially surged ahead of the convective line on its right side. Meanwhile, the cold pool stayed centered behind the already existing bowing segment. In the next figure in the sequence, Fig. 5.15b, one can see the new bowing development which formed on the right edge of the convective line, to the left of the pressure surge. Note the isotherms of the cold pool remained parallel to the convective line, even as it bowed. This same cycle was seen again in Figs. 5.16a,b. In Fig. 5.16a, the mesohigh again crossed partially ahead of the convective line with the cold pool remaining centered behind; this was followed

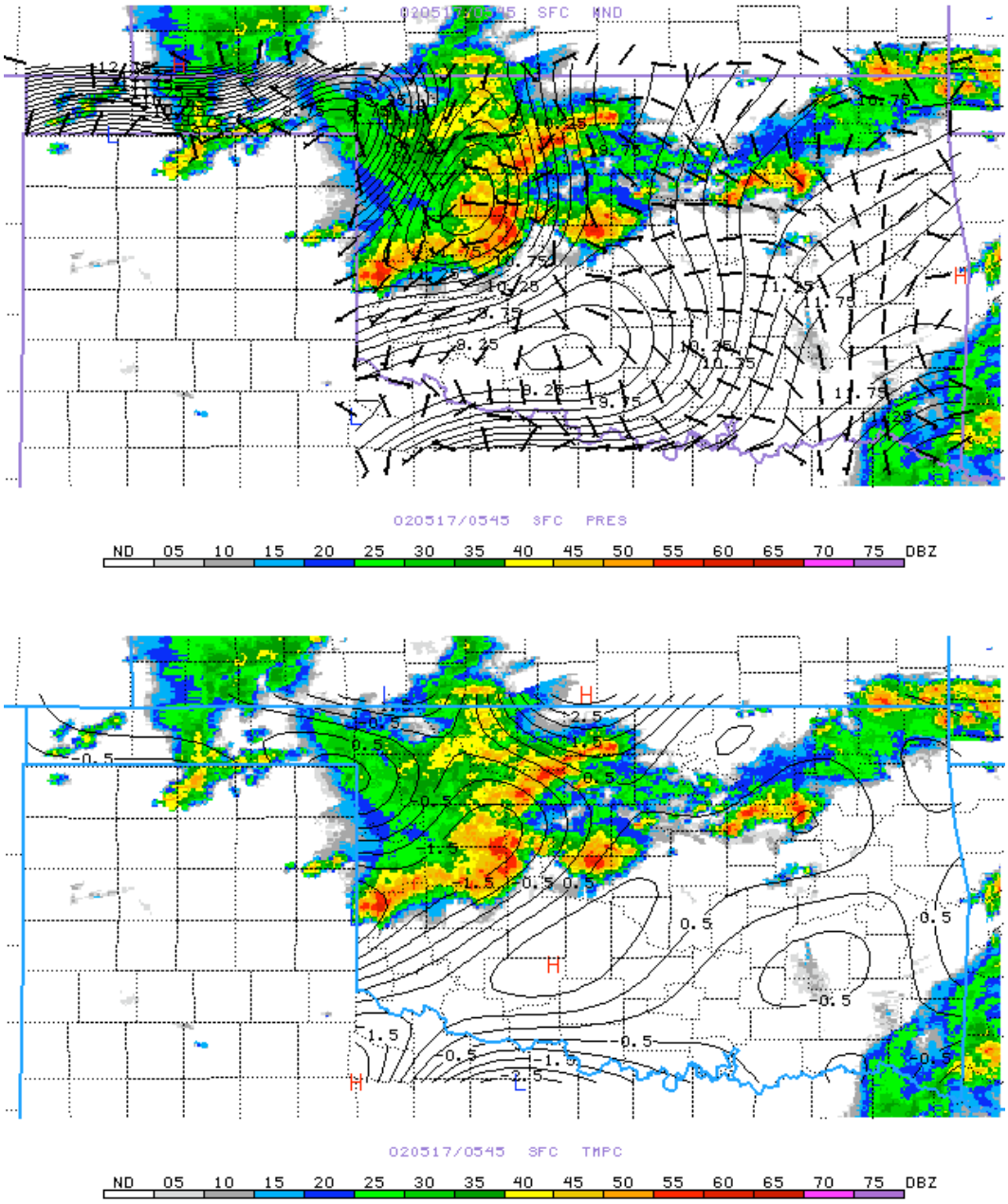

Figure 5.14: Figure (a): same as Fig. 5.1, but for 0545 UTC 17 May 2002. WSI NOWrad base reflectivity in color. Figure (b): high-pass temperature (0.5 °C) from the same time.

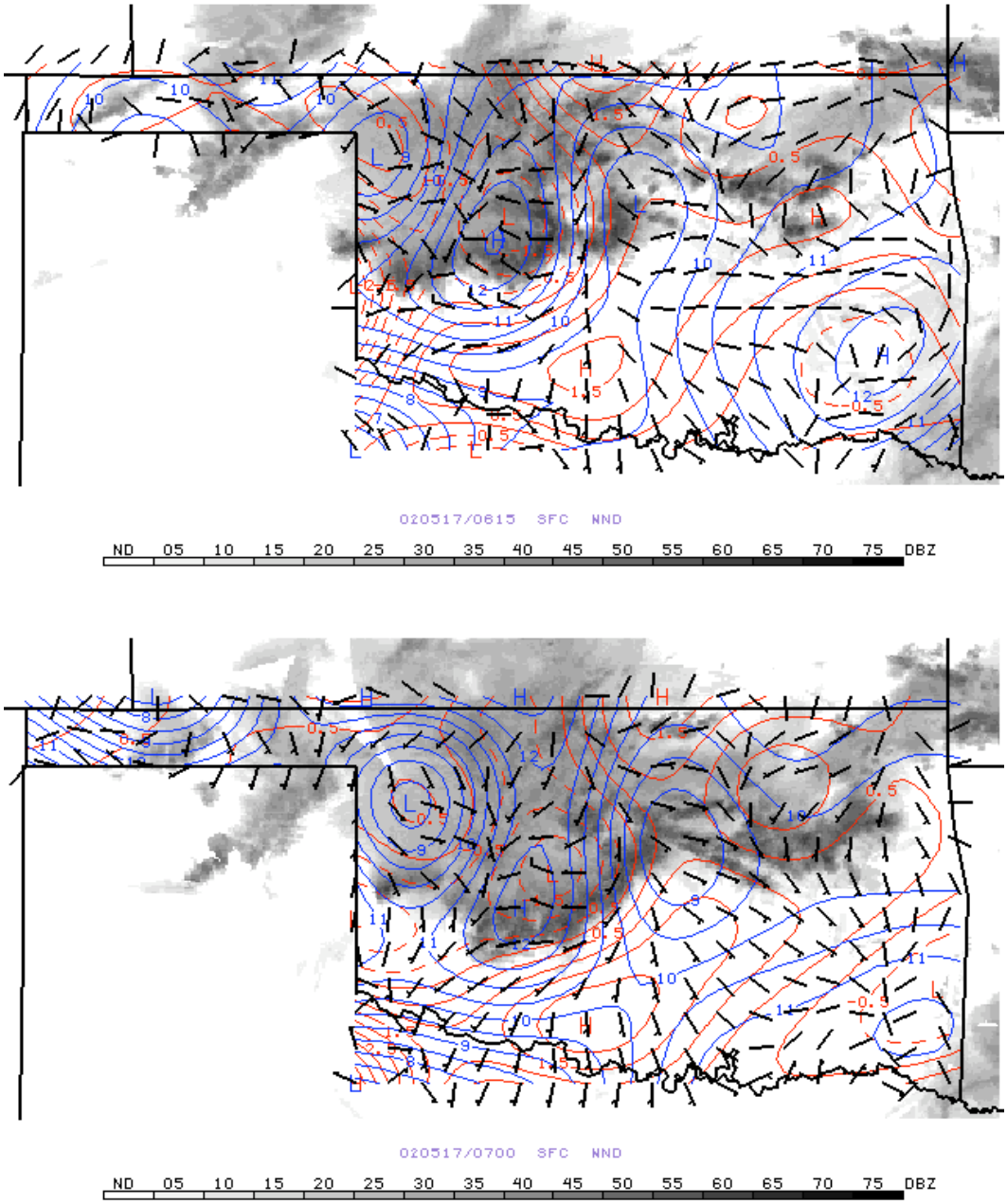

Figure 5.15: Figure (a): same as Fig. 5.2, but for 0615 UTC 17 May 2002. Figure (b): same as (a), but for 0700 UTC.

by the new bowing development to the left of the surge in Fig. 5.16b. Again, the cold pool remained centered behind this new bowing segment. While not all cases exhibited multiple bowing segments, as seen here, the pressure surge - new bowing behavior was evident in almost all.

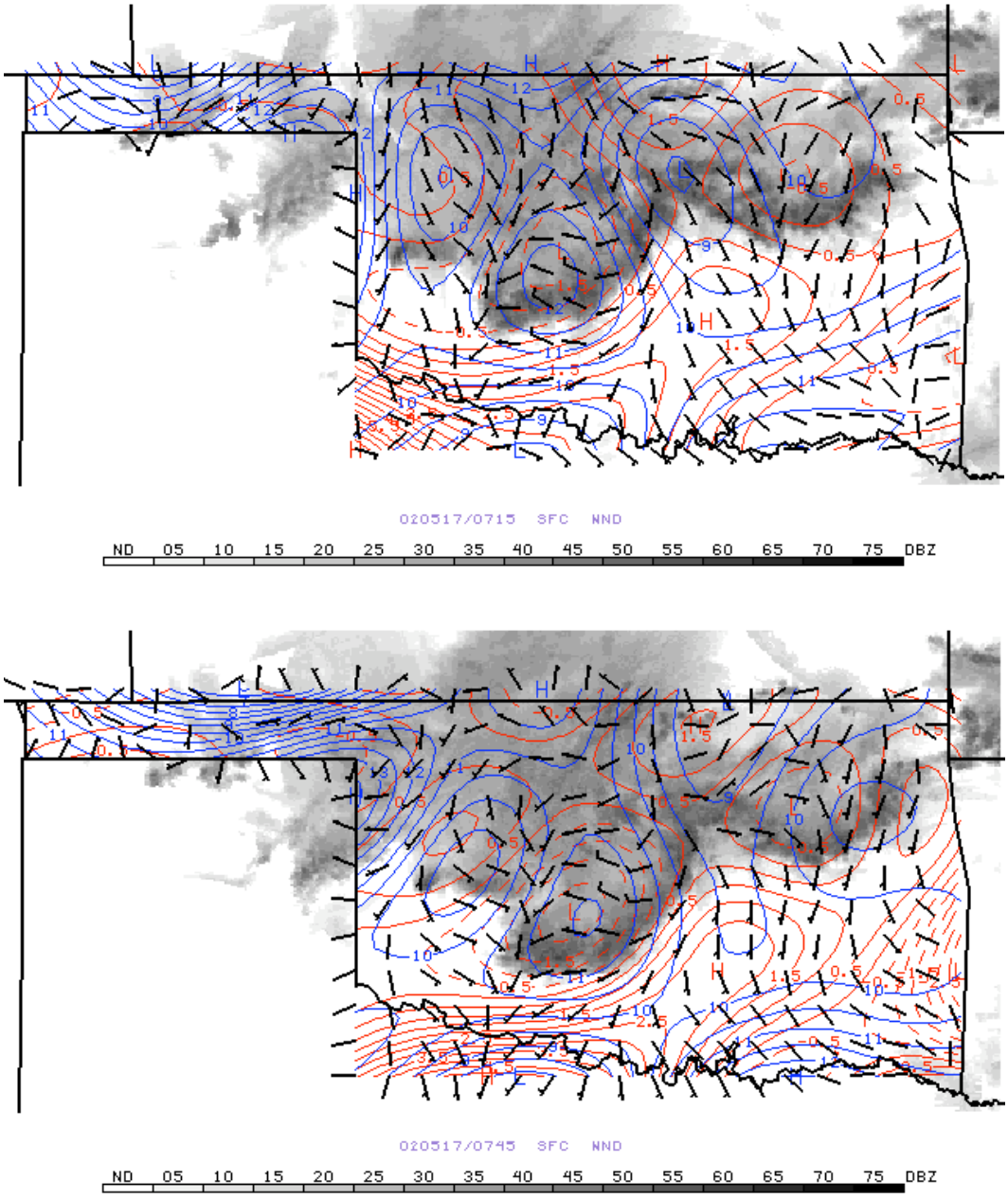

Figure 5.16: Figure (a): same as Fig. 5.2, but for 0715 UTC 17 May 2002. Figure (b): same as (a), but for 0745 UTC.

Timeseries from stations PAUL (which experienced the bowing portion of the convective line at 0800 UTC) and BOWL (passage of non-bowing convective line segment at 0820 UTC) are displayed in Figs. 5.17 and 5.18, respectively. The locations of these are given in Fig. 3.1. Noticeable in both segments was the start of a very gradual pressure rise. At station PAUL (Fig. 5.17) this was evident just before 0800 UTC. A wind shift, onset of stronger winds, and a sharp pressure rise began about 5 min later. The start of the rain and the passage of the cold pool occurred 7.5 min after that, when the convective line passed.

On the other hand, at station BOWL, a gradual pressure rise starting just before 0820 UTC occurred about 5 min prior to the wind shift, wind gust onset, and start of a sharp pressure rise. These things occurred almost simultaneously with the onset of the rain and cold pool, which arrived less than 5 min later. Thus, at the "bowing" station, the time interval between the start of the sharp pressure rise and the cold pool/rain arrival was about 10 min longer than at the non-bowing station. This could indicate that the front edge of the mesohigh was farther ahead of the convective line at the bowing station than the non-bowing one. Therefore, the mesohigh was much closer to the front of the convective line at times of new bowing (where it was positioned from its recent surge) than in times of non-bowing. In addition, the wind shift ahead of the convective line was clearly coupled to the pressure rise and not the temperature drop; therefore the convergence axis most likely did surge with the mesohigh. The implications of this will be discussed in Chapter 6.

As the complex began to dissipate, there were two distinctly different mesohigh behaviors, just like in the Classic Bow Echo category. In the case being presented, the mesohigh shifted so that a portion of it was far behind the left side of the convective line, in the stratiform precipitation region. It was also deformed from its originally circular shape: it now stretched from the stratiform region down to just behind the right side of the convective line. This can be seen in Fig. 5.19a. In some cases, like this

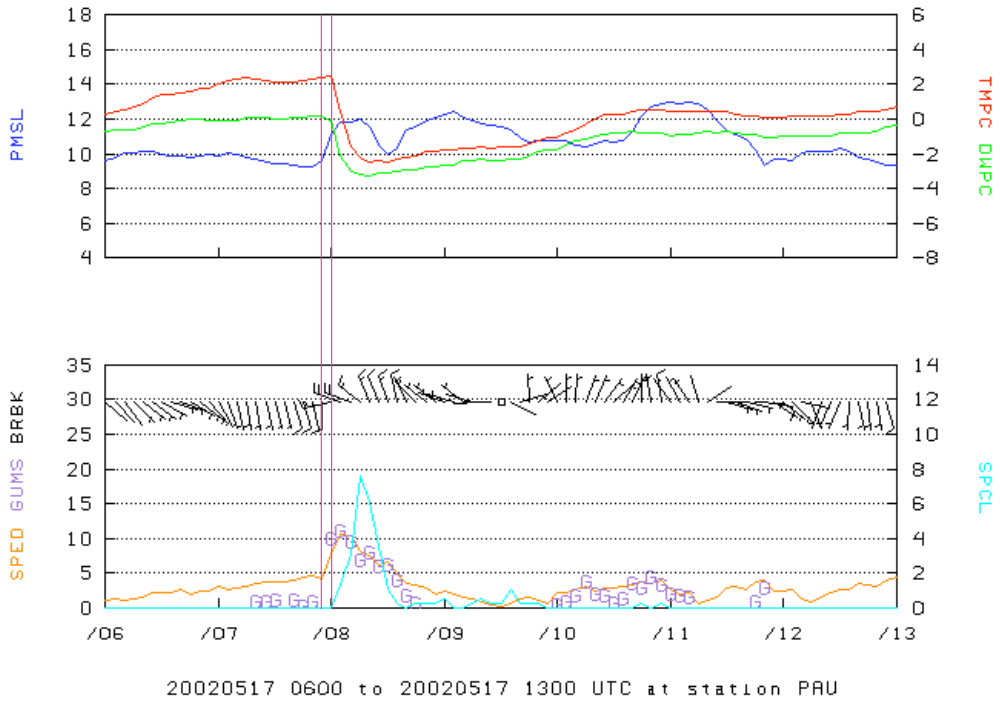

Figure 5.17: Timeseries display of high-pass filtered data for station PAUL, which experienced both the pressure surge and the newly bowed segment of the squall line. Plotting convention same as Fig. 5.3. Time increases to the right, running from 0600 UTC on 17 May 2002 to 1300 UTC, same date. The first pink line indicates the wind shift, wind gust onset, and start of the sharp pressure rise, at 0755 UTC. The second pink line signals the arrival of the cold pool and rain, when the bow echo passed at 0800 UTC.

one, the mesohigh actually split into two, with the second mesohigh located typically on or just behind the right end of the convective line. The cold pool still remained in its location centered about 100 km behind the convective line, and stayed in that location until the convective line fully dissipated. Fig. 5.19b shows this behavior for the 17 May 2002 case.

The other mesohigh behavior appeared in three smaller cases, again just like the Classic Bow Echoes. A dissipating Bow Echo Complex from 21 June 2004 provided an excellent example of this behavior. In Fig. 5.20a, the mesohigh in the dissipating, easternmost bow echo had shifted back behind the left end of the convective line into the stratiform region. It was still somewhat elongated toward the right side of

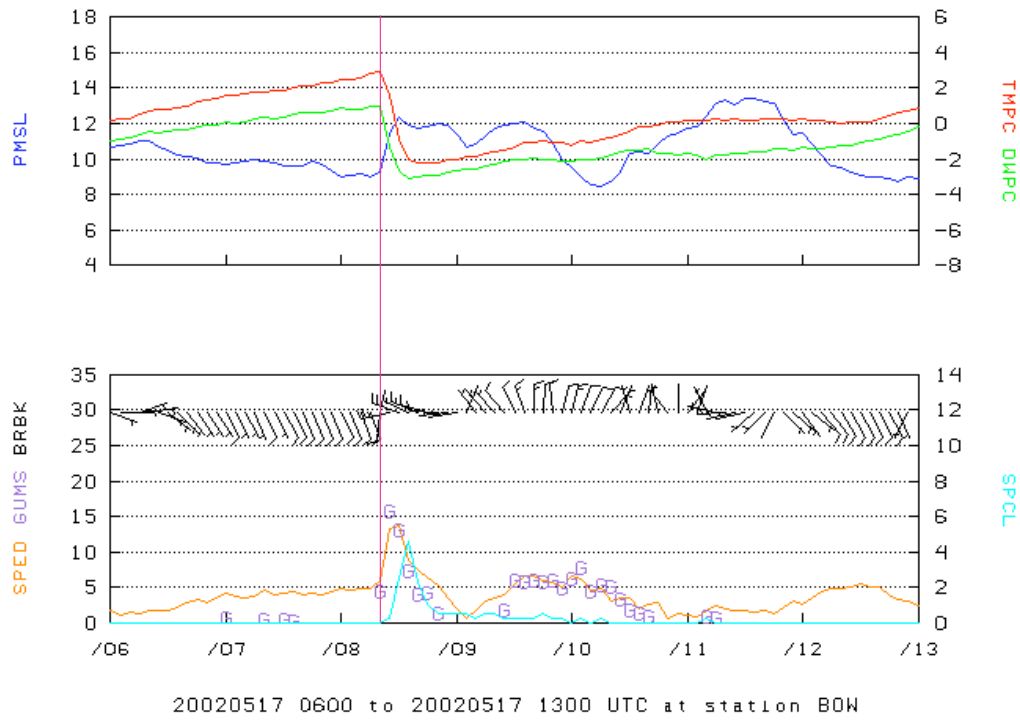

Figure 5.18: Same as (a), but for station BOWL, which experienced neither bowing nor pressure surge. The pink line indicates the wind shift, wind gust onset, start of the sharp pressure rise, temperature drop, and rain onset; all simultaneous when convective line passed around 0820 UTC.

the convective line, but not as much as the 17 May case; in the other smaller cases this elongation is still less. In addition, in some of the other smaller cases both the mesohigh and stratiform precipitation stayed more centered behind the convective line. The cold pool behavior remained the same in all cases, however - still centered around 100 km behind the dying convective line (Fig. 5.20b).

5.3.2 Bow Echo Complex discussion

The behavior of the surface patterns associated with Bow Echo Complexes were very similar to those of the Classic Bow Echoes. The only main difference was that both a mesohigh and cold pool were already associated with pre-existing surrounding precipitation. Once a convective line emerged from this, this mesohigh and cold pool

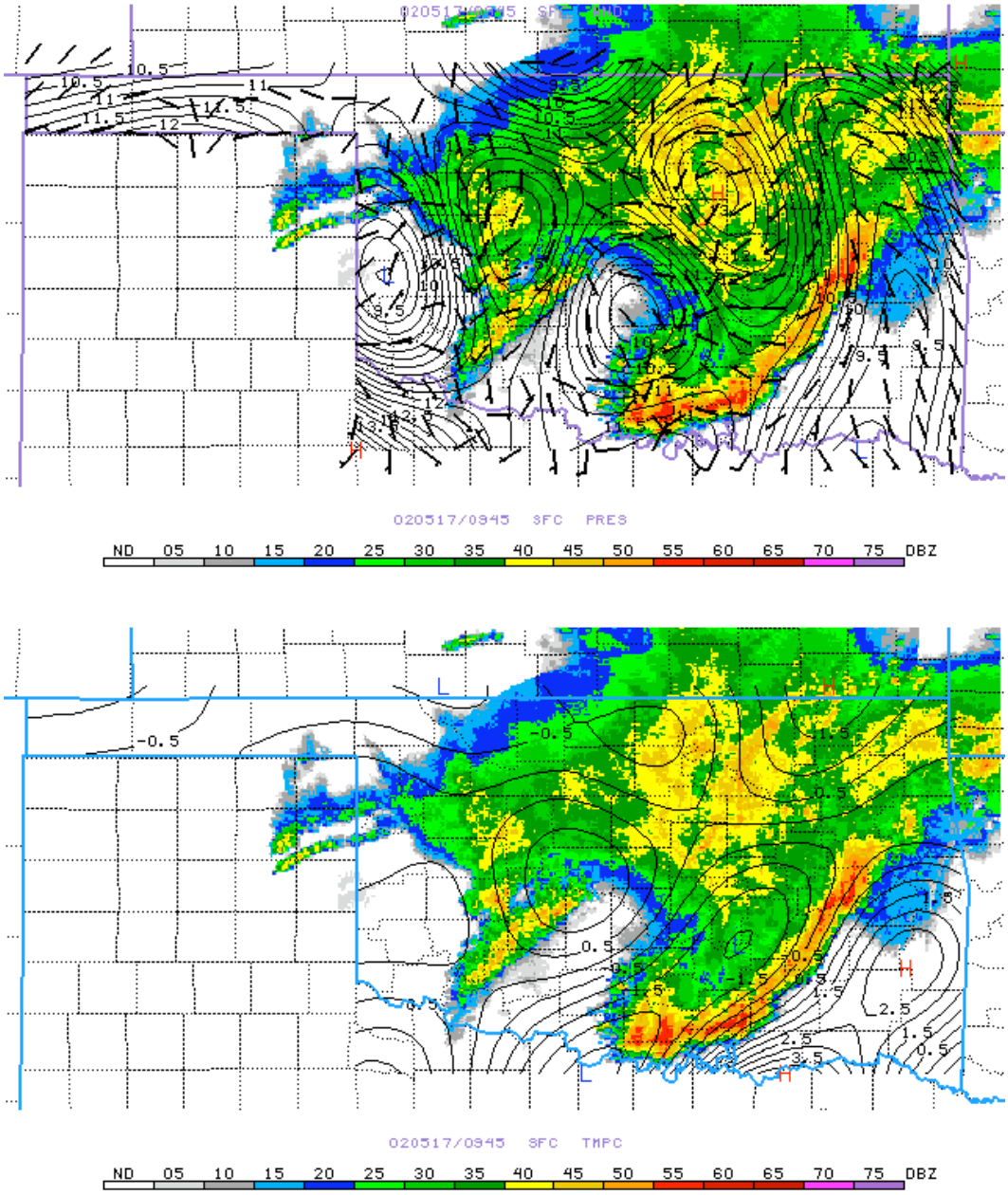

Figure 5.19: Figure (a): same as Fig. 5.1, but for 0945 UTC 17 May 2002. WSI NOWrad base reflectivity in color. Figure (b): high-pass temperature (0.5 °C) from the same time.

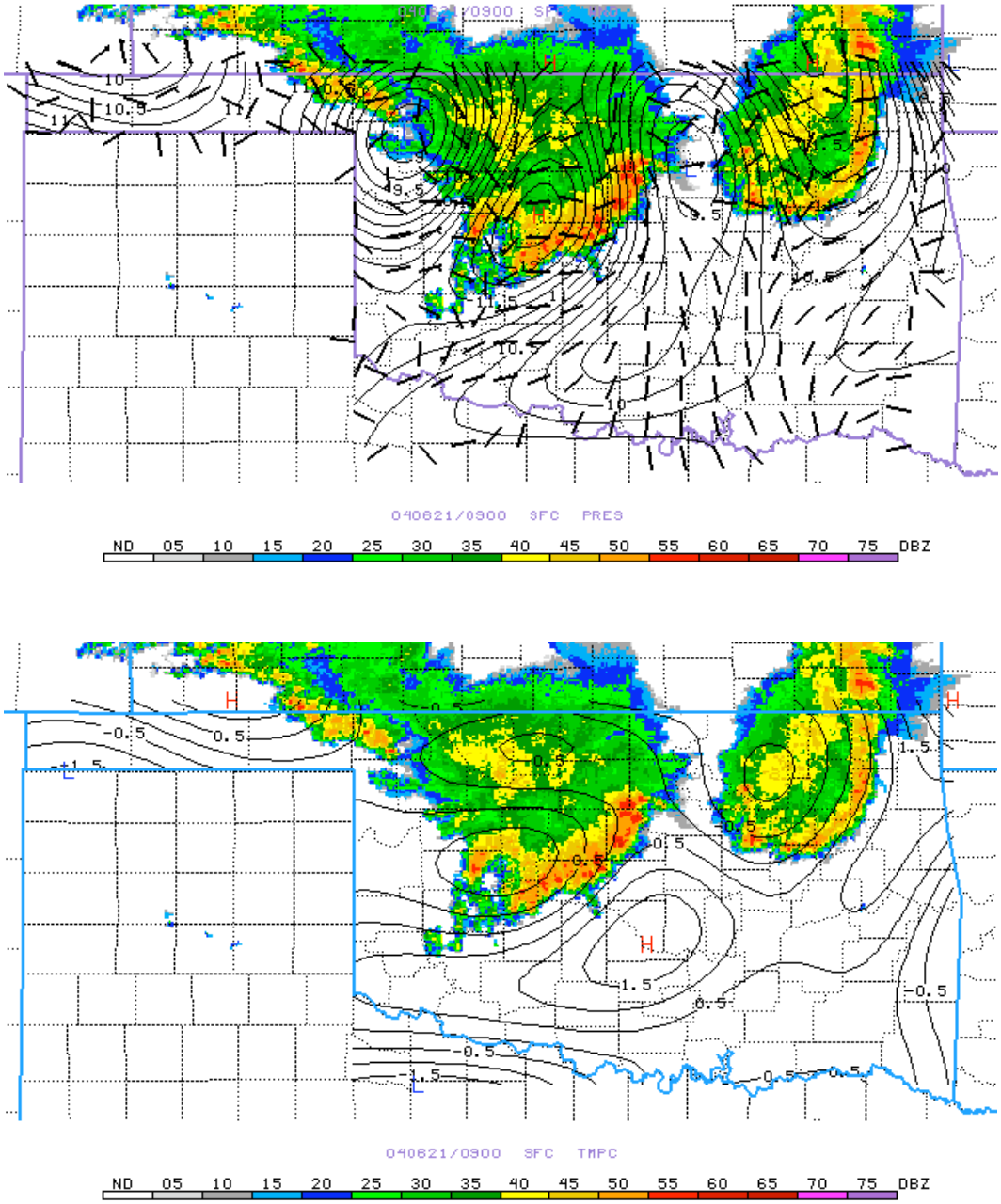

Figure 5.20: Figure (a): same as Fig. 5.1, but for 0900 UTC 21 June 2004. WSI NOWrad base reflectivity in color. Figure (b): high-pass temperature (0.5 °C) from the same time.

shifted to be associated with the new feature. Nearby stratiform precipitation also shifted to be behind the newly formed convective line's left side.

During the beginning stages, the mesohigh and cold pool were collocated, centered about 50-100 km behind the convective line. At a highly variable time later (30 min to 3 h), the mesohigh surged entirely or partly ahead of the convective line while the cold pool remained centered behind. A new bowing segment developed about 50-100 km to the left of this surge. The isotherms of the cold pool continued to run parallel to the convective line, conforming to it even as it bowed. Table 5.3 breaks down the timing relationship between this pressure surge and new bowing development. For Bow Echo Complexes, by far and large the most favored mode was the pressure surge preceding new bowing development. The time period between the two (an average of 35.8 min) was also greater for Bow Echo Complexes than either Squall Line Bow Echoes or Classic Bow Echoes (which had means of 25.7 and 20.0 min, respectively). However, the standard deviation of the BEC mean is quite wide: 22.5 min over the 13 'before' cases. As this structure type was less defined and not as tightly organized as the others, the wider array of time intervals makes sense.

Once the convective line began to dissipate, the mesohigh shifted about 100 km rearward and to the left into the region of stratiform precipitation. For larger complexes, the mesohigh also stretched toward the right end of the convective line; occasionally a second mesohigh formed in that location. The cold pool remained centered approximately 100 km behind the dissipating bow echo.

5.4 Synthesis

After examining the patterns associated with each of the active bowing structures in detail, it is evident that a common behavior exists. There were generally two different structures found: smaller bow echoes that when dissipating exhibited only one mesohigh (and usually still a centered area of stratiform precipitation), and larger

Bow Echo Complexes

	Pressure Surge - New Bowing Relationship					
Initiation Type	Before	Simul.	After	None	Total	Surge/No Bow
Isolated	2	0	0	0	2	0
Merge	11	1	0	2	14	3
Total	13	3	0	2	18	3
Percent of Total	72.2%	16.7%	0.0%	11.1%	100.0%	
Mean Interval (min)	35.8	0	N/A			

Table 5.3: As in Table 5.1, but for Bow Echo Complex bowing episodes.

bow echoes with an elongated mesohigh (or even two split mesohighs) apparent during dissipation, with stratiform precipitation shifted to the left. A conceptual model depicting the evolution of these two structures is proposed in Fig. 5.21. The top row of figures corresponds to the smaller, one mesohigh bow echo, and the bottom row the larger bow echo with an elongated mesohigh.

The first column in the figure illustrates the arrangement of a system immediately following the formation of the convective line. As was noticeable throughout this chapter, the manner of initiation of bow echoes was highly varied, even within the same initiation mode. The initial formation of each mesohigh and cold pool was just as varied. However, once the convective line developed, the positioning of these features was fairly systematic. The cold pool would be centered about 50 km behind the line. The mesohigh would be nearby, generally no more than 50 km to the right of the cold pool if not collocated. While there were a few of the larger, elongated mesohigh cases in which the stratiform precipitation had already shifted to the left when the convective line formed, the large majority of these bigger cases originally formed on a smaller scale with the stratiform region centered behind the convective line, as pictured in the lower left portion of Fig. 5.21.

The existence of a warm region and pre-squall mesolow, both in advance of the convective line, was observed throughout almost all of the cases. However, the positioning and intensity of both of these features were highly varied, particularly over

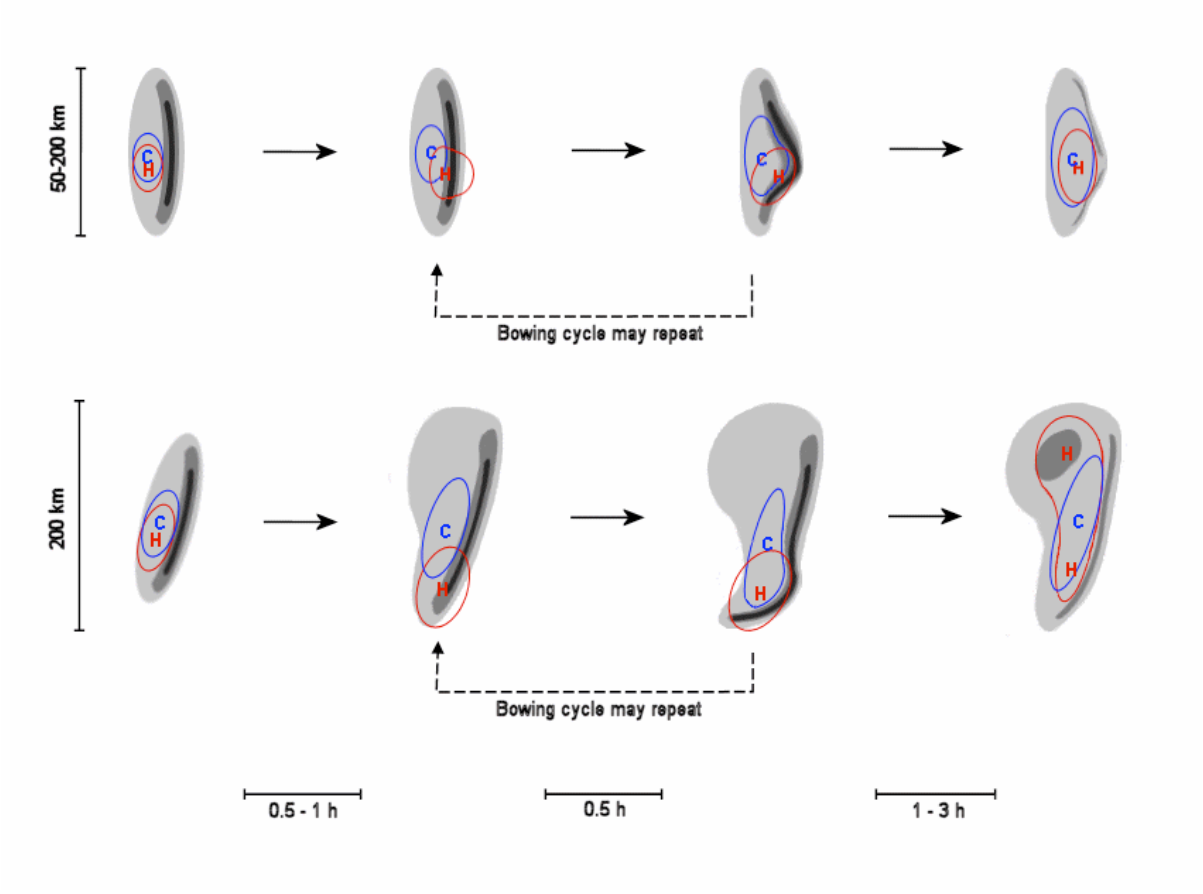

Figure 5.21: Conceptual model for the pressure surge - new bowing relationship. The shading roughly corresponds to radar reflectivity levels of 20, 40, and 50 dBZ. The blue contour surrounds the cool mesoscale temperature perturbations; the 'C' is where the lowest perturbation typically is found. The red contour surrounds the high mesoscale pressure perturbations, with the 'H' being the location of the highest perturbation. The top row represents smaller bow echo cases with centered stratiform precipitation throughout; the bottom row are larger cases which evolve into systems with left-shifted stratiform precipitation. Frequently observed length and time scales are noted for each type. Column 1: initial formation of the convective line. Column 2: pressure surge ahead of convective line. Column 3: period of new or increased active bowing. Column 4: dissipation.

the lifetime of the system. Therefore, a reliable "composite" of these could not be included in this conceptual model. The same is true of the post-system wake low.

Continuing to the right across the figure, the next stage is the surge of the mesohigh ahead of the convective line. This surge was almost always found to the right of center of the convective line. The cold pool remains centered behind the convective line, although it has grown in size since the last stage. The time interval between the first stage and the second broadly fluctuated among the cases examined, from 30 min to up to 3 h; however the majority of cases had an interval between 30 min and 1 h.

Step three in the figure shows the development of new bowing. The apex of the new bow forms to the left of the previous surge, and the bowing expands the convective line to almost eclipse the mesohigh. The cold pool expands with the new bow, resulting in the isotherms conforming with the new curvature of the convective line. As can be seen from Table 5.4, a full 59.0% of the cases examined followed this pattern of new bowing development preceded by a pressure surge. The second-highest arrangement, simultaneous new bowing and pressure surge, could possibly be decreased if higher temporal resolution radar data had been available. In any case, the pressure surge - new bowing feature is a highly common one which should be documented. On average, about 30 min would pass between the pressure surge and new bowing development (Table 5.4). Occasionally, one bow echo case might go through multiple pressure surge - new bowing cycles before dissipating, as is indicated by the dashed line in Fig. 5.21.

It should be noted that the location of the apex of the new bow, while almost always to the left of the pressure surge, did vary in its positioning along the convective line. Particularly with the elongated mesohigh cases, new bowing could occur anywhere from the very right end of the convective line (as pictured in stage three of the bottom row of Fig. 5.21) to its center. Generally, these cases would exhibit new bowing closer to the right end of the line than the smaller, one mesohigh cases.

All Bow Echoes

	Pressure Surge - New Bowing Relationship					
Initiation Type	Before	Simul.	After	None	Total	Surge/No Bow
Linear	6	1	0	0	7	0
Isolated	2	0	0	0	2	0
Merge	12	2	1	4	19	5
Total	23	8	3	5	39	7
Percent of Total	59.0%	20.5%	7.7%	12.8%	100.0%	
Mean Interval (min)	30.7	0	30.0			

Table 5.4: As in Table 5.1, but for all bowing episodes.

It is in the dissipation stage, shown in the fourth column of Fig. 5.21, that the differences in the two types are most readily apparent. In the smaller cases, the one mesohigh would shift behind the center of the bow apex into the stratiform precipitation region, as would the cold pool. The two would be more collocated than previously, although the mesohigh could still be closer to the convective line. The region of stratiform precipitation would also still likely be centered behind the bow.

In larger cases, however, the mesohigh is much larger and elongated. It would stretch from the center of the stratiform precipitation region to just behind the right end of the convective line, as displayed. Occasionally the portion of the mesohigh on the right end would be strong enough that the feature would actually split in two. The cold pool would remain centered behind the convection, although it might have shifted around 50 km farther backward into the stratiform region. If the system is very large, such as with Squall Line Bow Echoes, the cold pool associated with the system might actually split as well, with one pool located behind each mesohigh. However, such a phenomenon was not observed very often within this dataset and thus was not included in the figure; this might be due to the lack of SLBE systems. If further studies are done over a longer time period, this point is suggested for study.

The time interval between the last development of new bowing and the dissipation of the convective line (defined as when the convective line no longer contained any

radar echoes greater than or equal to 50 dBZ) varied even more widely than the period between stages one and two: intervals from 15 min to just under 6 h were noted. The most commonly observed interval was between 1 and 3 h.

It should also be noted that at any point in its lifecycle, a bow echo could develop into a much larger system, and thereby shift from exhibiting features like the top row in the conceptual diagram to exhibiting patterns more common to the bottom row. Specifically, the timing of the stratiform precipitation shift to the left varied, from starting that way or shifting there after stages one, two, or three. In other words, the two rows given in the diagram are not meant to be exclusive; systems frequently shift at some point from the top row to the bottom.

Chapter 6

Discussion

Recent simulations have suggested that the surface pressure patterns associated with MCSs, such as the mesohigh and wake low, can be attributed to a combination of gravity current and gravity wave dynamics produced by temperature perturbations within both the convective line and stratiform precipitation region (Schmidt & Cotton 1990; Nicholls et al. 1991; Haertel & Johnson 2000; Haertel & Johnson 2001). As this study is the first to offer enough detailed surface data to infer such processes, an examination of the dynamics behind the observed patterns noted herein would be instructive.

According to Nicholls et al. (1991) and Haertel et al. (2001), multiple gravity waves and currents are often generated by one single MCS (in the context of this study, a bow echo). The initial heating profile associated with a convective line, one of deep heating throughout the troposphere due to latent heating, deposition, and other factors, generates a fast-moving, deep gravity wave. Meanwhile, the low-level cooling associated with both a mature convective line and stratiform region (Gallus and Johnson 1991), produces a slow moving, "forced" gravity wave which often travels at a speed close to that of the bowing system (Haertel and Johnson 2000). This approximate matching of the two speeds amplifies both the wave and

the surface mesohigh associated with it. In addition, the low level cooling produces a cold pool which spreads along the ground as a gravity current.

Ideally, upper air observations should be examined to determine if such gravity wave and gravity current features took part in these cases, as the generation of a gravity current or a gravity wave depends on the stability of the troposphere and the depth of the temperature perturbation (Haertel et al. 2001). Unfortunately, as the Oklahoma Mesonet is only a surface observation network, such direct and timely "above ground" measurements were not available in this study. However, both station timeseries and plots of surface pressure can be used to infer gravity current and gravity wave generation and subsequent propagation. Nearby upper air soundings can also be utilized, if only to provide a first guess for the depth of the heating and cooling. Observations from the case of 13 March 2003 were selected for further examination, as not only did this case initiate entirely within Oklahoma, but it also best resembled the pressure surge - new bowing conceptual model presented above.

6.1 Gravity wave generated by deep heating

There are certain surface pressure patterns exhibited by MCSs which are indicative of overhead passage of a fast-moving gravity wave generated by deep heating. Figure 6.1, from Gallus and Johnson (1991), displays a heat source profile from the convective line of the 10-11 June 1985 squall line MCS, as well as several profiles from convective lines of tropical MCS case studies. Such a profile, of heating throughout almost all the troposphere, would result in a very deep gravity wave that propagates quickly away from the convective line, and warms the troposphere via subsidence throughout its entire depth (Nicholls et al. 1991). At the surface, this would be reflected as a lowering in surface pressure that quickly spreads away from the convective line, although an ambient shear vector could affect the speed of this propagation. Figures 6.2a,b display the start of initiation of the convective line from the 13 March 2003 case,

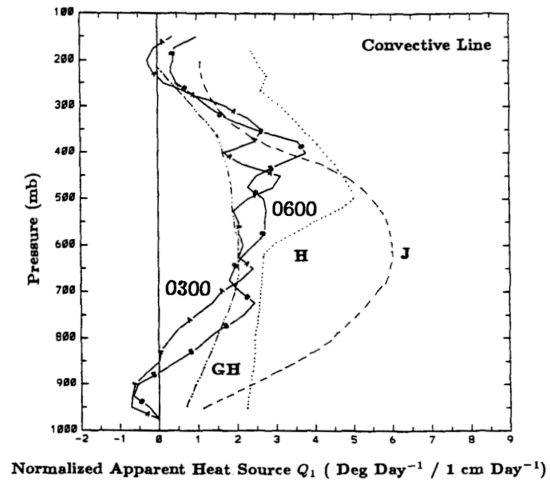

Figure 6.1: Mean vertical heating profiles, normalized by rain rate, over the convective line area from the 11 June 1985 squall line MCS at 0300 and 0600 UTC (labelled). The lines labeled R, Y, T, J are convective line tropospheric heating profiles from tropical or subtropical case studies by Reed and Recker (1971), Yanai et al. (1973), Thompson et al. (1979), and Johnson (1976), respectively. Figure from Gallus and Johnson (1991).

and the fully-formed convective line prior to development of stratiform precipitation. Note in Fig. 6.2a the low pressure region coincident with the emerging convective line; in Fig. 6.2b this low pressure has spread far from its source. Both plots are in agreement with a deep free wave propagating quickly away from the convective line. Such features, in the form of a pre-squall mesolow, were seen in almost all of the cases previously examined. Past studies, such as Hoxit et al. (1976), represent the pre-squall mesolow as a quasi-permanent feature; however, as will be seen later, this particular feature propagates rapidly away from the convection.

Figure 6.3, reproduced from Haertel et al. (2001), depicts an idealized timeseries of surface observations from a linear model at a station experiencing an acoustic wave, a forced gravity wave, and a gravity current all generated by a source of cooling 10 km away. The forced gravity wave and gravity current will be discussed later in Section 6.2. At approximately 1 min, a dip in pressure was seen in this Figure along with a modification in temperature and wind speed, reflecting the overhead passage of

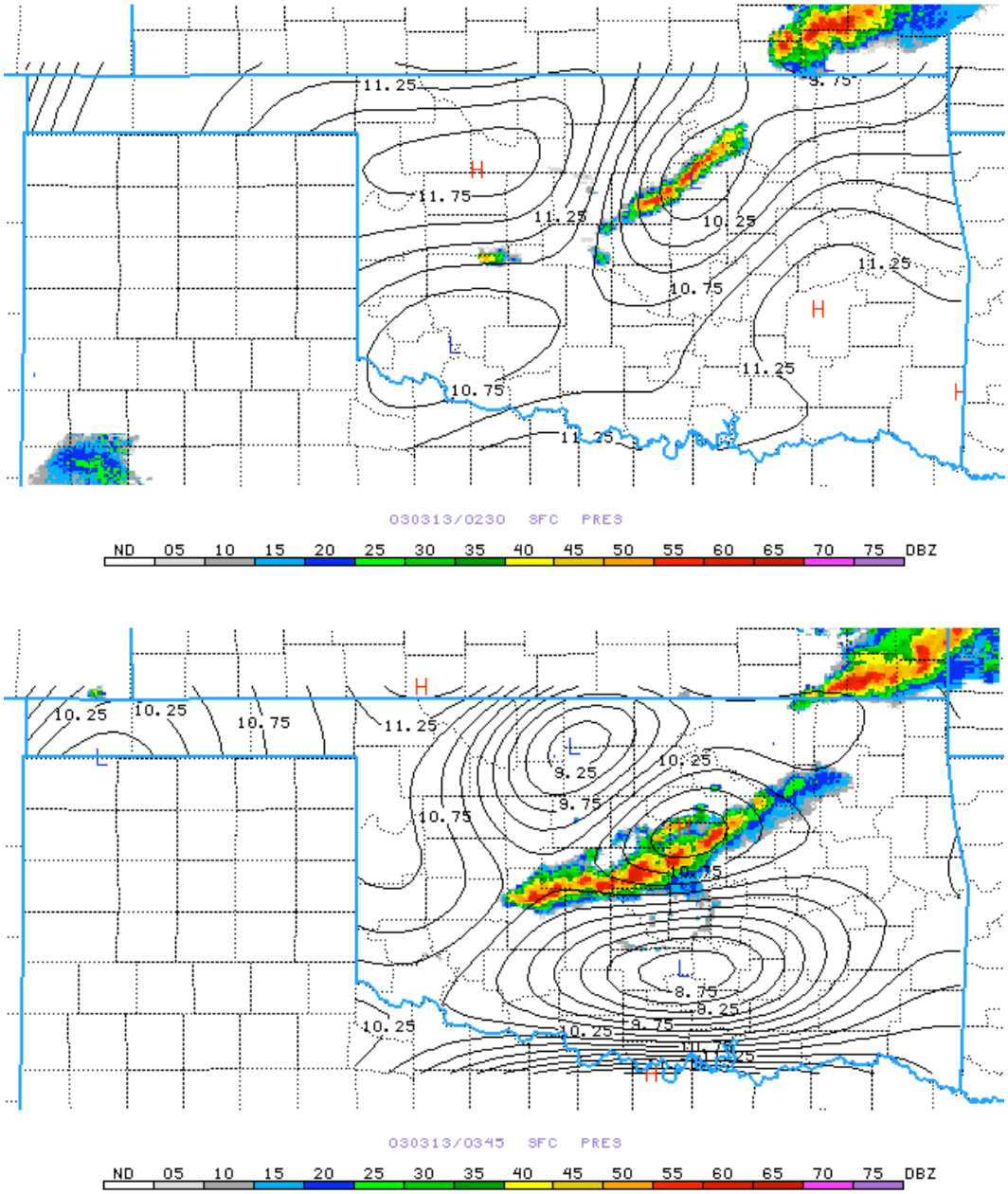

Figure 6.2: Figure (a): high-pass adjusted pressure (0.25 hPa) from 0230 UTC 13 March 2003. WSI NOWrad base reflectivity in color. Figure (b): same as (a), but for 0345 UTC.

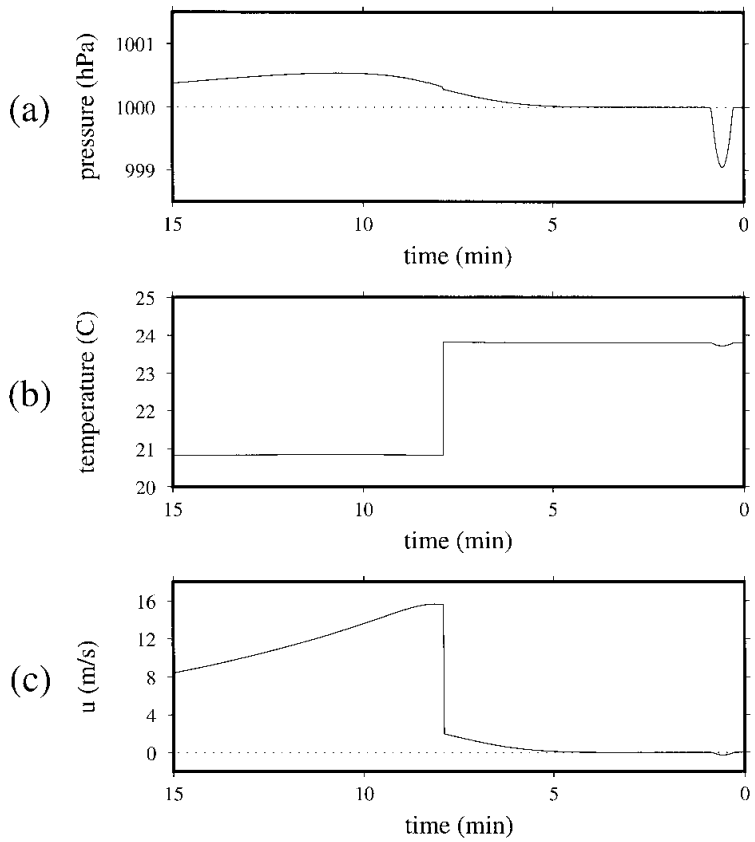

Figure 6.3: Pressure (a) hPa, temperature (b) C, and u (c) m/s observations from a station experiencing both gravity wave and gravity current outflow forced by low-level cooling. Time increases to the left. From Haertel et al. (2001).

the acoustic wave. While the fast-moving wave generated by deep heating is not an acoustic wave, it would produce a similar effect at the surface station it was overtaking – namely, a dip in pressure due to the subsidence warming this wave was effecting throughout the troposphere. The actual warming may not be reflected at the surface due to a nighttime stable layer or other reasons.

Figure 6.4 is a timeseries from station VANO on 13 March 2003. This timeseries was originally shown in Fig. 5.3, but is reproduced here with its time axis increasing to the left to allow for ease of comparison to Fig. 6.3. At approximately 0345 UTC, a temporary 2 hPa decrease in pressure was seen, with no (or very little) accompanying wind or temperature signature. This appears to be the passage of a fast-moving deep

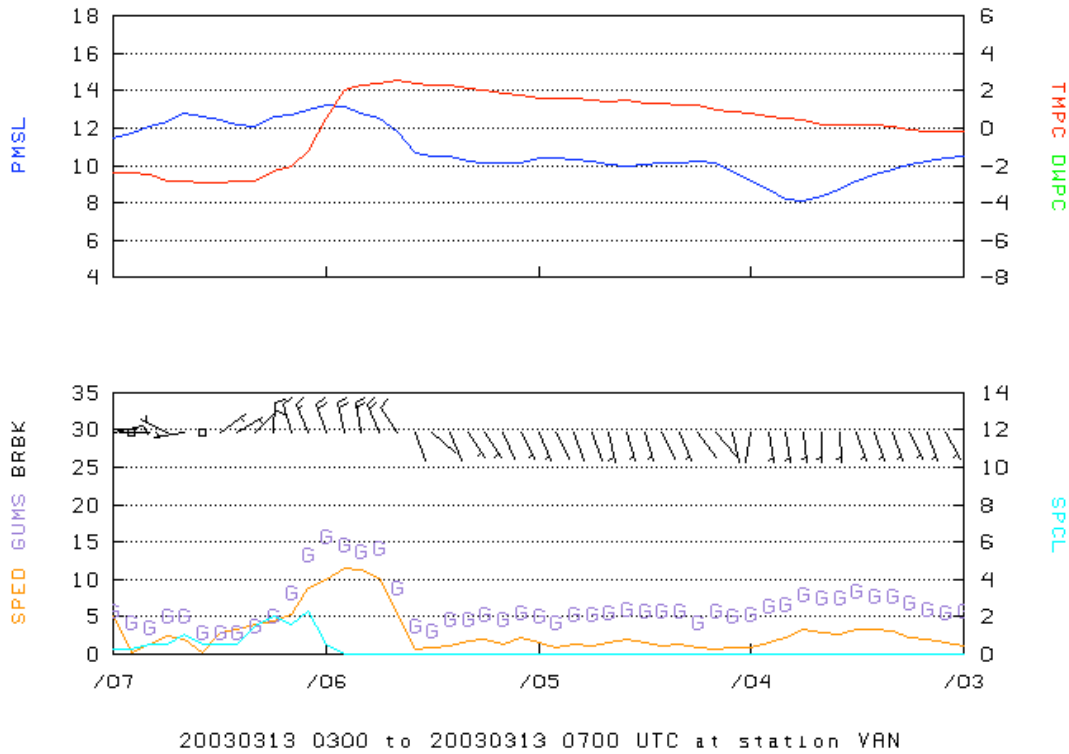

Figure 6.4: Same as Fig. 5.3, but with time increasing to the left, from 0700 to 0300 UTC.

gravity wave. These dips in pressure were noted at almost all stations impacted by the bow echo in this case. The times of passage at each impacted station are displayed in Fig. 6.5. The isochrones display a rapidly propagating wave-like feature, moving in the direction indicated by the red arrow. The following stations along this arrow were used to calculate an average speed: BRIS (time of passage 2.83 in decimal-hour notation, or 0250 UTC), OKEM (3.12, or 0305 UTC), STUA (3.67, or 0340 UTC), and ANTL (4.37, or 0420 UTC). The average speed found was 34.1 m s^{-1}.

This speed can be compared to theoretical gravity wave speeds, in order to further corroborate the idea of a gravity wave generated by deep heating. Nicholls et al. (1991) found that gravity wave speed can be given by Eq. 2.3, which can be rewritten as

$$c = \frac{N}{\pi}\frac{\lambda}{2} \tag{6.1}$$

where $\frac{\lambda}{2}$ is the depth of the source of heating or cooling. The 0000 UTC sounding from Norman, OK (KOUN, not pictured) was utilized to provide a rough guess at the environment experienced by the initiating convective line. From the case studies examined in Fig. 6.1, it appears the heating from the convective line often stretches the entire depth of the troposphere; Nicholls et al. (1991) utilized a similar height of 10 km for their simulations. The depth of the troposphere in this case was found to be 9844 m from the 0000 UTC sounding, which agrees well with these numbers. A mean N was calculated over this depth to be 0.0129 s^{-1}, using

$$N = \left(\frac{g}{\bar{T}_v} \frac{\partial \theta_v}{\partial z} \right)^{1/2}. \tag{6.2}$$

Combining these numbers in Eq. 6.1 gives a speed of 40.4 m s^{-1}. This is a little fast for the speed found from ground observations; however, it is possible that the heating did not extend the full height of the troposphere. A gravity wave moving at a speed of 34.1 m s^{-1}, at the N already found, would require heating over a depth of 8315 m, which is certainly not unreasonable. It is possible that N varied with height, which would also affect the gravity wave speed calculation.

6.2 Gravity wave generated by shallow, low-level cooling

Once the bow echo system in this case reached maturity, it was associated with both an intense convective line and large stratiform precipitation region. Both of these features would be associated with strong cooling in the lower levels of the troposphere, due to evaporating, melting, and sublimating precipitation, as well as other factors discussed in Chapter 2. This cooling will generate a slower-moving gravity wave as well as hydrostatically induce a surface mesohigh. However, if the gravity wave is moving at a similar speed to the bow echo/source of cooling, it will amplify the mesohigh (Haertel and Johnson 2000). Thus surface indications of a

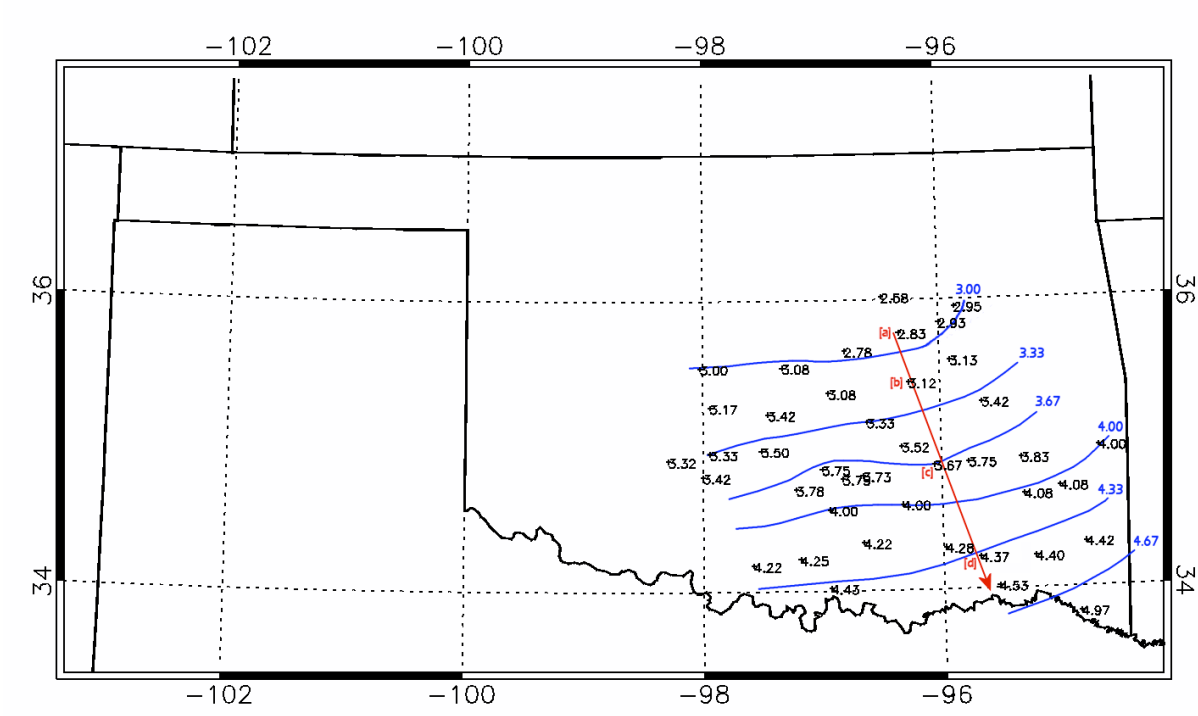

Figure 6.5: Isochrones of the fast-moving wave generated by deep heating in the convective line for the 13 March 2003 bow echo. The time the feature reached each affected station is noted. Times are displayed in decimal format; e.g. 3.50 is 0330 UTC. The red arrow displays direction of propagation. Stations labelled [a], [b], [c], and [d] are BRIS, OKEM, STUA, and ANTL, respectively.

forced gravity wave include a strong mesohigh which travels with the bowing system. This feature was evident not only throughout this case (see Figs. 5.2 and 5.5) but all cases examined in this study.

Naturally, a strong mesohigh alone is not fully indicative of a forced gravity wave. We refer again to Fig. 6.3 for an idealized example of a timeseries during forced gravity wave passage. Starting from 5 min, the pressure and wind speed began to gradually rise, revealing the effects of the overhead gravity wave and its attendant circulation. Finally, around 7 min, the gravity current arrived, with its further increase in pressure and wind speed, and large temperature drop.

Figure 6.4, the timeseries from station VANO during passage of the 13 March 2003 case, was examined for elements similar to Fig. 6.3. At 0535 UTC, a sharp increase in

pressure, wind shift, and increase in wind speed all occurred. This could correspond to a forced gravity wave passing above. Note that as both the pressure rise and wind shift are well before the sharp temperature drop, there are separate elevated gravity wave and surface gravity current passages. There was a significantly sharper increase in pressure and wind speed associated with this gravity wave than was suggested in the linear simulations in Haertel et al. (2001). Possibly part of this increase was due to the nonhydrostatic effect of colliding air masses ahead of the gravity current; these non-linear effects were not included in Haertel et al. (2001). Other non-linear effects, such as downward transport of momentum, could also be a cause.

A gravity current passage much like that at minute 7 in the idealized Fig. 6.3 occurred at station VANO just prior to 0600 UTC. A temperature drop accompanied its arrival, as in the model. However, both the wind speed and pressure had actually already begun to decrease at this time, unlike Fig. 6.3. This suggests non-linear effects associated with the forced gravity wave, ahead of the gravity current, actually did more in this case to increase the pressure and wind than the purely hydrostatic effects associated with the cold air in the gravity current. Again, the non-linear nonhydrostatic pressure increase due to colliding air masses ahead of the gravity current could also affect the rate of the pressure rise.

The start of the sharp increase in pressure (like that at 0535 UTC in Fig. 6.4), presumably the leading edge of the forced gravity wave, was noted for all stations affected by the bow echo. Figure 6.6 shows isochrones of this sharp pressure rise. A wave-like feature which closely hugs the bow echo is discernible here, although this wave moved at a slower pace than the previously examined wave generated by deep heating. The red arrow shows its direction of motion; stations along this arrow selected to calculate average speeds were CHAN (time of passage 3.67, or 0340 UTC), CALV (5.83, or 0540 UTC), and ANTL (7.17, or 0710 UTC). Two different speeds were calculated, one prior to most of the new bowing development (from CHAN

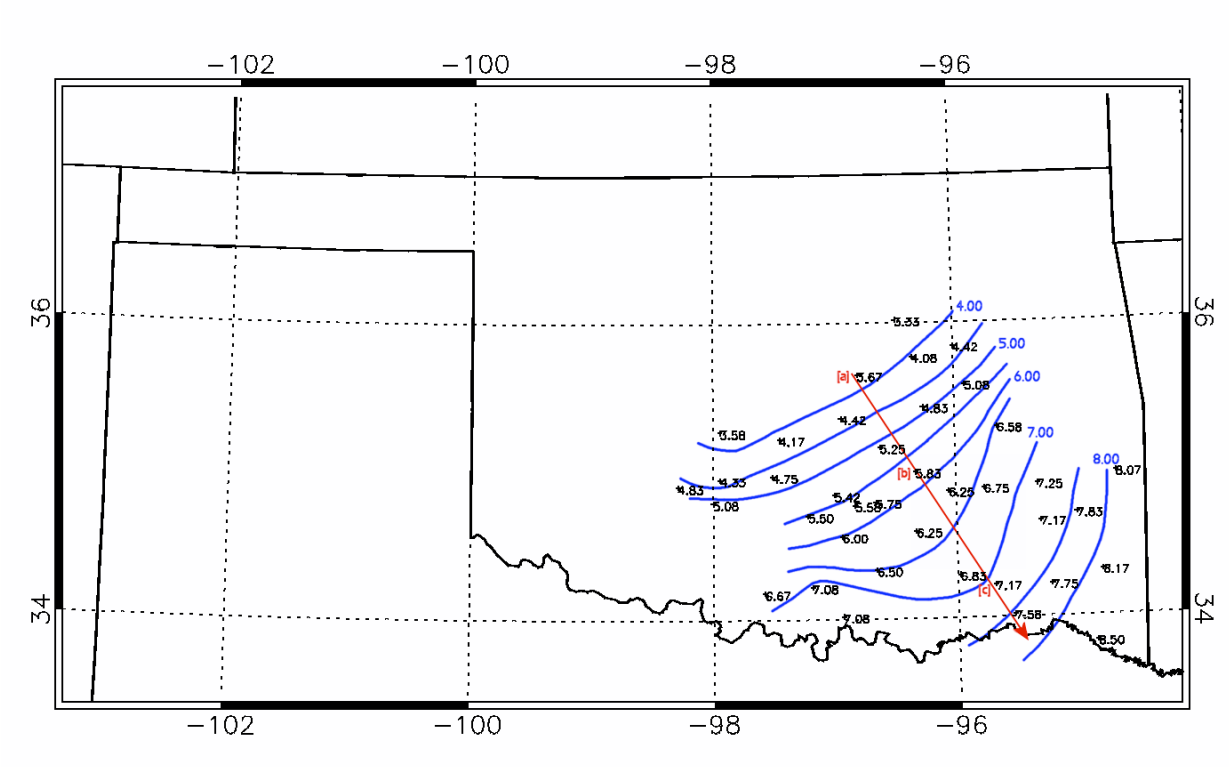

Figure 6.6: Isochrones of the slower-moving, forced wave generated by shallow, low-level cooling in both the convective line and stratiform region for the 13 March 2003 bow echo. The same format as Fig. 6.5 is used. Stations labelled [a], [b], and [c] are CHAN, CALV, and ANTL, respectively.

to CALV), and one during bowing (from CALV to ANTL). Unfortunately, because stations in a straight line parallel to the direction of motion were required to estimate the speed, the division between periods of "prior to" and "during" bowing was unable to be as exact as hoped. However, the average speeds found - 10.9 m s^{-1} and 21.6 m s^{-1} for prior to and during bowing, respectively - are very similar to the observed speed of the convective line at these same times: 9.8 m s^{-1} and 19.5 m s^{-1}. Therefore the numbers are reasonable. The slightly faster calculated speed of the tracked wave is likely partially due to including part of the bowing period in the "prior bowing" calculation. In any case, since this wave travelled at about the same speed as its forcing, it was possible for this gravity wave to be amplifying the mesohigh.

In order to calculate a theoretical forced gravity wave speed using Eq. 6.1, the depth of the cooling must be estimated. Prior to the start of new bowing, there was little stratiform precipitation associated with the system (see Fig. 6.2). Thus, at that time most of the cooling must have been associated solely with the convective line. The convective line passed upper air sounding station KOUN prior to developing large amounts of stratiform precipitation. The 1200 UTC sounding from KOUN (not shown) could then be used to estimate the depth of the cooling from the remaining cold pool. The sounding showed a layer of cold air above the surface reaching to 2022 m, or 800 hPa. Granted, the depth of the cold pool would not necessarily be equal to the depth of the cooling. However, this value fit well with the midlatitude case convective line heating profile in Fig. 6.1, in which there was also shallow cooling up to about 800 hPa. Using the N already calculated yields a wave speed of 8.3 m s^{-1} for the prior to bowing period. This is 2.6 m s^{-1} slower than the speed of the tracked wave, and 1.5 m s^{-1} slower than the actual bow echo. Part of this difference is likely due to the fact that a small amount of stratiform precipitation did form prior to the start of new bowing; this would have increased the depth of the cooling and sped the generated wave.

It is also possible to estimate the depth of the cold pool at this time by assuming the speed of the convective line was the same as the speed of the gravity current. This is a fairly safe assumption - examination of Fig. 6.4 shows that the temperature drop (leading edge of the gravity current) and onset of rain (leading edge of the convective line) occurred at the same time, 0555 UTC. The close association of the two was the same for all timeseries analyzed. Eq. 2.2 from Charba (1974),

$$V = k\sqrt{gd\frac{\rho_1 - \rho_2}{\rho_1}} \tag{6.3}$$

uses the difference in densities between the environmental air and within the cold

pool at a station, and the cold pool depth, to find the speed of the gravity current. (This equation does not include a term for mean synoptic flow; due to a lack of exact upper air measurements synoptic flow was not included in these calculations.) Thus, given the density difference and gravity current (bow echo) speed, the equation can be solved for the cold pool depth. Observations ahead of and following gravity current passage at station NRMN were used (at times 0420 and 0450 UTC, respectively). For a convective line speed of 9.8 m s^{-1}, this yielded a cold pool depth of 1265 m. Allowably, the change in density across the leading cold pool edge, found here, would not be the same as the mean change in density over the entire depth of the cold pool. However, this result can be used to suggest that, in general, the depth of cooling associated with this case prior to the development of new bowing is fairly similar to the squall line MCS cooling profiles shown in Fig. 6.1.

After bowing occurred, a large region of stratiform precipitation was associated with the system (Fig. 5.2). This would greatly increase the depth of the cooling. Unfortunately there were no direct measurements available to estimate this depth. Instead, an estimate of the depth of the cooling will be calculated from the given wave speed, and it will be compared to values in literature. The speed of the tracked wave, during bowing, was 21.6 m s^{-1}. Using the same N, this corresponds to a depth of cooling of 5269 m.

Figs. 6.7a,b show the heating profiles associated with the squall line studied by Gallus and Johnson (1991): Fig. 6.7a shows average profiles of the total system, and Fig. 6.7b shows average profiles of the stratiform precipitation region. The total system heating profile in Fig. 6.7a suggests a cooling depth of no higher than 800 hPa, very similar to the convective line profile. However, Nicholls et al. (1991) and Haertel and Johnson (2000) both suggest that the forced gravity wave is generated primarily by low-level cooling within the stratiform region. In Fig. 6.7b the stratiform cooling has a depth of around 700 hPa, which corresponds to 3000 m in the 13 March 2003

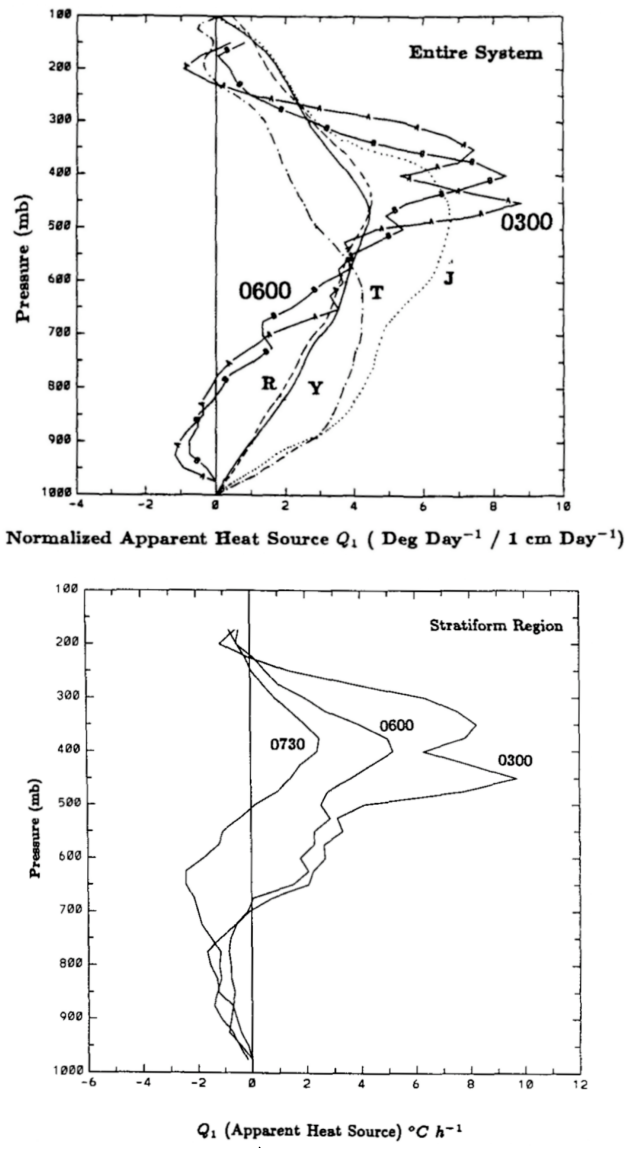

Figure 6.7: Mean vertical heating profiles, normalized by rain rate, over the total MCS system (a) and the stratiform region (b) from the 11 June 1985 squall line MCS at 0300 and 0600 UTC (labelled). In (a), the lines labeled R, Y, T, J are convective line tropospheric heating profiles from tropical or subtropical case studies by Reed and Recker (1971), Yanai et al. (1973), Thompson et al. (1979), and Johnson (1976), respectively. In (b), the profiles are from the studied MCS only, at 0300, 0600, and 0700 UTC (labelled). From Gallus and Johnson (1991).

case. Wakimoto's 1982 study of gust fronts associated with squall lines observed a gust front with cold pool depth of 3954 m moving at a speed of 20 m s^{-1}, a similar speed to this case. Nicholls et al. (1991) suggests that the stratiform region has a cooling depth of approximately half the troposphere, which would correspond to 4922 m in this case. However, the calculated cooling depth from this case of just over 5000 m would still be higher than previous values observed in the literature. Such a value indicates that, during new bowing development, the depth of the cooling is much larger than values observed in squall line MCSs (Gallus & Johnson 1991; Wakimoto 1982).

If the calculation from Eq. 6.3 estimating cold pool depth from gravity current/convective line speed is repeated, using data from station VANO (at times of 0535 or 0600 UTC) and the measured convective line speed during bowing of 19.5 m s^{-1}, a cold pool depth of 3186 m results. However, it should again be noted that the change in density across the leading cold pool edge at the surface, used here, would not be the same as the mean change in density over its entire depth, typically used in such calculations. This could account for the disparity in depths; in addition, the depth of the cold pool does not necessarily correspond exactly with the depth of the cooling. However, this depth found via Eq. 6.3 is still larger than the previously observed depths for most squall lines.

6.3 Summary

The gravity waves generated by temperature perturbations within this 13 March 2003 bow echo case were tracked using the reflections of these features in both surface plots and station timeseries. A fast-moving wave generated by the deep heating within the convective line, first modeled by Nicholls et al. (1991), was tracked via its pressure "dips" evident in timeseries from nearby stations. The speed of the slower-moving wave, forced by the shallow cooling within both the convective line and the stratiform

region, was also calculated using sharp increases in pressure as an indication of the leading edge of this wave.

It is clear from the calculations presented in this chapter that, prior to new bowing, the heating and cooling profile of the convective line is similar to profiles associated with squall line MCSs from Wakimoto (1982) and Gallus and Johnson (1991). However, during the period of new bowing, the cooling from the convective line and stratiform region was much larger than the depth of cooling associated with squall line MCSs. As most bow echoes examined in this study moved at speeds similar to or even faster than this case particularly during new bowing development - and their associated waves are likely moving as fast as well - such a result regarding the cooling depth might be applied to bow echo systems as a whole.

The large depth of the cooling could possibly also provide one dynamical explanation for the pressure surge - new bowing process noted extensively in Chapter 5. Prior to and during new bowing development, the bow echo system would receive a strong low-level influx of cooler air. Such an idea is not without precedent in the literature, as Przybylinski and Gery (1983) noted a rear-inflow notch radar signature which often occurred prior to new bowing development (see Section 2.2 for further discussion). This rear-inflow notch indicated a large influx of low- to mid-level cool, dry air. A quick incursion of such air would not only hydrostatically strengthen the mesohigh, but would also suddenly increase the depth of the cooling. This would in turn speed the forced gravity wave ahead of the system, causing the surge in the mesohigh as seen in the conceptual model. The convective line would then follow this gravity wave, resulting in new bowing development. However, while the data examined here does lend itself nicely to such a conclusion, it also does not eliminate the possibility that new bowing development could be caused by downward transport of momentum from strong rear inflow into the system. Further studies, particularly

with upper air observations, would need to be completed to fully examine the viability of either theory.

Chapter 7

Summary and Conclusions

7.1 Review of presented results

The Oklahoma Mesonet was used to create high-pass, temporally filtered mesoanalyses overlaid on WSI NOWrad composite radar data during years 2002 through 2005. Within these years, the radar data were examined for all bow echoes which were both large and long-lasting enough to be adequately sampled by the observation network. The resultant 36 cases were then subdivided into categories based on both mature structure, and type of initiation.

A climatology of the cases was presented. It was found that the most common method of initiation in these cases was a merging of previously formed convection (the "Merger" initiation type), and the most frequent active bowing structure was the Bow Echo Complex. (The BEC was defined here as a bow echo which contained more than one type of convection in its convective line.) Additionally, the direction of motion of all of these cases contained a west-to-east component; almost all cases moved either southwest-to-northeast or northeast-to-southwest. Upper-level "steering" winds over Oklahoma are most often from either of those directions, fitting well with the observations. Notably, a large portion of the Merger initiation type cases tracked southwest-to-northeast. Possibly this result is due to the fact that upper-level

southwesterly flow often brings more moisture to Oklahoma than northwesterly flow, which could precipitate more unorganized convection.

An instability-dynamics relationship was noted in the distribution of cases by season. Classic Bow Echoes (specified in this study as bow echoes larger than a single cell but smaller than a squall line, and isolated from other convection) occurred most often in the spring, implying both instability and synoptic forcing are favored for these cases. Merger initiations and Bow Echo Complexes were most frequent in the summer, when environments of greater instability and less synoptic forcing are common. Finally, Linear initiation (the bowing out of an straight convective line smaller than a squall line) and Squall Line Bow Echoes (bowing segments within a squall line structure) happen most regularly in the fall, suggesting the most synoptic or linear forcing is required for these cases. The Linear initiation type also had the highest percentage of cases with severe wind reports, possibly indicating strongly forced environments are more favorable for stronger winds. However, all of these results are strongly conditional upon the limited spatial and temporal scope of the cases.

Following the climatological discussion, case studies from each active bowing structure were presented. Features that have already been noted in the literature as common to squall lines were also frequently seen to be associated with bow echoes. A meoshigh and cold pool, located generally just behind the convective line, and a pre-squall mesolow and warm region ahead of the convective line were noted. These were observed in all initiation types and mature structures.

Most significantly, a surface pattern which preceded bowing, the "pressure surge - new bowing" pattern, was identified. While not all cases exhibited this behavior, a majority did, enough so that a conceptual model for the process was proposed. This model included only the behavior of the mesohigh and cold pool, as the behavior of

the pre-squall mesolow and warm region was too variable among these cases. The "pressure surge - new bowing" pattern included the following features:

1. Prior to formation of the convective line, the location of the mesohigh and cold pool are variable, depending on prior surrounding convection and type of initiation. Once the convective line forms, however, both the mesohigh and cold pool can typically be found no more than 50 km behind the line. The cold pool is centered behind the line with the mesohigh slightly to its right.

2. About 0.5 to 1 h later, the mesohigh surges closer to or ahead of the convective line, generally to the right of its center. The convective line might bow slightly at the same time, although bowing has not necessarily yet occurred. The cold pool remains centered behind the convective line.

3. New bowing develops slightly to the left of the pressure surge about 0.5 h later. As the convective line surges ahead, it almost surpasses the mesohigh. The cold pool remains centered close behind the convective line, and expands with the line as it bows out. The "pressure surge - new bowing" cycle (steps 2 and 3) might repeat several times before dissipation, particularly if the bowing segment is within a larger system.

4. At the time of dissipation of the convective line, the behavior of the bow echo varies as a function of its overall size, as well as the location of its stratiform precipitation region. The generally larger bow echoes, with a stratiform region shifted to its left side, exhibit an elongated or even split mesohigh, with centers both in the stronger portion of the stratiform rain and about 25 km behind the right end of the convective line. Smaller bow echoes, on the other hand, typically have only one mesohigh, which remains just to the right of and behind the dissipating bow apex within the convective line. The cold pool in both types stays centered 50-100 km behind the dissipating convective line.

Examination of observed timeseries during the 13 March 2003 bow echo displayed features very similar to the simulated combination gravity wave/current of Haertel et al. (2001). Hours ahead of the convective line passage, a dip in pressure with little associated change in winds or temperature was noted. This pressure trough, which propagated rapidly at a speed of 34.1 m s^{-1}, was a surface manifestation of a gravity wave generated by deep convective heating in the convective line.

A short time prior to the arrival of the convective line, a sharp increase in pressure and wind speed took place. This indicated the passage overhead of a gravity wave generated by low-level cooling, and was followed by the appearance of the surface gravity current and cold pool as the rain began and the temperature dropped. It was noted that the time interval between the start of the sharp increase in pressure (indicating the front edge of the mesohigh) and the start of the temperature drop (the front edge of the cold pool) was larger at stations that experience a pressure surge - new bowing cycle. This demonstrated that at these stations the front edge of the mesohigh was farther ahead of the convective line prior to the time of new bowing. This could be a surface reflection of the overhead gravity wave surging ahead of the surface gravity current. Such a result was further corroborated by the finding that the depth of the cooling in the 13 March 2003 system greatly increased just prior to new bowing development. A quick increase in the height of the cool perturbation would increase the speed of the gravity wave, allowing it to surge ahead of the gravity current. The convective line would follow, creating a new bowing segment. Thus, from this study it could be suggested that a sudden influx of cold air into the system at low-levels is at work in initiating new bowing.

7.2 Suggested future work

A number of goals were set forth and the beginning of this work: to determine if surface pressure and temperature patterns associated with squall line MCSs were

applicable to the smaller bow echo MCSs, to establish a dynamic distinction between bow echoes and squall lines, and to identify a surface pattern which preceded new bowing development. Good progress was made on two of these goals with this study. The mesoscale pressure and temperature features of bows were examined and found to correspond well with those already associated with squall line MCSs. A common surface pattern which precedes new bowing development was also discovered which hints at a gravity wave mechanism behind the bowing process. Unfortunately, it would be difficult at this time to fully utilize the pressure surge as a forecasting aid for bow echo development. A much denser surface observation network (such as a mesonet) would be required than is currently available across much of the United States, in order to resolve the pressure surge feature. However, as more mesonetworks are established throughout the country, such a forecasting technique would become more valuable.

The authors were also unable to fully infer a dynamic distinction between squall lines and bow echoes. It is possible that the depth of cooling (and therefore the speed of the associated gravity wave) is lesser in squall lines than in bow echoes, particularly during new bowing development. It is also likely that the sudden increase in cooling depth, feasibly leading to the surging behavior of the gravity wave and mesohigh, are also not exhibited in squall lines. The method used in this study of tracking these waves via surface data could be applied to more bow echo cases, to see if similar results occur as expected. However, observations above the surface would be required to fully explore this possibility.

The lack of observations at elevations other than the surface was one of the most significant limiting factors in this study. These measurements are necessary to fully confirm the existence of the elevated gravity waves. They would also prove very useful in examining if the source of new bowing is either the sudden surge of said gravity wave ahead of the convective line, the result of rear inflow downward momentum

transport, or as is most likely, a portion of both. Granted, dense networks of upper air soundings close to bowing convection are unfortunately rather rare; the recent BAMEX experiment may provide excellent analyses to confirm or disprove the suggested bowing mechanism. The use of wind profiler data, if located close enough to the bowing system, could also confirm the theory of a gravity wave surge prior to new bowing development. Level-II WSR-88D data, from a radar site at a favorable position and distance from the bow, could be utilized to explore the source of the suggested low-level influx of cold air. Numerical modeling of bow echoes may be profitable as well, particularly as a high resolution surface dataset is available for initiation.

The study was additionally limited in space by the extent of the Oklahoma Mesonet. If mesoscale observation networks were established in other regions of the United States or the world, additional analysis of bow echoes from other climatological areas would be highly beneficial. While the pressure surge - new bowing behavior was exhibited in all types of bow echoes in Oklahoma, it would be valuable to track its appearance in bow echoes that form in a wider range of synoptic and mesoscale environments. Even analysis of further years using the Oklahoma Mesonet could prove fruitful, if only to provide a wider sample size. Moreover, this would allow further investigation into the placement of the pre-squall mesolow and wake low in relation to the bowing system.

Bow echoes have been a relatively unpredictable phenomenon throughout meteorological history. Due to their somewhat undefinable qualities, intensive studies on their inner workings were not as frequent as other, more definable subjects. Moreover, because of their small spatial and temporal scale, the observational networks available to analyze them, until recently, were few. This study, as well as the suggested future work, all aims to provide forecasters with a better understanding of the processes which initiate new bowing development. When the cause of new bowing is

fully revealed, the aid to those warning the public about possible dangers from these ever-evolving storms would be significant.

References

American Meteorological Society, 2000: Glossary of meteorology. This is an electronic document. Date of publication: June, 2000. Date retrieved: May 10, 2007. Date last modified: [unavailable].
URL `http://amsglossary.allenpress.com/glossary/preface2`

Burke, P. and D. Schultz, 2004: A 4-year climatology of cold-season bow echoes over the continental United States. *Weather and Forecasting*, **19**, 1061–1074.

Byers, H. and R. Braham, Jr., 1949: *The Thunderstorm*. U.S. Government Printing Offices, Washington, D.C., 287 pp.

Charba, J., 1974: Application of gravity current model to analysis of squall-line gust front. *Monthly Weather Review*, **102**, 140–156.

Coniglio, M., D. Stensrud, and M. Richman, 2004: An observational study of derecho-producing convective systems. *Weather and Forecasting*, **19**, 320–337.

DeWald, V. and T. Funk, 2000: WSR-88D reflectivity and velocity trends of a damaging squall line event on 20 April 1996 over south-central Indiana and central Kentucky. *Preprints, 20th Conference on Severe Local Storms*, Amer. Meteor. Soc., Orlando, FL, 177–180.

Duchon, C., 1979: Lanczos filtering in one and two dimensions. *Journal of Applied Meteorology*, **18**, 1016–1022.

Evans, J. and C. Doswell, 2001: Examination of derecho environments using proximity soundings. *Weather and Forecasting*, **16**, 329–342.

Fujita, T., 1955: Results of detailed synoptic studies of squall lines. *Tellus*, **7**, 405–436.

— 1959: Precipitation and cold air production in mesoscale thunderstorm systems. *Journal of Meteorology*, **16**, 454–466.

— 1978: Manual of downburst identification for project NIMROD. Technical report, Dept. of Geophysical Sciences, University of Chicago, Chicago, IL.

— 1979: Objective, operation, and results of project NIMROD. *Preprints, 11th Conference on Severe Local Storms*, Amer. Meteor. Soc., Kansas City, MO, 259–266.

Funk, T., K. Darmofal, J. Kirkpatrick, V. Dewald, R. Przybylinski, G. Schmocker, and Y.-J. Lin, 2003: Storm relectivity and mesocyclone evolution associated with the 15 April 1994 squall line over Kentucky and southern Indiana. *Monthly Weather Review*, **131**, 2804–2823.

Gallus, J., W.A., 1996: The influence of microhysics in the formation of intense wake lows: A numerical modeling study. *Monthly Weather Review*, **124**, 2267–2281.

Gallus, W., Jr. and R. Johnson, 1991: Heat and moisture budgets of an intense midlatitude squall line. *Journal of the Atmospheric Sciences*, **48**, 122–146.

— 1995: The dynamics of circulations within the trailing stratiform regions of squall lines. Part I; The 10-11 June PRE-STORM system. *Journal of the Atmospheric Sciences*, **52**, 2161–2187.

Haertel, P., 2007: personal communication.

Haertel, P. and R. Johnson, 2000: The linear dynamics of squall line mesohighs and wake lows. *Journal of the Atmospheric Sciences*, **57**, 93–107.

Haertel, P., R. Johnson, and S. Tulich, 2001: Some simple simulations of thunderstorm outflows. *Journal of the Atmospheric Sciences*, **58**, 504–516.

Hilgendorf, E. and R. Johnson, 1998: A study of the evolution of mesoscale convective systems using WSR-88D data. *Weather and Forecasting*, **13**, 437–452.

Houze, R., Jr., S. Rutledge, M. Biggerstaff, and B. Smull, 1989: Interpretation of Doppler weather radar displays of midltatiude mesoscale convective systems. *Bulletin of the American Meteorological Society*, **70**, 608–619.

Hoxit, L., C. Chappel, and J. Fritsch, 1976: Formation of mesolows or pressure troughs in advance of cumulonimbus clouds. *Monthly Weather Review*, **104**, 1419–1428.

Johnson, R., 1976: The role of convective-scale precipitation downdrafts in cumulus and synoptic-scale interactions. *Journal of the Atmospheric Sciences*, **33**, 1890–1910.

— 1983: The heat burst of 29 May 1976. *Monthly Weather Review*, **111**, 1776–1792.

— 2001: Surface mesohighs and mesolows. *Bulletin of the American Meteorological Society*, **82**, 13–31.

Johnson, R. and P. Hamilton, 1988: The relationship of surface pressure features to the precipitation and air flow structure of an intense midlatitude squall line. *Monthly Weather Review*, **116**, 1444–1472.

Klimowski, B., M. Bunkers, M. Hjelmfelt, and J. Covert, 2003: Severe convective windstorms over the Northern High Plains of the United States. *Weather and Forecasting*, **18**, 502–519.

Klimowski, B., M. Hjelmfelt, and M. Bunkers, 2004: Radar observations of the early evolution of bow echoes. *Weather and Forecasting*, **19**, 727–734.

Klimowski, B., R. Przybylinski, G. Schmocker, and M. Hjelmfelt, 2000: Observations of the formation and early evolution of bow echoes. *Preprints, 20th Conference on Severe Local Storms*, Amer. Meteor. Soc., Orlanda, FL, 44–47.

Klimwoski, B., 2007: personal communication.

Loehrer, S. and R. Johnson, 1995: Surface pressure and precipitation life cycle characteristics of pre-storm mesoscale convective systems. *Monthly Weather Review*, **123**, 600–621.

Miller, D. and R. Johns, 2000: A detailed look at extreme wind damage in derecho events. *Preprints, 20th Conference on Severe Local Storms*, Amer. Meteor. Soc., Orlando, FL, 52–55.

Nicholls, M., R. Pielke, and W. Cotton, 1991: Thermally forced gravity waves in an atmosphere at rest. *Journal of the Atmospheric Sciences*, **48**, 1869–1884.

Nuss, W. and D. Titley, 1994: Use of multiquadric interpolation for meteorological objective analysis. *Monthly Weather Review*, **122**, 1611–1631.

Parker, M. and R. Johnson, 2000: Organizational modes of midlatitude convective systems. *Monthly Weather Review*, **128**, 3413–3436.

Przybylinski, R., 1995: The bow echo. observations, numerical simulations, and severe weather detection methods. *Weather and Forecasting*, **10**, 203–218.

Przybylinski, R. and W. Gery, 1983: The reliability of the bow echo as an important severe weather signature. *Preprints, 13th Conference on Severe Local Storms*, Amer. Meteor. Soc., Tulsa, OK, 270–273.

Reed, R. and E. Recker, 1971: Structure and properties of synoptic-scale wave disturbances in the equatorial western Pacific. *Journal of the Atmospheric Sciences*, **28**, 1117–1133.

Rotunno, R., J. Klemp, and M. Weisman, 1988: A theory for strong, long-lived squall lines. *Journal of the Atmospheric Sciences*, **45**, 463–485.

Schmidt, J. and W. Cotton, 1990: Interactions between upper and lower tropospheric gravity waves on squall line structure and maintenance. *Journal of the Atmospheric Sciences*, **47**, 1205–1222.

Skamarock, W., M. Weisman, and J. Klemp, 1994: Three-dimensional evolution of simulated long-lived squall lines. *Journal of the Atmospheric Sciences*, **51**, 2563–2584.

Smull, B. and R. Houze, Jr., 1985: A midlatitude squall line with a trailing region of stratiform rain: Radar and satellite observations. *Monthly Weather Review*, **113**, 117–113.

Stensrud, D., R. Maddox, and C. Ziegler, 1991: A sublimation-initiated mesoscale downdraft and its relation to the wind field below a precipitation anvil cloud. *Monthly Weather Review*, **119**, 2124–2139.

Stumpf, G., R. Johnson, and B. Smull, 1991: The wake low in a midlatitude mesoscale convective system having complex organization. *Monthly Weather Review*, **119**, 134–158.

Thompson, R., Jr., S. Payne, E. Recker, and R. Reed, 1979: Structure and properties of synoptic-scale disturbances in the intertropical convergence zone of the eastern Atlantic. *Journal of the Atmospheric Sciences*, **36**, 53–72.

Trapp, R. and M. Weisman, 2003: Low-level mesovortices within squall lines and bow echoes. part II: Their genesis and implications. *Monthly Weather Review*, **131**, 2804–2823.

Trapp, R., D. Wheatley, N. Atkins, R. Przybylinski, and R. Wolf, 2006: Buyer beware: Some words of caution on the use of severe wind reports in postevent assessment and research. *Weather and Forecasting*, **21**, 408–415.

Vescio, M. and R. Johnson, 1992: The surface-wind response to transient mesoscale pressure fields associated with squall lines. *Monthly Weather Review*, **120**, 1837–1850.

Wakimoto, R., 1982: Life cycle of thunderstorm gust fronts as viewed with Doppler radar and rawinsonde data. *Monthly Weather Review*, **110**, 1060–1082.

Wakimoto, R., H. Murphey, C. Davis, and N. Atkins, 2006a: High winds generated by bow echoes. part I: Overview of the Omaha bow echo 5 July 2003 storm during BAMEX. *Monthly Weather Review*, **134**, 2793–2812.

— 2006b: High winds generated by bow echoes. Part II: The relationship between the mesovortices and damaging straight-line winds. *Monthly Weather Review*, **134**, 2813–2829.

Weisman, M., 1992: The role of convectivley generated rear-inflow jets in the evolution of long-lived mesoconvective systems. *Journal of the Atmospheric Sciences*, **49**, 1826–1847.

— 1993: The genesis of severe, long-lived bow-echoes. *Journal of the Atmospheric Sciences*, **50**, 645–670.

Weisman, M. and C. Davis, 1998: Mechanisms for the generation of mesoscale vortices within quasi-linear convective systems. *Journal of the Atmospheric Sciences*, **55**, 2603–2622.

Weisman, M. and R. Trapp, 2003: Low-level mesovortices within squall lines and bow echoes. Part I: Overview and dependence on environmental shear. *Monthly Weather Review*, **131**, 2779–2803.

Williams, D., 1963: The thunderstorm wake of May 4, 1961. Technical report, U.S. Department of Commerce, Washington, D.C.

Yanai, M., S. Esbensen, and J. Chu, 1973: Determination of bulk properties of tropical cloud clusters from large-scale heat and moisture budgets. *Journal of the Atmospheric Sciences*, **30**, 611–627.

Appendix A

Bow Echo Cases Included in This Study

Table A.1: Information about each bow echo case included in this study. The first column is the date of each case. The second contains either the time (UTC) the convective line of the case first formed, or when the bow apex entered the state. The third column is the time (UTC) the convective line contained no reflectivity values greater than 50 dBZ, or the time the bow apex exited the state. The fourth and fifth columns are the active bowing structure and initiation type, respectively. Abbreviations are as explained in Chapter 3.

Date	Start (UTC)	End (UTC)	Mature Structure	Initiation Type
23 Apr 2002	0915	1200	CBE	merge
17 May 2002	0415	1130	BEC	isolated
24 May 2002	0500	0800	CBE	merge
29 July 2002	0545	0800	BEC	unknown
27 Aug 2002	0415	1145	CBE	unknown
19 Sep 2002	0230	0730	SLBE	linear
13 Mar 2003	0530	0745	CBE	linear
24 Apr 2003	0200	0345	CBE	linear
16 May 2003	0415	1030	BEC	merge
16 May 2003	0700	1100	BEC	merge
16 May 2003	0915	1200	BEC	merge
24 May 2003	1215	1715	CBE	unknown
06 Jun 2003	0100	0400	SLBE	linear
12 Jun 2003	0230	0645	BEC	merge
11 Sep 2003	1200	1515	SLBE	linear

Date	Start (UTC)	End (UTC)	Mature Structure	Initiation Type
04 Mar 2004	1945	2345	BEC	unknown
22 Apr 2004	0345	0745	CBE	merge
30 Apr 2004	0030	0415	BEC	merge
21 Jun 2004	0330	1000	BEC	merge
21 Jun 2004	0645	1200	BEC	merge
01 Jul 2004	0500	1045	BEC	merge
06 Jul 2004	0545	1030	CBE	unknown
11 Apr 2005	0130	0445	CBE	isolated
20-21 Apr 2005	2345	0245	BEC	merge
13 May 2005	0345	0845	CBE	merge
05 Jun 2005	0345	0515	BEC	merge
07 Jun 2005	0545	0745	CBE	merge
10 Jun 2005	0600	0815	CBE	merge
13 Jun 2005	0000	0300	BEC	merge
17 Jun 2005	0400	0530	BEC	merge
17 Jun 2005	0500	0600	BEC	merge
01 Jul 2005	0700	0845	CBE	isolated
01 Jul 2005	1130	1330	BEC	merge
04 Jul 2005	0430	0745	BEC	unknown
15 Sep 2005	0545	0800	CBE	linear
01 Oct 2005	1045	1215	CBE	unknown